Alma Mater Studiorum – Università di Bologna

DOTTORATO DI RICERCA IN Scienze Chimiche
Ciclo XXIII

Settore scientifico-disciplinare di afferenza: CHIM/12

DEVELOPMENT OF ADVANCED ANALYTICAL APPROACHES FOR THE CHARACTERIZATION OF ORGANIC SUBSTANCES IN ARTISTIC AND ARCHEOLOGICAL SAMPLES

Presentata da: GIORGIA SCIUTTO

Coordinatore Dottorato

Prof. Giuliano Longoni

Relatore

Prof. Rocco Mazzeo

Co-relatore

Prof. Aldo Roda

Esame finale anno 2011

The work described in this thesis was performed at

M2ADL - Microchemistry & Microscopy Art Diagnostic Laboratory,
Università di Bologna, Ravenna Campus,
Via Guaccimanni 42, 48100 Ravenna, Italy

This research has been carried out with the support of the European Union, within the European project "CHARISMA" Cultural heritage Advanced Research Infrastructures: Synergy for a Multidisciplinary Approach to Conservation/Restoration, VII Framework INFRASTRUCTURE n.228330,
and the Italian Ministry of Instruction, University and Research (MIUR) through the PRIN 2008 project "Sviluppo di metodologie diagnostiche integrate per la caratterizzazione e la localizzazione stratigrafica della componente organica in manufatti policromi artistici ed archeologici" (prot. 2008ZRSHHB).

"Di nostro non abbiamo che il tempo, nel quale vive chi non ha neppure dimora"
Oracolo manuale e arte di prudenza – Baldasar Gracian

A mio fratello Alessio, perché il mio tempo è ancora per lui

DEVELOPMENT OF ADVANCED ANALYTICAL APPROACHES FOR THE CHARACTERIZATION OF ORGANIC SUBSTANCES IN ARTISTIC AND ARCHEOLOGICAL SAMPLES

GIORGIA SCIUTTO

ABSTRACT

Polychrome artworks are usually characterised by a complex structure, made by the superimposition of different components. Their chemical characterisation and spatial location within these multilayered structures is of the outmost importance in the study of ancient painting techniques, as well as for the understanding of causes and degradation phenomena in view of the planning for appropriate conservation measures to be adopted by painting conservators.

The analytical studies presented in this thesis have been focused on the development of advanced approaches aimed at the characterisation of organic substances, which are usually the most difficult to be characterised among the various components in artistic and archaeological samples, due to their low concentration and to their wide chemical variety.

The microscopic and molecular characterisation of organic materials developed have been performed by means of different imaging and spectroscopic techniques, applying innovative analytical protocols, in order to provide a deep understating of their chemical identification and location in paint stratigraphies.

The potentialities and advantages of immunological approaches in combination with chemiluminescence imaging techniques have been deeply investigated to propose alternative methods for the localisation of proteins in paint cross-sections. FTIR spectroscopic and microscopic techniques have been also applied in combination with chemometric multivariate data analysis, to extract the maximum useful information embodied in the analytical signals.

Moreover, the crucial role played by sample preparation methods in the characterisation of the organic substances in paint cross-sections by chemical

imaging techniques has been taken into account. Alternative sample preparations have been proposed and evaluated to improve the traditional methodologies.

Contents

Chapter 1

Chapter 2

Chapter 3

Chapter 1

Introduction

Chemistry was first applied to the conservation field in the 18th Century, gradually assuming a fundamental role due to the increased number of collections exhibited in the museums of Europe [1].

Nowadays, chemistry for cultural heritage is widely employed in the field of conservation science, both in technical studies concerning attribution purposes and conservation-restoration issues [2]. Through the ages, in fact, the field of conservation science has become an interdisciplinary discipline, by the use of scientific inquiry and analytical equipment applied to the wide area of studies including the technology, structure and materials of artworks and their historical background.

The scientific approach is usually aimed at characterising the original artwork constituents as well as the restoration materials and their degradation products. Ancient artefacts can be considered as heterogeneous systems where several interactions between substances present in the complex matrix, as well as degradation and aging phenomena, can occur. In particular, polychrome objects are characterised by a multilayered structure made by the superimposition of different components, which constitute the preparation, priming, paint and varnish layers, depending on the working practices and techniques of the artist, as well as on the state of conservation of the object (Figure 1.1). Samples collected from a painting usually show a multilayered structure composed by mixtures of organic and inorganic substances. Their complete characterisation – and in particular their spatial

location within the layer structure and even within a single paint layer – is fundamental in the determination of adequate methodologies for conservation and restoration practices. Over the last decade, researches in the field of the science for conservation have been mainly focused on the development of advanced analytical methods and on the evaluation of instrumental performances aimed at characterising heterogeneous mixtures of components and their localisation.

The complexity of such kind of investigation is generally engendered by the wide chemical variety of components, their sensibility to the degradation phenomena (in particular of organic substances) and their modality of use. Moreover, the identification of materials may be difficult due to the thickness of layers, ranging from 1 to 100 μm. Therefore, the spatial resolution of the analytical techniques and the setup employed are of great importance in the characterisation of thin layers and small particles dispersed into each layer.

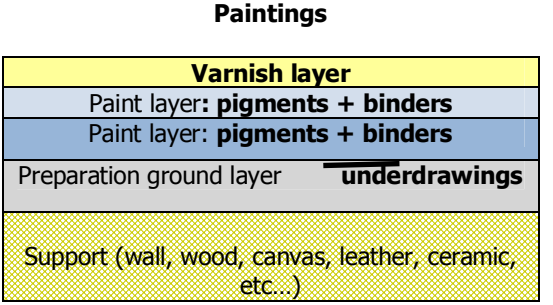

Figure 1.1 – Schematic view of a paint stratigraphy structure

On the other hand, it is worth noticing that, being one of the first stages, the sampling procedure is always one of the most critical and relevant phases of the whole analytical process.

In 1964, O. Karmie Galle observed that "no analysis is better than the sample itself" [3], highlighting the relevance of a proper deployment of sampling methodologies and criteria for the achievement of valuable results. In fact, lacks and faults affecting the sampling phase may determine gross errors and considerable losses in the significance of the final outcomes.

Even more in the conservation science, the correct collection and preparation of samples is one of the most important and challenging steps, due to both the heterogeneity of artwork matrices and the uniqueness and rarity of specimens. Actually, a number of difficulties may arise in the collection of sample sets, since two opposite criteria have to be addressed: the minimum invasiveness – i.e., the minimum number of specimens, and the maximum representativeness of the system under study and of the problems encountered.

Recently, the use of non-invasive techniques, which do not require the destruction of samples, have been strongly developed, allowing the characterisation of the whole artwork surface without damages. These techniques allow to obtain information about the distribution of materials and their degradation products. The first screening with non-destructive techniques allows, in fact, the documentation of chemical heterogeneity of the artworks, thus providing a reliable identification of the areas to be sampled.

For this purpose, spectroscopic techniques and imaging systems such as X-ray radiography, X-ray fluorescence (XRF), multispectral imaging system, and portable FTIR (Fourier transform infrared) or Raman spectroscopies are widely employed for such survey investigation on art objects.

In particular, based on the different X-ray energies emitted by a sample after excitation, XRF is an important tool to perform single-spot elemental analysis. This technique enables the identification of numerous inorganic compounds employed as painting materials [4 - 6]; the alloy composition and the nature

of corrosion patinas can also be determined for metal artworks [7], as are the different components used in the manufacture of glasses.
However, the information is simultaneously obtained from all the paint layers and should be carefully interpreted due to the penetration depth of X-rays and the resulting difficulties in distinguishing between the different layers beneath the surface.
It is worth saying that non-destructive approaches alone are often insufficient for fully characterising an art object and, as a consequence, a sample collection is required, not only for a deepened chemical analysis but also for detailed stratigraphical characterisation. For this reason, it is recommendable to follow a methodological approach, combining non-destructive and micro-destructive techniques in an integrated way.

1.1 ORGANIC SUBSTANCES IN ARTISTIC SAMPLES

Organic substances present as constituents into artworks are characterised by a large chemical variety and, consequently, by different properties and behaviour.
Natural and synthetic materials have been widely employed in museum objects and monuments. In fact, their use and manipulation were well known since ancient times and applied in artistic processes and techniques by artisans [8].
Even if most of the organic materials incorporated into artworks could be used without any pre-treatments, as row components, others required a higher technical knowledge and development to be obtained or utilised. Until the expansion of synthetic chemical industry, these treatments were probably devised empirically in the absence of any concept of the chemistry involved.

Synthetic polymers were introduced by Schonbein in 1846, a few years after the invention of the first synthetic polymer, cellulose nitrate [9].

Indeed, in the field of art and conservation, organic compounds could be employed alone or, more often, in highly complex mixtures in order to provide appropriate systems for different uses. Thanks to their abilities to form uniform and elastic films, different organic materials have been applied as binders, primers, finishing layers and protective coatings, as well as adhesives.

Among the natural products, proteins, lipids, polysaccharides and terpenoids have been widely used in art objects.

Lipids are defined as a mixture of mixed mono, di and triglycerides, which are esters of glycerol and carboxylic acids characterised by carbon chains ranging up to more than 30 atoms. Their chemical properties are related to their structure. In particular, the presence of double bounds confers to the molecules a higher susceptibility to the oxidation processes characteristic of drying oils, which are of basic importance to oil painting and the coating technology. Linseed, walnut and poppy oils have been widely used in western European painting.

Proteins, which are usually of animal origin, have usually been incorporated into paintings as binding media and adhesives. Form, physical characteristics and biological functions are widely variable, on the basis of the sequence of amino acids present.

Glues are obtained by dissolving collagen, the fibrous protein constituting the connective tissues in animals. Their use as adhesive is widespread in the preparation of grounds or binding media in easel paintings.

Egg white and yolk have quite a complex composition in terms of individual proteins, including glycoproteins, ovoalbumin and lysozyme in the white and phosphorous-containing lipids, such as phosphovitin, and also lipovitellins, lipoproteins and livetins in the yolk. In the history of painting techniques, they

have played a crucial role, thanks to their ability to form stable emulsions with pigments and other organic substances [10].
Casein is the first protein of milk and was mainly applied as a glue and eventually as a tempera medium.
Gums are polysaccharides exuded by trees and plants. They are water soluble or water-dispersive materials with a high molecular weight. Gums are the principal medium in watercolour paintings, miniatures and manuscript illumination.
Natural resins are a secretion or excretion of plants, mainly composed of terpenoid substances, which are made up of units of isoprene. These substances, widely used as varnishes can be characterised by the presence of mono- and sesquiterpenoids (essential oils) or di- or triterpenoids as well as mono- and sesquiterpenoids (solid resin). They show an amorphous - often glassy, rarely crystalline – structure [10].
Beeswax contains long chains of hydrocarbons, acids, alcohols or esters. They have been employed as adhesives and surface coatings, and particularly as waterproofing agents and occasionally as ingredients of binding media.

Among the materials composing the art object, organic compounds used as binding media or protective coatings have attracted the attention of the conservation professionals because of their noticeable ability to undergo physicochemical changes on ageing.
The stability of an organic compounds depends on its chemical structure and composition, which determines the alteration mechanisms.
The deterioration of artistic media and varnishes is mainly a result of oxidation processes involving free radicals and hydrolytic processes.
Auto-oxidation reactions are initiated by a thermal or photochemical input and, more rarely, by ionising radiations without oxygen intervention.

Hydrolysis reactions are catalysed by acids or other catalysts, which can be present in the atmosphere as pollutants. These processes are particularly important in proteins, drying oils and polysaccharides as they result in a significant change in the chemical and mechanical properties of the film [9].
Moreover, different agents can interact with painting materials, triggering degradation processes. A particularly well-known reaction involves pigments and oil binding media, producing metal soaps on the surface of paintings and modifying their visible appearance and state of conservation.

In the last decades, a particular attention has been devoted to the deep understanding of organic materials employed in art and of the ageing effects of conservation environments. Scientific researches, in fact, have mainly addressed the development of analytical methods for the characterisation of such compounds.
However, it is worth noting that, due to their complexity in composition, use and degradation, it is difficult to identify a general and common analytical strategy for their complete characterisation.
In addition, a restriction in the analysis is also determined by the limited number and amount of available samples. Indeed, non-invasive/non-destructive techniques would be favourable, as well as high-sensitive techniques, which require sub-milligrams of sample.
On the other hand, it is important to consider approaches which are able to obtain as much information as possible on the same sample by following an appropriate analytical protocol.
Recently, advanced methods have been developed and combined in order to provide detailed information on organic materials in paintings concerning their chemical composition and location in a heterogeneous multilayered system.

1.2 SCOPE OF THE THESIS AND OVERVIEW

The present research has been focused on the development of advanced approaches aimed at the characterisation of organic substances, which are the most difficult to be characterised among the various components in artistic and archaeological samples, due to their wide chemical variety and to their high sensitivity to degradation processes [8]. In order to overcome drawbacks and limits of the traditional techniques in terms of selectivity and location of analytes, different analytical purposes have been followed to optimise and define innovative methodologies addressing specific conservation issues.

The potentialities and advantages of immunological techniques have been deeply investigated to propose alternative methods in the localisation of proteins in paint cross-sections (Chapter 2). In fact, immunological approaches, thanks to the high selectivity of antigen-antibody reactions, are widely used in bioanalytical and clinical chemistry. In particular, a new ultrasensitive immunochemical procedure has been developed for the detection - in paint cross-sections - of the protein ovalbumin (chicken egg white albumin), present in binding media or varnishes,. The technique is based on chemiluminescence imaging detection combined with optical microscopy, and allows the sensitive localisation of the target protein in cross-sections with high spatial resolution. In order to evaluate its performance, the method was first applied to standard samples (also containing different common pigments), then used for the localisation of ovalbumin in samples from a Renaissance wood painting. Furthermore, a CL immunochemical procedure has been developed for the simultaneous identification and localisation of ovalbumin and casein, another protein which may be found as binding medium or varnish in artistic and archaeological samples. The

immunochemical analysis is performed by means of specific primary antibodies, revealed by enzyme-labelled secondary antibodies and suitable CL substrates. The possibility to simultaneously detect different proteins has been evaluated and confirmed, in order to allow a complete characterisation of the organic binding media in paint cross-sections.

An overview of the recent advances of FTIR microscopy in artwork diagnostic is provided. Moreover, considering the main drawbacks encountered in the past, new or less studied instrumental configurations have been evaluated and compared (Chapter 3.1).

A core part of the thesis is dedicated to the definition of a suitable approach for the analysis and interpretation of the large amount of data typically obtained by μFTIR-ATR hyperspectral arrays obtained from the analyses of paint cross-sections (Chapter 3.2). Chemical maps are usually re-constructed by the selection of a given absorption band, which is considered as a marker of a specific compound, known or supposed to be present inside the micro-area of the investigated paint cross-section. Nevertheless, by using the univariate approach, problems related to the presence of mixtures, the overlapping of characteristic bands, as well as changes in their relative intensity may arise, which affect the correct compound identification and localisation. In order to overcome such limitations and to extract the maximum useful information embodied in the hyperspectral data, an exploratory multivariate approach has been adopted. Principal component analysis (PCA) was performed, after application of proper signal pre-processing, and the score values were converted into chemical maps. The methodology has been positively tested on samples collected from painted artworks.

One of these, which concerns the application of FTIR spectroscopy in the far infrared region (FIR), has been proposed as an alternative method for the characterisation of natural resins (Chapter 3.3). For this purpose, standards of

natural resins used as paint varnishes have been analysed by FIR spectroscopy in the ATR mode. In accordance with the requirements in examinations of cultural heritage materials, ATR analysis allows the non-destructive investigation of micro-samples without any prior chemical nor mechanical treatment. Discrimination between spectral data for all the resin specimens and the repeatability of measurements have been magnified and verified using principal component analysis (PCA).

The crucial role played by preparation sample methods in the characterisation of the organic substances in paint cross-sections by chemical imaging techniques (such as μFTIR, μRaman, etc.) has been taken into account. In fact, the final investigation outcomes may be considerably influenced by the sample preparation phase, which is accomplished through embedding the paint fragment into a polymer resin followed by grinding, polishing or microtoming the block to produce either cross-sections or thin sections.

Chapter 4 deals with a critical definition of the state of the art on sample preparation procedures. Initially, different embedding and polishing methods are compared, evaluating the sample morphology and the pollution effects. With this aim, fragments coming from the same area of a real sample were embedded following different approaches and compared in terms of cross-section morphology and pollution. The cross-sections were observed with optical microscopy, ESEM and confocal microscopy, and analysed with FTIR microscopy both in ATR and in total reflection modes (Chapter 4.1).

Subsequently, in the second part of the chapter 4 (Chapter 4.2), alternative sample preparations are proposed and evaluated to improve the traditional methodologies. In particular, the use of infrared-transparent salts as the embedding material for cross-sections was introduced in order to avoid interferences. A first attempt with the use of potassium bromide (KBr) was proposed in previous research works. The performances of different inorganic salts used as embedding materials have been compared and evaluated. In

particular, sodium chloride (NaCl), calcium fluoride (CaF_2) and barium fluoride (BaF_2) were selected according to their chemical and physical properties: solubility, colour, transparency and stability. Pressure and application time necessary for the embedding procedure were defined for each mounting material. In particular, NaCl has shown better performances in terms of physical stability. Furthermore, systems aimed at stabilising salt embedding medium, and which are suitable for semi-automatic polishing procedures with the use of the sample holder, were developed.

Moreover, the well known KBr embedding method was optimised using the inorganic salt as a barrier against the resin infiltration, obtaining promising results. In fact, the double embedding system (with KBr and polyester resin) showed high performance in terms of physical stability and proved to be also suitable for a polishing sample holder, which is needed in order to obtain a high surface quality.

1.3 BIBLIOGRAPHY

1. Spoto, G. (2002) Past Restorations of Works of Art, Acc. Chem. Res. 35, 652-659
2. Ciliberto, E. Spoto, G. (2000) Modern Analytical Methods In Art And Archaeology. Wiley
3. Karmie Galle, O. (1964) Transactions of the Kansas Academy of Science Vol. 67, No. 1 pp. 100-110
4. Moioli, P. and C. Seccaroni (2000) Analysis of art objects using a portable x-ray fluorescence spectrometer X-Ray Spectrometry 29(1): 48-52.
5. Mazzeo, R. Sciutto, G. Prati, S.. Amadori, M.L (2009) in Techne: La technique picturale d'Andrea Mantegna, C2RMF, Paris, 46-66

6. Mazzeo, R. Menu, Amadori, M.L. Bonacini, I. Itié, E. Eveno, E. Joseph, E. Lambert, E. Laval, E. Prati, S. Ravaud, E and Sciutto, G. (2011) Studying Old Master Paintings: Technology and Practice, Archetype Publications. London, 44-51
7. Cesareo, Ridolfi et al. 2006; Karydas 2007; Bonizzoni, Galli et al. 2008
8. Mills J.; White R. (1999) in Organic material in museum objects, 2d ed. Oxford, Butterworth Heinemann, 95-129
9. Doménech-Carbò M.T. (2008) Anal. Chim. Acta 621: 109–139;
10. Gettens, R. J. and G. L. Stout (1966) Painting Materials. New York, Dover Publications, Inc.

1.4 LIST OF PUBBLICATIONS

- G. Sciutto, L.S. Dolci, A. Buragina, S. Prati, M. Guardigli, R. Mazzeo, A. Roda, Development of a multiplexed chemiluminescent immunochemical imaging technique for the simultaneous localization of different proteins in painting micro cross-sections, Accepted by Analytical and Bioanalytical Chemistry vol. 399, n. 9, 2889-2897
- S. Prati, G. Sciutto, R. Mazzeo, C. Torri, D. Fabbri, Application of ATR-Far Infrared Spectroscopy to the analysis of natural resins. Accepted by Analytical and Bioanalytical Chemistry vol. 399, n. 9, 3081-3091
- C. Samorì, G. Sciutto, L. Pezzolesi, P. Galletti, F. Guerrini, R. Mazzeo, R. Pistocchi, S. Prati, E. Tagliavini, (2011) Effects of imidazolium ionic liquids on growth, photosynthetic efficiency, and cellular components of the Diatoms *Skeletonema marinoi* and *Phaeodactylum tricornutum, Chem. Res. Toxicol.*, Article ASAP, DOI**:** 10.1021/tx100343p Publication Date (Web): February 25, 2011
- S. Prati, E. Jospeh, G. Sciutto, R. Mazzeo, (2010) New Advances in the Application of FTIR Microscopy and Spectroscopy for the Characterization of Artistic Materials, Accounts of chemical research, ISSN 0001-4842, vol. 43, n. 6, 792-801, 2010
- E. Joseph, S. Prati, G. Sciutto, M. Ioele, P. Santopadre, R. Mazzeo, (2009) Performance evaluation of mapping and linear imaging FTIR microspectroscopy for the characterisation of paint cross sections, Analytical and Bioanalytical Chemestry, Vol 396, 899-910
- E. L. Kendix, S. Prati, E. Joseph G. Sciutto, R. Mazzeo, (2009) ATR and transmission analysis of pigments by means of far infrared spectroscopy, Analytical and Bioanalytical Chemistry, Vol. 394, 1023-1032
- Mazzeo, R. Menu, Amadori, M.L. Bonacini, I. Itié, E. Eveno, E. Joseph, E. Lambert, E. Laval, E. Prati, S. Ravaud, E and Sciutto, G. (2011)

Studying Old Master Paintings: Technology and Practice, Archetype Publications. London, 44-51

- R. Mazzeo, G. Sciutto, S. Prati, M.L. Amadori, Scientific examination of the Mantegna's paintings in Sant'Andrea, Mantua: the families of Christ and St. John the Baptist and the baptism of Christ, in *La technique picturale d'Andrea Mantegna,* Techne, C2RMF, Paris, 46-66
- R. Mazzeo, G. Sciutto (2009) Spot and staining test in *Scientific examination for the investigation of paintings. A handbook for conservator-restorers*, Firenze, Centro di, pp. 56-57, 80-82, 92-93, 124-125, ISBN 978-88-7038-474-1
- L. Cartechini, R. Mazzeo, L. Pitzurra, S. Prati, G. Sciutto, M. Vagnini (2009) Immunological tests in *Scientific examination for the investigation of paintings. A handbook for conservator-restorers*, Firenze, Centro di, pp. 93 – 94, ISBN 978-88-7038-474-1
- L.S.Dolci, G. Sciutto, M. Guardigli, M. Rizzoli, S. Prati, R. Mazzeo, A. Roda, (2008) Ultrasensitive chemiluminescent immunochemical identification and localization of protein components in painting cross-section by microscope low-light imaging, Analytical and Bioanalytical Chemistry 392:29-35.
- R. Mazzeo, E. Joseph, G. Sciutto, (2007) Indagini di imaging multispettrale e analisi microFTIR per la caratterizzazione dei materiali originali e di restauro del globo celeste di V. Coronelli, in *Restaurare il cielo. Il restauro del globo celeste faentino di VincenzoCoronelli*. N. Scianna, Bologna, CLUEB**:** 48-61. ISBN 978-88-491-3006-5

Chapter 2

Characterisation of organic substances in paint cross-sections:

Immunological approach

2.1 ULTRASENSITIVE CHEMILUMINESCENT IMMUNOCHEMICAL DETECTION OF PROTEINS IN PAINT CROSS-SECTIONS

In the last decade, a considerable part of the research in the field of the science for conservation has been aimed at the development and optimisation of analytical methods for the characterisation and localisation of components of heterogeneous mixtures in paint samples.

Indeed, polychrome artworks are usually made by the superimposition of several layers containing different substances according to the painting technique. In addition, the characteristics of the painting layers are affected by degradation processes, reflecting the state of conservation of the artwork.

Until now, chromatographic techniques have represented the most commonly used analytical technique for the analysis of organic components of paintings thanks to their high selectivity and applicability to a wide range of natural organic materials. Nevertheless, chromatographic techniques require the extraction of the analytes from the sample, thus losing the information concerning stratigraphic localisation. Moreover, chromatographic procedures for the analysis of proteins are quite complicated and require long extraction protocols [1].

Another analytical technique that has been extensively applied in the field of cultural heritage is the micro Fourier transform infrared spectroscopy (μ-FTIR) [2]. This technique allows the stratigraphic characterisation of both organic

and inorganic materials in painting cross-sections, and its performance in terms of spectral and spatial resolution is continuously improving thanks to the development of alternative analytical approaches for the measurement of microsamples and the implementation of new-generation instruments [3]. However, in spite of these achievements, an important limit of μ-FTIR is still its lack of selectivity: it only allows to recognise functional groups, not the whole molecular structure. Therefore, proteinaceous materials can be easily detected but specific proteins cannot be identified.

Immunological techniques represent a promising alternative for the detection and identification of organic materials (particularly proteins) used as painting materials. Thanks to the high selectivity of the antigen-antibody reaction, which would allow one to distinguish between different proteins and also to determine the biological source of a protein (e.g., bovine collagen vs. rabbit collagen). Such techniques are widely employed, particularly in bioanalytical and clinical chemistry, in applications ranging from microtiter plate-based quantitative assays to immunohistochemistry [4].

Moreover, immunohistochemical techniques have been proven suitable for the sensitive localisation of target proteins in cells and tissue samples with spatial resolution of the order of the micrometer [5]. After the early sporadic applications in the field of cultural heritage [6-8], in the last years a growing attention is being focused on the potential of enzyme-linked immunosorbent assays (ELISA) [9-10] and the use of immunochemical imaging methods employing different detection techniques for the location of protein components in multilayer cross-sectioned paint samples.

Among the different detection techniques, chemiluminescence (CL) has shown remarkable performances in terms of spatial resolution and detection limit. Indeed, CL imaging has already proven to be more sensitive than fluorescence detection for the localisation of target molecules in tissues and cells [11-14]. In addition, CL detection does not require a excitation source.

Therefore, the CL technique is not affected by the autofluorescence of sample components, which is of particular relevance for the analysis of paintings' cross-sections because several components of paintings are natively fluorescent.

Ultrasensitive chemiluminescent immunochemical procedures for the detection of ovalbumin as well as for the simultaneous localisation of ovalbumin and bovine casein (two common proteins in binding media or varnishes of artistic and archaeological samples) in resin-embedded painting micro cross-sections have been developed during this PhD thesis.

2.2 CHEMILUMINESCENCE

The phenomenon of chemiluminescence can be defined as the emission of light (usually in the visible spectral region) due to a chemical reaction that produces molecules in the excited state. The CL emission is utilized in various analytical techniques, in which analytes are detected and quantified by measuring light emission [14-15].

Light-emitting chemical reactions can be grouped into three classes:

1. Chemiluminescent reactions, i.e., chemical reactions involving strongly oxidant species (e.g., peroxides) and natural or synthetic compounds.
2. Bioluminescent reactions, i.e., light-emitting reactions that take place in a living organism, such as the firefly or the jellyfish.
3. Electrochemiluminescent reactions, i.e., chemical reactions in which light emission is triggered by a redox process.

In more detail, in order to produce light a chemical reaction should possess some essential requirements:

1. The reaction must be sufficiently exothermic to produce molecules in an electronically excited state. The free energy requirement can be calculated using the following equation:

$$-\Delta G \geq \frac{hc}{\lambda_{ex}} = \frac{28600}{\lambda_{ex}} \qquad (2.1)$$

Therefore, the free energy change for CL reactions producing photons in the visible range (400–750 nm) must be at least 40–70 kcal mol^{-1}. Peroxides, especially cyclic peroxides, are often involved in light-emitting reactions because the relatively weak peroxide bond is easily cleaved and the resulting molecular reorganisation liberates/releases a large amount of energy.

2. This electronically excited state has to be accessible on the reaction coordinate (i.e., it should be obtained with a high yield as the product of the reaction).

3. Photon emission has to be a favourable decay process of the excited state, which means that the excited product of the reaction must be a fluorescent molecule.

The CL quantum yield, defined as the number of photons emitted per reacting molecule, of a CL reaction can thus be expressed as:

$$\Phi_{CL} = \Phi_R \times \Phi_{ES} \times \Phi_F \qquad (2.2)$$

where Φ_R reflects the chemical yield of the reaction, Φ_{ES} is the fraction of the product obtained in an excited state, and Φ_F is the fluorescent quantum yield of the product.

When the excited product of the chemical reaction is poorly fluorescent (low Φ_F) the yield of chemiluminescence can be increased by employing a fluorescent acceptor: in such type of chemiluminescence (indirect CL) the excited product transfers its energy to an highly fluorescent energy acceptor, which then emits. The CL quantum yield of an indirect CL reaction can be obtained by the equation:

$$\Phi_{CL} = \Phi_R \times \Phi_{ES} \times \Phi_{ET} \times \Phi_F' \qquad (2.3)$$

where Φ_{ET} expresses the efficiency of the energy transfer from the excited donor to the acceptor and Φ_F' is the fluorescence quantum yield of the acceptor.

As concerned chemical analysis, CL represents a powerful detection techniques due to features that make them superior to other detection principles involving light, such as spectrophotometry and fluorometry. Indeed, since the light is emitted by a specific reaction no excitation source is required, thus avoiding interferences from light scattering and background emission due to sample matrix components. Thanks to the wide dynamic range of CL measurements, samples can be measured over several decades of concentration without dilution or modification of the analytical procedure. In addition, the onset of light emission usually takes place in seconds or minutes (thus rendering CL techniques very rapid), minimal instrumentation is required and CL can be measured in a wide range of analytical formats

(tubes, microtiter plates, etc.). On the other hand, a potential disadvantage of CL systems is that the light-emitting chemical reaction could be uncontrollably inhibited, enhanced, or triggered by sample matrix constituents.

2.3 ENZYME CHEMILUMINESCENT SYSTEMS

Chemiluminescent reactions involving simple CL reagents usually have flash-type kinetics, in which light lasts only a few seconds. To obtain higher CL signals and longer CL emissions, enzymes can be used in the presence of an excess of a suitable CL enzyme substrate. In addition, suitable enhancers can be added to a CL substrate to obtain steady-state emission lasting several minutes, thus improving analytical signal handling (modes of triggering and measuring the signal) and measurement reproducibility [16].
Horseradish peroxidase (HRP) and alkaline phosphatase (AP) are the most commonly employed enzymes detectable by CL.

2.3.1 HORSERADISH PEROXIDASE

The luminol CL reaction catalyzed by HRP in the presence of an oxidizing agent (e.g., hydrogen peroxide) is widely employed in analytical chemistry [17] and is commonly used in bioanalysis (e.g., in immunoassays and gene probe assays) for the determination of HRP biospecific probes. In addition to HRP, several transition metal ions (including Fe^{2+}, Co^{2+}, Cu^{2+} and others) and their complexes can be used to trigger the reaction [18].
Luminol (LH_2) can be considered a diprotic acid. During the chemiluminescence reaction under basic conditions the prevalent luminol anion (LH^-) is oxidised to luminol radical anion (LH^*). As shown in Figure 2.1, in a second oxidation step LH^* is further oxidised to either aminodiazaquinone

(L) or directly (by superoxide anion) to hydroperoxide adduct (LO_2H^-). Another reaction that takes place is the dismutation of two molecules of LH_d, forming L and LH^-. Addition of hydrogen peroxide to L can also give the hydroperoxide adduct (LO_2H^-). From this adduct an endoperoxide species can be formed, from which molecular nitrogen (N_2) is expelled, generating excited state 3-aminophthalate dianion (AP).

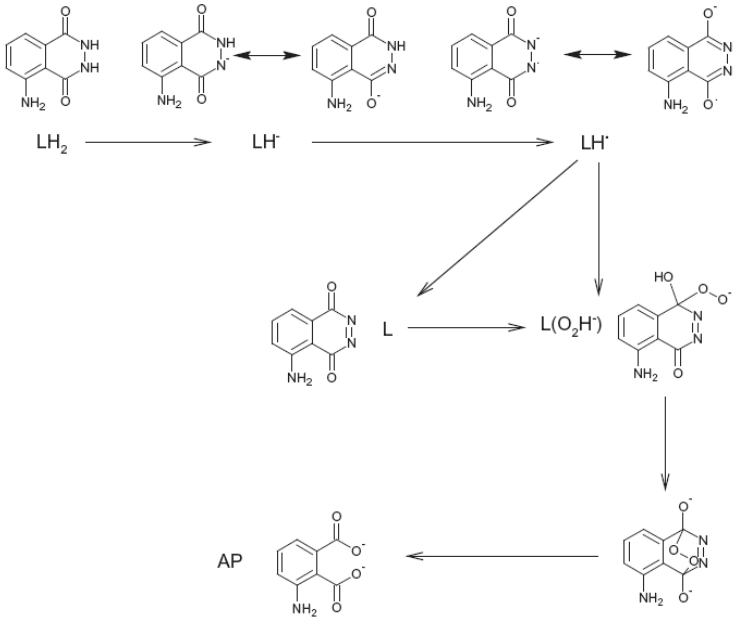

Figure 2.1 - Scheme of chemiluminescent luminol oxidation

Moreover, the intensity and duration of the luminol CL emission can be greatly increased by adding a molecule (e.g., 4-iodophenol) in the substrate solution, which works as an enhancer. The mechanism of this enhanced chemiluminescence involves the very efficient generation of enhancer radicals (En*) increasing HRP turnover.

2.3.2 ALKALINE PHOSPHATASE

The alkaline phosphatase is another quite common tracer in immunoassay and molecular biology especially when coupled with chemiluminescent detection. APL catalyses the dephosphorylation (hydrolysis of phosphatase esters) in many type of molecules and it is are most effective in an alkaline environment.

Dioxetanes such as the stabilised adamantyl 1,2-dioxetane (3-(4-methoxyspiro[1,2-dioxetane-3,20-tricyclo[3.3.1.13,7]decan]4-yl)phenyl phosphate, AMPPD) are appropriate substrates for the detection of AP, thanks their high efficiency and availability [20-21].

The chemiluminescent substrate undergoes hydrolysis in the presence of AP to yield an unstable intermediate with light emission at 470 nm (Figure 2.2).

The AP reactions are basically free of interferences and AP itself is very highly stable and has a high turnover rate [19].

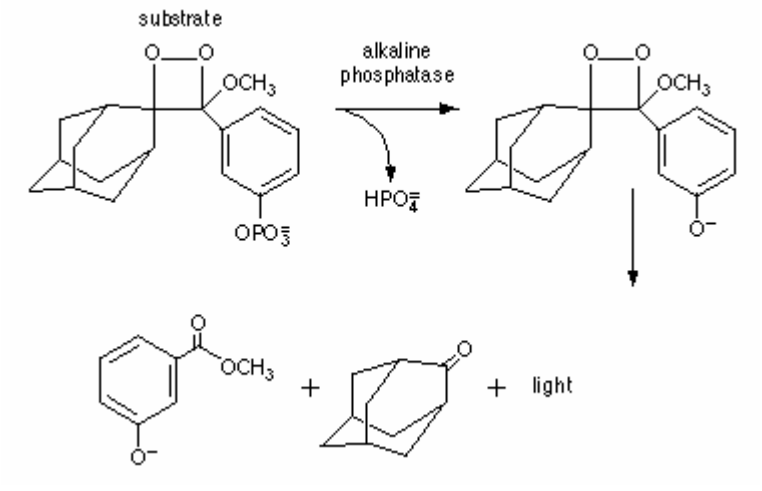

Figure 2.2 - Scheme of chemiluminescent AMPPD dephosphorylation

2.4 CHEMILUMINESCENCE IMMUNOASSAYS

Immunoassays are quantitative analytical techniques that uses antibodies as specific recognition elements and rely on the high selectivity of the binding of an antibody (Ab) to its specific antigen (Ag). Antibodies bind to various important analytical targets, including small organic molecules (pesticides, hormones, drugs) and biopolymers (peptides, proteins, DNA). Therefore, immunoassays can be designed for a wide range of analytes and are applied in various fields, such as life sciences, clinical chemistry, and pharmaceutical, toxicological, environmental and food analysis

Antibodies are immunoglobulin proteins produced by the immune system of organisms in response to the presence of specific antigens. The antigen is the counterpart to the antibody and, due to its chemical structure, it binds to the antibody with high affinity (i.e., high equilibrium constant). The antigen molecular sequence recognized by the antibody is called the epitope or antigenic site. Depending on their structure and immune function, antibodies are divided into five classes: IgM, IgG, Iga, IgD and IgE. Immunoglobulins G (IgG) are the antibodies commonly used in immunoassays. The IgG molecule presents four polypeptide chains (two heavy chains and two light chains) joined to form a "Y" shaped structure (Figure 2.3). The variable region includes the ends of the light and heavy chains and is characterised by a great variability, giving the antibody its specificity for the binding antigen. The constant region (the other part of the antibody) is specific of the animal species in which the antibody is produced.

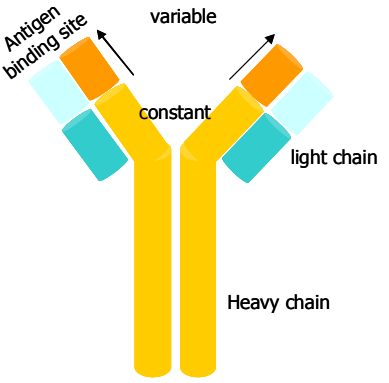

Figure 2.3 – Antibody stricture

Monoclonal (mAb) and polyclonal (pAb) antibodies are available for immunoassays. Differently from a monoclonal Ab, which recognises only one antigenic site, a polyclonal Ab is a mixture of antibodies able to bind to different epitopes within the same antigen. Polyclonal antibodies are usually employed in immunoassays to increase the possibilities of identifying the target protein.

In order to be detectable using a proper technique, an antibody needs to be labeled with a suitable marker. Instead of direct labeling, it is a common procedure to detect the antigen-specific antibody (primary antibody) with a secondary labeled antibody. Such labeled antibody is an anti-species antibody, i.e., it is directed against primary antibodies depending on their biological source (mouse, goat, sheep, rabbit, etc). This approach is called indirect antibody detection and it is shown in Figure 2.4. It is worth noting that the labelling process requires significant amounts of antibody, reduces its activity and may be quite complex. Therefore, the indirect approach is more convenient in terms of cost and efficiency (only one anti-species secondary antibody needs to be labelled, which can in all the immunoassays employing

primary antibodies from the same species), even if this requires an additional reaction step and thus a longer assay time.

Different markers and detection techniques can be used for the visualisation of the antigen-antibody complex (e.g., radioisotopes, fluorophores, gold nanoparticles, enzymes). In any case, the marker should be characterized by a high signal/mass ratio to detect low antigen concentrations. Enzyme markers are particularly interesting from this point of view, because allow one to obtain high sensitivity thanks to their catalytic activity. Indeed, nowadays about 80% of immunoassays for routine clinical analysis are based on the use of enzymatic labels.

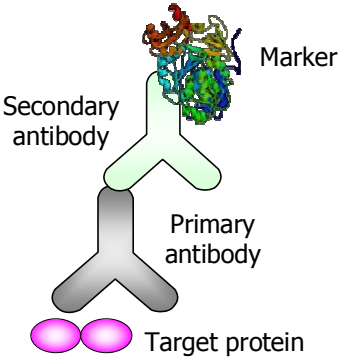

Figure 2.4 – Scheme of indirect approach in immunoassay

Chemiluminescence immunoassays are more sensitive than chromogenic and fluorogenic enzyme immunoassays and often exceed radioimmunoassay [22-23].

In principle, an antibody can be labelled either with a CL molecule or with an enzyme detectable by CL in the presence of a suitable CL enzyme substrate. Nevertheless, the latter labelling approach allow to achieve a much higher CL

signal/mass ratio of the labelled antibody, and therefore it is preferred when a high detectability is required. The HRP and AP enzymes are the main enzyme labels employed in chemiluminescent enzyme immunoassays.

2.5 CHEMILUMINESCENCE IMAGING

The availability of low-light imaging devices based on high-sensitivity and highresolution video cameras, such as intensified, or cooled, charge-coupled devices (CCD) or complementary metal oxide semiconductor (CMOS) image sensors, has allowed the development of bio- and chemiluminescence imaging methods, which rely not only on the detection of light emission down to the singlephoton level, but also on the localization of the signal on the sample surface with excellent spatial resolution [24].

A wide number of applications have been described, for both macro- and microsamples in various fields, such as drug development, diagnostic applications, agrofood and environmental analysis and, recently, in cultural heritage.

The possibility of localizing and quantifying the light emission on a target surface through chemiluminescence imaging represents a powerful tool for a wide range of applications. When microsamples are analyzed, the distribution of the target analyte on the sample surface can be assessed, even on irregular surfaces. Coupling the imaging detector with a microscope also allows the localization and quantification of target molecules, taking the advantage of high detectability and possibility of quantification of the labeled probes.

Low-light imaging devices, such as high-sensitivity CCD, are currently employed for bio- and chemiluminescence imaging in macro- and microsamples.

Luminographs consist of an ultrasensitive video camera and an optical system enclosed in a light-tight box to prevent interference from ambient light. The sample under investigation is placed in the luminograph and the pattern of light emission from its surface is recorded and converted into a digital image.

The grayscale image can be converted into pseudo-colors to emphasize the differences in signal intensity, and then overlapped to the image acquired in transmitted light (live image) to obtain accurate analyte localization on the sample surface. Resolution of luminescence imaging by employing standard or customs optics ranges from 100 to 200 μm for macro-samples analysis to a micrometer or sub-micrometer level when imaging measurements are performed by coupling the imaging detector to an optical microscope, thus enabling analysis at cellular and subcellular level.

Consequently, chemiluminescence imaging techniques have been proposed as a powerful tool in the characterization and of artworks materials in stratigraphic micro-sample.

2.6 CHEMILUMINESCENT IMMUNOCHEMICAL IMAGING FOR THE LOCALISATION OF OVALBUMIN IN PAINT CROSS-SECTIONS

The CL immunochemical method for the localisation of ovalbumin relied on the binding to the target protein of a specific primary antibody, which was then detected by a horseradish peroxidase (HRP)-labelled secondary antibody and a CL enzyme substrate. The imaging of the CL signal produced by the enzyme-catalysed reaction allowed the detection and the stratigraphic localisation of the target protein. To evaluate the performance of the method, whole egg tempera standard samples (with or without pigments) were used as models, then the immunolocalisation assay was applied for the detection of ovalbumin in samples obtained from a Renaissance wood painting.

2.6.1 MATERIALS AND METHODS

2.6.1.1 Reagents

Anti-chicken egg albumin antibody (whole antiserum, produced in rabbit), horseradish peroxidase (HRP)-conjugate polyclonal anti-rabbit IgG antibody (produced in goat), albumin from chicken egg white (ovalbumin), bovine serum albumin, gelatin (type A, from porcine skin), and bovine nonfat dried milk were purchased from Sigma-Aldrich Co. (St. Louis, MO). The luminol-based HRP CL detection reagent WESTAR Supernova was from Cyanagen

(Bologna, Italy). The smalt (ground glass colored with cobalt(II) salts), azurite and malachite ($Cu_3(CO_3)_2(OH)_2$), hematite (Fe_2O_3), cinnabar (HgS), and minium (Pb_3O_4) pigments were obtained from Zecchi (Florence, Italy). Polyester resin for sample embedding (SeriFix Resin and SeriFix Hardener) was purchased from Struers A/S (Ballerup, Denmark). All the other chemicals used were of analytical grade. Experiments on membranes were performed on Protran® nitrocellulose membrane (Whatman, Maidstone, England).

2.6.1.2 Instrumentation

Chemiluminescence imaging microscopy experiments were carried out by a home-made imaging system composed by a BX 60 epifluorescence microscope (Olympus Optical, Tokyo, Japan) connected to a liquid nitrogen-cooled ultrasensitive CCD camera (LN/CCD Princeton Instruments, Roper Scientific, Trenton, NJ). The microscope, which was enclosed in a dark box to avoid interference from ambient light, was also equipped with an OptiScan ES103 XYZ stage system (Prior Scientific Instruments Ltd., Fulbourn, England) to allow reproducible sample positioning and focusing without opening the dark box. Live images of the samples were obtained using the LN/CCD camera and a RGB filter (CRI Inc., Woburn, MA): separate grayscale images for red, green and blue channels were acquired, then they were then merged in a single color image. Image processing and quantitative analysis were performed using the image analysis software Metamorph v. 4.5 (Universal Imaging Corporation, Downington, PA).

Visible and fluorescence images of painting cross-sections under UV excitation at 313 nm were acquired by a BX 51M optical microscope (Olympus Optical) connected to a DP70 digital camera (Olympus).

Chemiluminescence imaging of nitrocellulose membranes was performed by a Night Owl LB 981 low-light luminograph (Berthold Technologies GmbH, Bad

Wildbad, Germany) equipped with a thermoelectrically-cooled, back-illuminated CCD camera.

2.6.1.3 Samples

Standard samples were prepared according to traditional painting techniques [25]. Briefly, a layer of whole egg tempera, i.e., a mixture of egg white, yolk and water in a 1:1:1 (v/v) ratio, was applied on a preparation layer made of gypsum (obtained from Zecchi) and rabbit glue (purchased from Phase, Bologna, Italy). To evaluate the effect of pigments on the CL immunolocalisation procedure, standard samples were also prepared using a mixture of pigments and whole egg tempera. The relative ratio between binding medium and pigments was depended on their nature. To obtain homogenous mixtures, suited to be applied as thin layers on the preparation ground, the following pigment/egg (w/w) ratios were adopted, according with artists' traditional recipes: 4:1 for azurite, malachite, smalt and hematite; 3:1 for cinnabar and minium.

The samples prepared from the mock ups (with size of a few mm^2) were embedded in polyester resin and polished with silica abrasive papers (grit from 120 to 1000) and water as a cooling medium. Then, to obtain a high-quality surface in terms of planarity and roughness (i.e., to reduce the surface porosity of the cross-section) [26], a dry polishing procedure was performed using SiC papers graded from 2400 up to 12000 purchased from Micro-Surface Finishing Products Inc., Wilton, IA.

2.6.1.4 Experimental procedure

Sample cross-sections were treated for 1h at room temperature with the blocking solution (5% dried milk in water) then, after washing (3X) with PBS/milk (10 mM phosphate buffer saline, pH = 7.4, containing 1.25% dried

milk), they were incubated overnight at 4°C with the anti-chicken egg albumin antibody (primary antibody) diluted 1:4000 (v/v) in PBS/milk. Afterwards, the samples were washed (5X) with PBS/milk and incubated for 4h at 4°C with the HRP-labeled anti-rabbit IgG antibody (secondary antibody) diluted 1:2000 (v/v) in PBS/milk. Samples were washed again (5X) with PBS, then the HRP CL detection reagent was added to cover the cross-section and the CL images were acquired using an integration time of 120 sec. For each CL image, a live image of the sample was also acquired to assess the localisation of the CL signal (therefore of the ovalbumin protein) in the sample through comparison of the CL and live images.

2.6.2 RESULTS AND DISCUSSION

2.6.2.1 Optimisation of experimental conditions

Optimisation of the experimental conditions of the immunoreactions was performed by preliminary measurements on ovalbumin samples spotted on nitrocellulose membranes. In order to select the most suitable concentrations of the antibodies, different dilutions of the primary and secondary antibody were employed for the detection of ovalbumin (data not shown). The highest CL signal/background ratios were obtained using 1:4000 (v/v) and 1:2000 (v/v) dilution factors for the primary and the secondary antibody, respectively. Even though higher concentrations of the primary antibody led to stronger CL signals from the ovalbumin spots, the CL signal/background ratios were lower, due to the concurrent increase of the background signal, thus such concentrations were not employed in the assay. Experiments on membranes also allowed the selection of the most suitable blocking agent to reduce the non-selective adsorption of the immunoreagents on the surface of the cross-section. Among the tested substances (bovine serum albumin,

gelatine and dried milk) the highest signal/background ratios were obtained using a 5% solution of non-fat dried milk in water (Figure 2.5). Interestingly, bovine serum albumin was the less efficient blocking agent and led to a diffuse background signal over the whole membrane, which might be attributed to a small cross-reactivity of the protein with the anti-ovalbumin antibody.

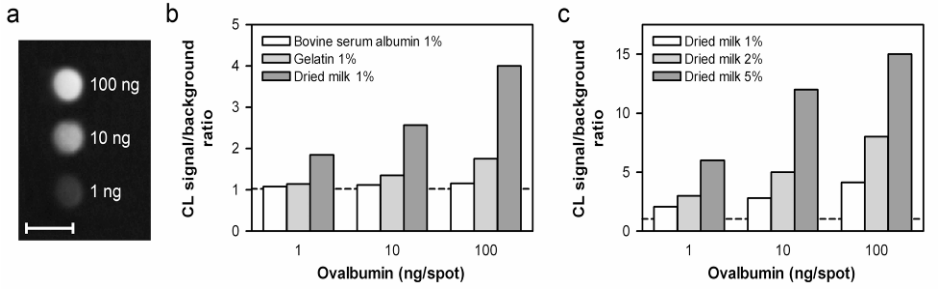

Figure 2.5 - Selection of (b) the blocking agent and (c) its optimal concentration performed on nitrocellulose membranes on which different amounts (1, 10 and 100 ng) of ovalbumin were spotted. The cross-sections were incubated for 1h at room temperature with both the blocking agent and the primary and secondary antibodies (used at their optimal concentrations). Data are reported as ratios between the CL signals of the spots and the background signal of the membrane. Panel (a) shows the CL image of a nitrocellulose membrane. Bar represents 5 mm

To evaluate the detectability of ovalbumin by using the CL immunolocalisation procedure, a calibration curve was obtained in the optimised experimental conditions for protein amounts ranging from 0.1 to 100 ng/spot. The CL signal showed a good correlation with the amount of protein, as shown in Equation 2.4 where Y is the mean CL signal of the spot (RLU) and X is the amount of ovalbumin (ng/spot).

$$Y = (128.6 \pm 4.3)\log X + (132.2 \pm 4.9) \quad (n = 7, r^2 = 0.996) \quad (2.4)$$

In such experimental conditions, the detection limit of the assay, estimated as the protein amount giving a CL signal corresponding to the background signal plus three times its standard deviation, was about 0.2 ng/spot (or 0.03 ng/mm^2). Even though the amounts of ovalbumin spotted on the membrane could not easily compared with those present in painting cross-sections, the low value of the detection limit suggested that the CL immunolocalisation procedure was sensitive enough to allow the detection of the protein in egg tempera paintings.

Due to the porosity of the cross-sections, optimisation of blocking and incubation steps was critical to avoid non-selective adsorption of the immunoreagents, which would determine high background signals and decrease the detectability of the target protein. Indeed, when the assay was performed in cross-sections of standard samples with a layer of whole egg tempera using the same experimental protocol employed for nitrocellulose membranes (1h-incubations at room temperature with the blocking agent and the two antibodies) the CL signal/background ratio was low due to the non-selective adsorption of the antibodies on the ground layer (Figure 2.6a). However, the non-selective binding of the immunoreagents could be controlled, other than by careful preparation of the cross-section with a dry polishing method to reduce the heterogeneity of the surface, by decreasing the incubation temperature.

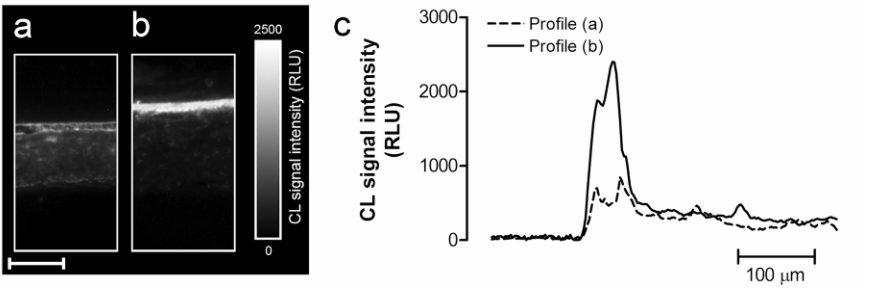

Figure 2.6 - Chemiluminescence images obtained for the immunolocalisation of ovalbumin in cross-sections of standard samples with a layer of whole egg tempera, performed (a) with 1h-incubations at room temperature with the primary and secondary antibodies and (b) according to the optimised experimental protocol. Panel (c) shows the profiles of the CL signal across the cross-sections. Bar represents 200 μm.

In fact, the signal/background ratio significantly improved when incubations with the primary and secondary antibodies were performed for longer times (overnight and 4h for the primary and secondary antibody, respectively) and at 4°C rather than at room temperature (Figure 2.6b). As shown by the CL profiles (Figure 2.6c), in such incubation conditions the CL signal from the tempera layer increased while the background was much less affected, thus resulting in a higher signal/background ratio. We also investigated the effect of different incubation times with the blocking agent, but no significant improvement was obtained with incubations longer than 1h (data not shown). Thus, it appeared that a 1h-incubation at room temperature with a 5% solution of non-fat dried milk was sufficient to saturate the non-specific binding sites of the sample.

2.6.2.2 Assay selectivity

The selectivity of the assay was assessed by performing the immunolocalisation of ovalbumin in standard samples with a layer of whole egg tempera either with or without the primary antibody. When the assay

was performed using the anti-ovalbumin antibody, a sharp, intense CL signal was obtained in the correspondence of the tempera layer (Figure 2.7a) while, in absence of the antibody, such CL signal was not detected (Figure 2.7b). Nevertheless, a much weaker emission (whose intensity was about 20 times lower than that of the ovalbumin-specific CL signal) was still observed in the whole cross-section (Figure 2.7c), which could be attributed to the non-selective binding of the secondary antibody. As expected, no specific CL signals were also observed in cross-sections of standard samples obtained using other organic binding media (fish glue, oil).

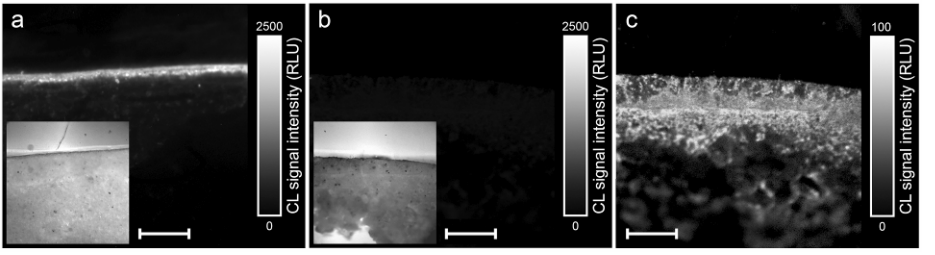

Figure 2.7 - Chemiluminescence images obtained for the immunolocalisation of ovalbumin in cross-sections of standard samples with a layer of whole egg tempera performed either with (a) or without (b) the primary antibody. The CL images in panels (a) and (b) are shown using the same greyscale, corresponding to the different CL intensities. The CL image obtained without the primary antibody is also shown in panel (c) using a different greyscale to highlight the weak CL signal due to the non-specific adsorption of the secondary antibody (insets: live images of the samples). Bars represent 200 µm.

The spatial association of the CL signal with the binding medium was also clearly demonstrated by the results obtained in standard samples with a layer of tempera containing the smalt pigment (Figure 2.8c, d). In such samples, the relatively large size of the pigment particles allowed to confirm the

localisation of the CL signal only in the correspondence of the binding medium.

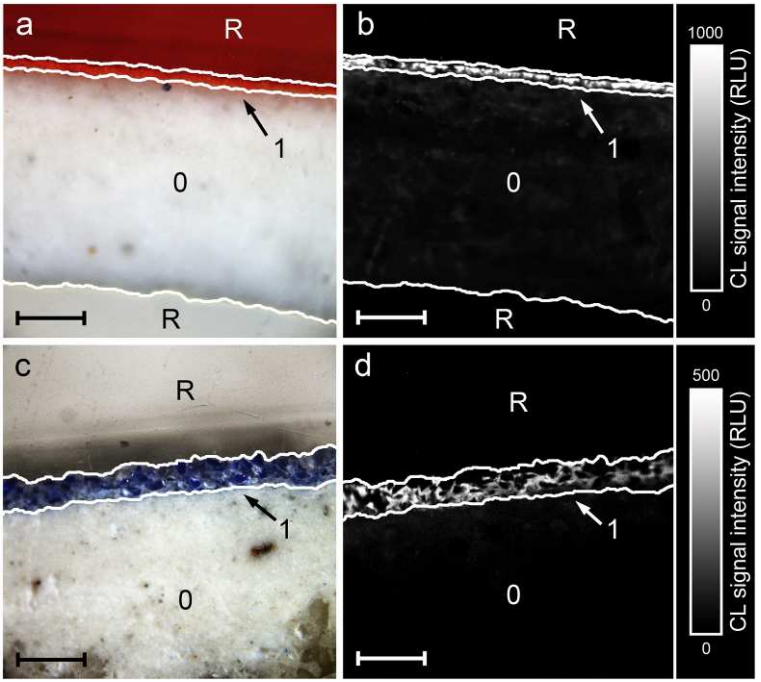

Figure 2.8 - Chemiluminescence immunolocalisation of ovalbumin in cross-sections of standard samples with a layer of whole egg tempera containing cinnabar (top) or smalt (bottom) pigments. Panels (a) and (c) show the live images of the cross-sections, panels (b) and (d) show the CL images, confirming the localisation of the CL signal in the egg tempera layer and in the correspondence of the binding medium. The different parts of the cross sections are indicated (R = resin, 0 = ground layer, 1 = egg tempera layer with pigments). Bars represent 200 µm.

2.6.2.3 Effect of pigments

To assess the suitability of the assay for the localisation of ovalbumin in real paint cross-sections, the possible interferences due to painting pigments were investigated. Indeed, several metal ions contained in pigments, especially the Co^{2+}, Cu^{2+}, Fe^{3+}, Mn^{2+}, and Pb^{2+} ions, are known inhibitors of HRP [27]. Thus, release of such ions during the CL detection step could affect the enzyme

activity, leading to enzyme inhibition and weak – or even absent – CL signal. In addition, metal ions can also directly influence the CL luminol reaction, either by acting as catalysts (the Co^{2+} ion is the most sensitive catalyst for the luminol-H_2O_2 reaction [28]) or inhibiting the CL process (for example, the Cu^{2+} ion [29]). In order to study such interferences we analysed standard samples of whole egg tempera containing different common inorganic pigments (smalt, azurite, malachite, hematite, cinnabar, and minium). The cross-sections either following the protocol described above were analysed to assess negative effects on the HRP enzyme activity and/or the CL process or by omitting the secondary antibody to detect possible catalysis of the CL oxidation of luminol. The experiments performed in the absence of the immunoreagents did not show any catalysis of the CL reaction, and for all the pigments the CL emission from the tempera layer was observable, even though the CL signal was significantly weaker for the hematite-containing samples. The absence of detectable effects for the other pigments containing metal ions known to affect the CL reaction (e.g., the Co^{2+} ion) was attributed to a low release of metal ions in the solution or, possibly, to the loss of the soluble metal ion fraction during the sample processing steps prior to the measurement. Further experiments other inorganic and organic pigments of historical interest are planned, also performing investigations on artificially aged samples to assess the effect of degradation processes.

2.6.2.4 Case study

The CL method for the immunolocalisation of ovalbumin was applied to cross-sections of samples taken from a wood painting by Baldassarre Carrari (c. 1450 – c. 1510), an Italian painter of the Renaissance period, active mainly in Ravenna. The CL images obtained for such samples (Figure 2.9a) showed a strong emission indicating the presence of ovalbumin in the most upper layer of the painting, even though such layer appeared discontinuous. This result

was confirmed by IR reflectance spectroscopy and by the observation of the sample fluorescence under UV excitation. In fact, the IR reflectance spectra of the cross-section (Figure 9b) showed absorptions at 1655 and 1545 cm^{-1} in the upper painting layer, which can be assigned to the protein amide I (C=O stretching) and amide II (NH bending) bands. In addition, a bluish fluorescence emission under UV excitation (typical of proteins) with a spatial distribution strongly resembling that of the CL signal was observed in the top layer of the painting (Figure 2.9c). Therefore, all the experimental findings suggested the presence of a proteinaceous material in the most upper painting layer, but only the CL immunolocalisation method gave information on its nature, allowing us to hypothesise the use of an egg-based varnish.

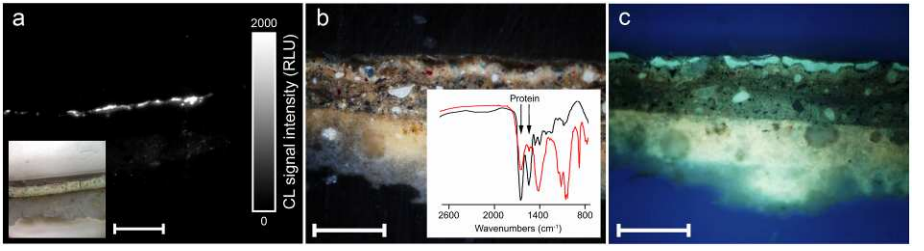

Figure 2.9 - Localisation of organic components in cross-sections of samples from the wood painting of Nicolò Rondinelli. (**a**) Chemiluminescence image of a cross-section showing the localisation of the CL signal in the upper painting layer (inset: live image of the sample); (**b**) live image of another cross-section from the same portion of the painting and (in the inset) comparison between the IR reflectance spectrum measured in the correspondence of the upper painting layer (red) and a reference IR spectrum obtained from an aged egg white sample (black); (**c**) fluorescence image of the same cross-section under UV irradiation. Bars represent 200 µm.

2.7 DEVELOPMENT OF A NEW MULTIPLEXED CHEMILUMINESCENT IMAGING TECHNIQUE FOR THE SIMULTANEOUS LOCALISATION OF DIFFERENT PROTEINS IN PAINT CROSS-SECTIONS

On the basis on the promising results obtained in the previously presented work, new immunochemical approaches to the localisation of common proteinaceous painting materials have been investigated.

Consequently, the research have been aimed at the development of a CL immunolocalisation protocol for the simultaneous detection of ovalbumin and bovine casein (two protein binders widely employed in ancient paintings) in the same sample. Following an approach already used in multiplexed immunoassays [30], primary anti-ovalbumin and anti-casein antibodies, each of them detected by a specific secondary enzyme-labelled antibody have been employed. Use of different enzyme labels - HRP and alkaline phosphatase (AP) - for the secondary antibodies allowed the separate localisation of each target protein by adding the proper CL enzyme substrate.

2.7.1 MATERIALS AND METHODS

2.7.1.1 Reagents

Monoclonal mouse anti-ovalbumin antibody (raised against purified chicken egg albumin), HRP-conjugated polyclonal goat anti-mouse antibody,

polyclonal rabbit anti-bovine casein antibody (raised against purified bovine casein isolated from milk), AP-conjugated polyclonal goat anti-rabbit antibody, ovalbumin, bovine casein, bovine serum albumin (BSA), and gelatin (type A, from porcine skin) were purchased from Sigma-Aldrich Co. (St. Louis, MO). Soybean milk (total protein content: 3.5%) was purchased in a local drugstore. The luminol-based HRP CL detection reagent Westar Supernova and the acridan-based AP CL substrate Lumigen APS-5 were obtained from Cyanagen (Bologna, Italy) and Lumigen, Inc. (Southfield, MI), respectively. Polyester resin (Inplex) for sample embedding was purchased from Remet (Bologna, Italy). Gypsum ($CaSO_4 \cdot 2H_2O$) and rabbit glue for the preparation layer of the mock ups were from Zecchi (Florence, Italy) and Phase (Bologna, Italy), respectively. Blue smalt (ground glass colored with cobalt(II) salts), azurite ($Cu_3(CO_3)_2(OH)_2$), malachite ($Cu_2CO_3(OH)_2$), hematite (Fe_2O_3), cinnabar (HgS), and minium (Pb_3O_4) pigments were obtained from Zecchi (Florence, Italy). All the other chemicals used were of analytical grade. The Protran® nitrocellulose membrane used for preliminary measurements was obtained from Whatman, Maidstone, England.

2.7.1.2 Instrumentation

The description of the home-made CL imaging system and the optical microscope employed are previously reported.

2.7.1.3 Standard samples

Standard samples were obtained from mock ups prepared according to ancient painting techniques [25]. The preparation layer of the mock ups was made by a mixture of rabbit glue (5 g, previously melted in 50 mL of water) and gypsum (12 g). Egg-tempera was obtained using a mixture of egg white, yolk and water in a 1:1:1 (v/v) ratio, while milk-tempera was prepared using

commercial whole milk. For the preparation of painting layers containing pigments, the relative ratio between pigments and binding medium was changed on basis of the grinding size and the chemical composition of the pigment as previously reported, in order to obtain homogenous mixtures suitable for application as thin layers.
The sample preparation followed the above described procedure.

2.7.1.4 Experimental procedure

The spatial distribution of ovalbumin and bovine casein in the resin-embedded painting cross-sections was determined using non-competitive sandwich-type immunoassays with CL imaging detection. Embedded samples were incubated for 1 h at room temperature under stirring with the aspecific binding blocking solution (soybean milk added with BSA to achieve a 5% total protein concentration) and washed three times with TRIS/BSA (0.1 M Tris-HCl buffer, pH = 7.4, containing 1% of BSA). Subsequently, the cross-sections were incubated with a mixture of preformed antibody complexes for the CL detection of the two target proteins. Preformed antibody complexes were obtained in TRIS/BSA by mixing primary and secondary antibodies for each analyte (anti-ovalbumin mouse antibody/HRP-labelled goat anti-mouse antibody for the detection of ovalbumin and anti-casein rabbit antibody/AP-labelled anti-rabbit goat antibody for the detection of bovine casein). After a 15 min-incubation at room temperature, the resulting solutions were mixed and used for the incubation of the cross-sections. Antibody dilutions (v/v) in the final solution were: 1:8,000 (anti-ovalbumin mouse antibody), 1:1,000 (HRP-labeled goat anti-mouse antibody), 1:4,000 (anti-casein rabbit antibody), and 1:2,000 (AP-labeled anti-rabbit goat antibody). The incubation was carried out under gentle stirring for 1 h at room temperature. Then, the samples were washed five times with TRIS/BSA and the CL signals from the enzyme-labeled secondary antibodies were sequentially detected by CL

microscope imaging. First, the CL detection of HRP was performed by covering the cross-sections with the HRP CL substrate and acquiring the CL images (10X objective magnification) using an integration time of 60 s. Afterwards, the samples were washed with TRIS/BSA to remove the HRP CL substrate and the CL detection of AP was performed with a procedure similar to that described above and using an integration time of 300 s. To perform the localisation of the two target proteins in the same areas of the cross-sections, the microscope stage system was used to achieve reproducible positioning of the samples. For each CL image, a live image of the cross-section was also acquired. Finally, superimposition of the live images of the cross-sections and the CL images corresponding to the different CL signals was used to assess the localisation of the CL signals, hence of the target proteins, on the cross-sections.

2.7.2 RESULTS AND DISCUSSION

2.7.2.1 Optimisation of the experimental procedure

The simultaneous immunolocalisation of ovalbumin and bovine casein in painting cross-sections was performed by using two specific immunoreactions based on a non-competitive assay format. Ovalbumin was detected by a mouse anti-ovalbumin primary antibody, followed by a HRP-conjugated goat anti-mouse secondary antibody, while bovine casein was detected by a rabbit anti-casein primary antibody and an AP-conjugated goat anti-rabbit secondary antibody. After the immunoreactions reached the equilibrium and the excess of immunoreagents was removed by extensive washing steps, the enzyme-labeled secondary antibodies were sequentially revealed by CL by adding the proper CL enzyme substrates (a luminol/enhancer/hydrogen peroxide CL system for HRP and an acridan-based CL substrate for AP). By exploiting the

selectivity of the antigen-antibody and the enzyme-catalysed CL reactions, selective localisation of the two target proteins could be achieved by microscope CL imaging on the micrometer scale.

The preliminary optimisation of the CL immunolocalisation procedures was firstly carried out by experiments performed on target proteins spotted on nitrocellulose membrane. For the optimal performance of the immunoassays, an excess of both the primary and the secondary antibodies is required to bind all the target protein molecules in the sample and to reveal all the target-bound primary antibody, respectively. Nevertheless, a high excess of the immunoreagents should be avoided because it would increase the amount of non-selectivity binding to the cross-section, thus giving stronger background CL signals. In the first step, the optimisation of the experimental conditions was separately performed for each immunoassay. To identify the antibody concentrations giving the highest detectability of the target proteins, various protein amounts (ranging from 0.1 to 100 ng/spot) were spotted on nitrocellulose membrane and revealed by CL imaging using different dilutions of the appropriate antibodies. Differently from the study previously presented, instead of performing sequential incubations of the membranes with primary and secondary antibodies, a single incubation with a preformed complex between the primary and the secondary antibody (obtained by mixing appropriate dilutions of the antibodies before use) was employed. This allowed to shorten the analysis time because only two incubation steps (i.e., saturation of the cross-section with the blocking agent and incubation with the antibody complex) were necessary. The best analytical performance in terms of target protein detectability were obtained with preformed antibody complexes made by mixing the primary and secondary antibodies at the following final dilution factors (v/v): 1:8,000 (primary antibody) and 1:1,000 (HRP-labelled secondary antibody) for ovalbumin, and 1:4,000 (primary antibody) and 1:2,000 (AP-labelled secondary antibody) for bovine casein.

Figure 2.10a shows the CL images obtained for the different proteins spotted on nitrocellulose membrane in the optimised experimental conditions. According to these data, calibration curves were obtained for the two proteins (Figure 2.10b) and the detection limits of the assays, estimated as the amount of protein giving a CL signal corresponding to the background signal plus three times its standard deviation, were estimated. The limits of detection were 0.3 and 0.8 ng/spot (corresponding to about 0.05 and 0.12 ng/mm^{-2} of protein) for ovalbumin and bovine casein, respectively. These values were of the same order of magnitude of the detection limit previously reported for the CL immunolocalisation of ovalbumin, therefore suggesting that both the immunolocalisation procedures were sufficiently sensitive for the localisation of the target proteins in cross-sections of painting samples obtained with conventional sampling procedures. According to the data shown in Figure 2.10b and 2.10d, the CL signals measured for bovine casein were significantly lower than those obtained for ovalbumin. This was presumably related to an intrinsic lower CL emission of the AP-catalysed reaction in comparison to the HRP-catalysed one and/or to a lower binding efficiency of the anti-bovine casein primary antibody and the AP-labelled secondary antibody for their respective targets. Nevertheless, the background CL signal of the AP-catalysed reaction was also weaker, therefore the detectability of bovine casein remained similar to that of ovalbumin.

2.7.2.2 Chemiluminescent multiplexed immunolocalisation

After the separate optimisation of each immunoassay, the multiplexed immunolocalisation procedure was performed on nitrocellulose membrane containing spots of both bovine casein and ovalbumin target proteins. The membranes were incubated with a mixed immunoreagent containing both primary and enzyme-labeled secondary antibodies at the optimal concentrations reported above, then the target proteins were detected by CL

imaging upon sequential addition of the HRP and AP CL enzyme substrates. The order of detection was chosen on the basis of the kinetics of the CL reactions. The HRP-catalysed CL reaction is faster than the AP-catalysed one (the maximum emission of the HRP-catalysed CL reaction is reached after a few minutes upon addition of the CL substrate), thus this order of addition of the CL enzyme substrates minimises the possibility that a residual emission due to the first CL reaction, even after a thorough rinsing to eliminate the HRP CL substrate, might interfere in the subsequent CL immunolocalisation of bovine casein. Figure 2.10c shows the CL images of a nitrocellulose membrane with ovalbumin and bovine casein spots after addition of the CL substrates for HRP and AP.

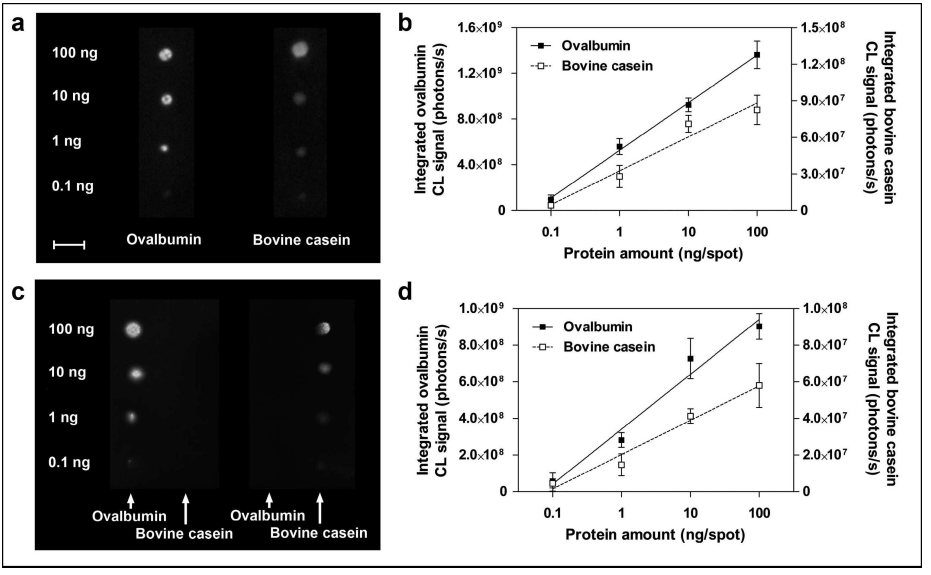

Figure 2.10 - Chemiluminescent immunolocalization of ovalbumin and bovine casein on nitrocellulose membranes. Panel (a): CL images of nitrocellulose membranes with different amounts (0.1-100 ng/spot) of ovalbumin (left) and bovine casein (right) obtained in the optimized experimental conditions with the separate immunolocalization procedures; panel (b): calibration curves for the separate immunolocalization of ovalbumin and bovine casein; panel (c): CL images of a nitrocellulose membrane with different amounts (0.1-100 ng/spot) of ovalbumin and

bovine casein obtained with the multiplexed immunolocalization procedure and measured upon addition of the CL substrates for HRP (left) and AP (right); panel (d): calibration curves for the multiplexed immunolocalization of ovalbumin and bovine casein. Measures were performed in triplicate. Bar represents 5 mm

Only the spots of the specific target protein were detectable upon addition of each CL substrate, thus confirming the possibility to perform a selective localisation of the proteins. The calibration curves for the two proteins (Figure 2.10d) were quite similar to those obtained for the separate CL immunolocalisation procedures, and the limits of detection of the multiplexed immunolocalisation assay were about 0.3 and 1.0 ng/spot for ovalbumin and bovine casein, respectively, thus proving that the analytical performance of the single immunoassays were maintained in the multiplexed assay.

As reported, any cross-reaction between the different specific antibodies in the simultaneous detection of bovine casein and ovalbumin spotted on nitrocellulose membrane have been observed. In addition, no selective CL signals were observed in cross-sections of standard samples containing other organic painting components (i.e., rabbit glue and oil). The selectivity of the immunolocalisation procedure was further confirmed by the localisation of the CL signals in the proper tempera layer of single- and multi-layer standard samples containing ovalbumin and/or bovine casein (Figure 2.11).

A critical step in the development of CL immunolocalisation procedures applied to painting cross-sections is the reduction of the non-selective adsorption of the immunoreagents on the porous sample surface, which causes poor repeatability and increases the background CL signal. Different blocking agents were evaluated to replace dried bovine milk, which was previously used to suppress non-selective adsorption. The evaluation of the blocking agents was carried out on nitrocellulose membranes for both immunoassays, to find the most suitable agent to be employed in the

multiplexed immunolocalisation assay. Among the different blocking agents evaluated (BSA, soybean milk, and gelatine at different concentrations) the highest CL signal/background ratios were obtained by employing soybean milk added with BSA to achieve a 5% (w/v) total protein concentration. The more efficient suppression of the non-selective adsorption obtained using soybean milk in the blocking solution could be ascribed to the presence of a mixture of different non-animal proteins, which could reduce possible cross-reactions with the immunoreagents.

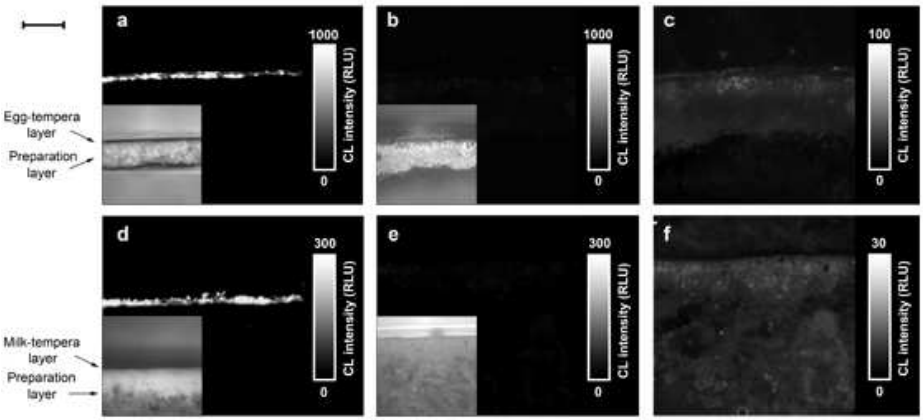

Figure 2.11 - Chemiluminescence images obtained for the immunolocalization of ovalbumin and bovine casein in cross-sections of single-layer standard samples with egg- (top) and milk-tempera (bottom). The CL images shown in panels (a) and (d) were obtained by processing the samples with the complete immunolocalization protocol, while the CL images shown in panels (b) and (e) were acquired without the primary antibodies. The latter images are also shown using a different grayscale in panels (c) and (f), in order to highlight the weak CL signal due to the aspecific adsorption of the immunoreagents on the cross-sections (insets: live images of the cross-sections). All images were acquired using a 10X objective magnification. Bar represents 200 μm.

Inorganic pigments commonly used in paintings may interfere with the enzyme-catalysed CL reaction by acting as enzyme inhibitors or activators, or could catalyse the oxidation or decomposition processes of the CL substrates

leading to light emission. It has been previously demonstrated that pigments such as blue smalt, azurite, malachite, hematite, cinnabar, and minium do not interfere in the HRP-catalysed CL reaction or, at least, their interference does not hamper the observation of the CL signal due to the presence of ovalbumin. In this work, the study of the interferences due to inorganic pigments has been extended to the AP-catalysed CL reaction used for the immunolocalisation of bovine casein. Inhibition of AP due to various metal ions has been already reported [31]. In particular, the strongest enzyme inhibitor was the Be^{2+} ion (enzyme inhibition was higher than 50% in the presence of 5 □mol L^{-1} Be^{2+}) while other metals (Co^{2+}, Ni^{2+}, Cd^{2+}, Cr^{3+}, $A1^{3+}$, Fe^{3+}, Mn^{2+}, and Sn^{2+}) were less efficient inhibitors and significantly affected the enzyme activity only at concentrations greater than 20-100 □mol L^{-1}. To evaluate the inhibition of the CL reaction due to inorganic pigments the CL immunolocalisation of bovine casein in cross-sections of single-layer standard samples with milk-tempera containing inorganic pigments were performed. In addition, to investigate possible catalytic effects of the pigments on the CL substrates (potentially leading to false positives) the CL signal of the cross-sections upon addition of the AP CL substrate alone was acquired and measured. As previously found for the HRP-catalysed reaction, the experiments performed in the absence of the immunoreagents did not show any catalysis of the CL reaction, and for all the pigments the CL emission from the milk-tempera painting layer could still be observed (see, for example, Figure 3 for blue smalt pigment). The apparent absence of AP inhibition for hematite and blue smalt pigments (containing Fe^{3+} and Co^{2+} ions, respectively) can be explained considering that the release of metal ions from those insoluble inorganic pigments is too slow to achieve the metal ion concentrations required to obtain enzyme inhibition. It should be also noticed that alkaline phosphatases from different sources showed different sensitivity to metal ions, and sometimes enzyme inhibition was only observed for AP

from certain sources [31]. Therefore, the findings reported in the literature may be not necessarily valid for the AP enzyme used as label in the secondary antibody.

2.7.2.3 Imaging of standard samples

Microscope CL imaging was performed on cross-sections of single-layer painting standard samples obtained from the mock ups prepared in our laboratory with a layer of egg- or milk-tempera. Using such samples, the performance of the CL immunolocalisation procedure was evaluated and the effectiveness of the blocking agent in reducing the non-selective adsorption of the immunoreagents on the porous painting layers was assessed. As found in the previous work, the incubation times and temperatures and the sample preparation procedures were crucial in the control of the non-selective adsorption. Differently from the previously published procedure, incubations of the cross-sections with the blocking agent and the preformed immunocomplexes were performed in stirred solution, allowing a further reduction of the overall analysis time by shortening the incubation steps. Indeed, instead of the long incubations used in the previously published assay (4-hours and overnight incubations with the primary and secondary antibodies, respectively), a 1-hour incubation at room temperature with the preformed immunocomplexes were suitable for performing the assay avoiding a significant non-selective adsorption of the immunoreagents to the cross-sections. Figure 2.11 showed the CL images obtained for the immunolocalisation of ovalbumin and bovine casein in cross-sections of single-layer standard samples with layers of egg- or milk-tempera. The sharp localisation of the CL signals in the correspondence of the tempera layers, as well the absence of significant CL signals in cross-sections processed without the primary anti-ovalbumin and anti-casein antibodies confirmed the selectivity of the immunolocalisation procedure, as well as the efficient

suppression of the non-selective adsorption of the immunoreagents. Moreover, according to the CL images, the spatial resolution achieved was adequate to perform the localisation of the target protein within the single painting layers, whose thickness is of the order of 5–50 µm.

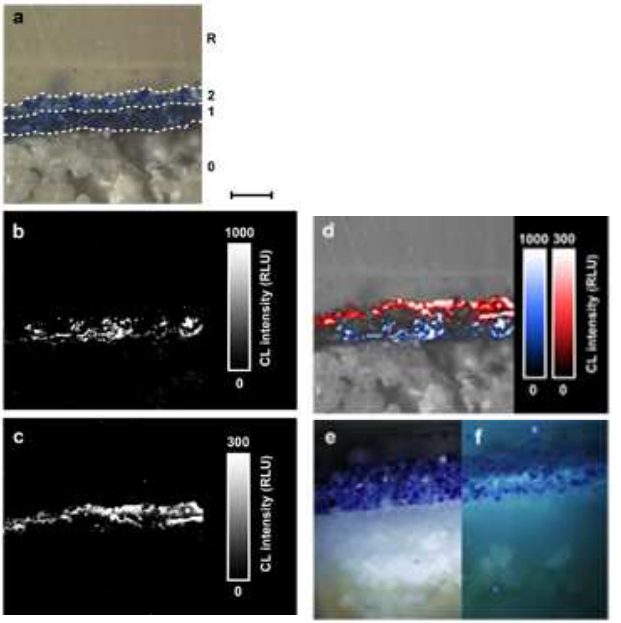

Figura 2.12 - Chemiluminescence immunocolocalization of ovalbumin and bovine casein in cross-sections of standard samples with layers of milk- and egg-tempera with smalt pigment. Panel (a) shows the live image of the cross-section; panels (b) and (c) show the CL signals corresponding to the CL immunolocalization of ovalbumin and casein, respectively; panel (d) shows the overlay of the live image of the cross-section and the pseudocolored CL images (CL signals corresponding to ovalbumin and bovine casein are displayed in shades of red and blue, respectively); panels (e) and (f) show the live image and the visible fluorescence image of the cross-section under UV excitation at 313 nm, respectively. The different parts of the cross-section are indicated (R = resin, 0 = preparation layer, 1 = egg-tempera layer with smalt pigment, 2 = milk-tempera layer with smalt pigment). All images were acquired using a 10X objective magnification. Bar represents 200 µm.

To demonstrate the suitability of the multiplexed CL assay for the simultaneous localisation of bovine casein and ovalbumin, the procedure was

applied to cross-sections of multilayer standard samples with layers of milk- and egg-tempera containing blue smalt pigment (Figure 2.12). Even though the two different tempera layers contain the same pigment, they can be easily discriminated in the visible fluorescence image of the cross-section under UV irradiation at 313 nm (Figure 2.12e and 2.12f) due to the stronger fluorescence emission of the egg-tempera layer. The overlay (Figure 2.12d) between the pseudocolored CL images corresponding to the localisation of the different proteins (also shown in greyscale in Figure 2.12b and 2.12c) and the live image of the cross-sections clearly demonstrated that each CL signal is produced only in the painting layer containing the proper target protein, thus confirming the validity of the immunocolocalisation CL assay.

2.8 FURTHER RESEARCH PERSPECTIVES: μFTIR MAPPING FOR THE DETECTION OF METAL CARBONYL DENDRIMER LABELED ANTIBODIES

Thanks to the high selectivity of antigen-antibody reactions, the potentialities of immunological techniques have been combined with different detection approaches, in order to design a suitable system for the characterisation of proteins in paint cross-sections.

Several detection procedures can be applied for the recognition of antibodies and immuno-complexes using specific labels, which can be revealed by adequate analytical techniques.
In particular, enzyme-conjugated secondary antibodies allow to obtain high sensitivity, thanks to the enzyme activity. The action of the enzyme is to kinetically promote the formation of reaction products when a substrate is added to the sample. The molecules which are generated have specific properties which allow their signal to be detected by microscopy.
As already reported, chemiluminescence detection is widely used in analytical issues, and CL imaging has already proved to be more sensitive than colorimetric – enzyme-mediated – detection techniques, allowing the localisation of target molecules in cells and tissues with a good spatial resolution and a feasible quantitative evaluation of the signal. More interestingly, due to the absence of an excitation source, CL imaging detection is not affected by interferences due to the autofluorescence of the sample components.

Concerning the immunological approach for the localisation of a protein in a paint stratigraphy, some of the applications reported were based on the deployment of immunofluorescence (IFM) for the recognition of different proteinaceous binders [32].
In the IFM technique, the antigen is detected by coupling the secondary antibody with a fluorescent marker that – by external excitation – emits fluorescence in the visible or near-infrared spectral regions. The acquisition of immunofluorescence images of the sample by means of a fluorescence microscope allows identifying and localising the target antigen. The fluorochromes most commonly used for IFM are fluorescein isothiocyanate (FITC), which has a green emission (515 – 530 nm) when excited with the blue light (490-495 nm), or tetramethyl rhodamine isothiocyanate (TRITC), which emits a red signal (615-630 nm) when excited with a green light (525-540 nm). Significant interferences were observed due to sample fluorescence. In fact, painting materials can show an intense autofluorescence due to the presence of pigments and/or binding media, which could hamper the use of immunofluorescence techniques. In attempt to overcome this shortcoming, different analytical procedures and strategies have been developed for IFM application. In particular, in confocal microscopy, sample fluorescence is excited by a monochromatic laser source eliminating the problem of filtering the incident light and an effective suppression of scattering phenomena is obtained.

In this research, alternative detection system were investigated in order to combine different imaging techniques, providing a wide collection of information on the same sample stratigraphy.
Starting from the advantages offered by μFTIR techniques in studies on paint layers, related to the acquisition of information for both inorganic and organic materials, a new immuno-detection approach has been proposed.

Indeed, the attention has been initially focused on the selection of suitable labeled-secondary antibody for the infrared microscopy detection.
Thanks to the collaboration with the France National Research Center (CNRS, Chimie ParisTech – *Ecole Nationale Supérieure de Chimie de Paris (ENSCP), Laboratoire de Chimie et Biochimie des Complexes Moleculaires),* the application of a poly(amidoamine) (PAMAM) dendrimers carrying (η^5-cyclopentadienyl) iron dicarbonyl succinimidato complexes as infrared probes for carbonyl metallo-immunoassay have been investigated.

Dendrimers play a crucial role in the field of bioconiugation. In fact, thanks to their properties, such as water solubility, lack of immunogenicity, availability in different sizes (generations) [33], they represent a suitable platform for the construction of complex labeled-antibodies. Moreover, the possibility to introduce a high number of active compounds on the antibody molecule, allows a signal enhancement in immunoassay and the amplification of the IR signal in carbonyl metallo-immunoassay.
The introduction of transition metal carbonyl complexes using amino-terminated PAMAM dedrimers as labels allowed the introduction of new detection reagents.
In particular, the (η^5-cyclopentadienyl) iron dicarbonyl succinimidato complex (Fp) presents a specific signal generated by the transitional metal carbonyl vibration bands in the mid-infrared region, related to the stretching of C=O. This allows the selective recognition of the IR markers and their quantification by measuring the height of the ν_{CO} bands. In fact, the intensity of the bands depends on the number of organometallic Fp labels present.
Recently, the optimisation of the bio-conjugation condition allowed to obtain PAMAM dendrimers carrying 20 to 30 Fp complexes, providing a more efficient infrared detection of the amplified signal [33].

The present research work was addressed to the evaluation of the Fp-labeled antibody immunoreactivity in the identification of ovalbumin in standard paint cross-sections.

2.8.1 METHODS AND MATERIALS

2.8.1.1 Reagents and samples

Anti-chicken egg albumin antibody (whole antiserum, produced in rabbit) purchased from Sigma-Aldrich Co. (St. Louis, MO).

The Fp-labeled anti-rabbit IgG antibody (produced in goat), was provided by the CNRS of Paris.

Details are reported in Table 2.1

Antibody	**[IgG]**	**Label**
F10-264-1	5.85 mg/mL	29 Fp complexes /IgG
F10-186-1	3.23 mg/mL	36 Fp complexes /IgG

Table 2.1 - Fp-labeled anti-rabbit IgG antibody

Standard samples were obtained from mock-ups prepared in laboratory by application of a layer of whole egg, prepared according to the ancient painting receipts. Namely, a mixture of egg white, yolk and water in a 1:1:1 (v/v) ratio, was applied on a preparation layer made of gypsum (obtained from Zecchi) and rabbit glue (purchased from Phase, Bologna, Italy).

2.8.1.2 Instrumentation

The sample cross-sections were primarily documented by means of an optical microscopy. Visible and fluorescence images under UV excitation at 313 nm

were acquired by a BX 51M optical microscope (Olympus Optical) connected to a DP70 digital camera (Olympus).

A Thermo Nicolet (Thermo Fisher Scientific, Waltham, MA, USA), iN™10MX imaging microscope, fitted with a mercury-cadmium-telluride (MCT) detector cooled by liquid nitrogen, was used for mapping analysis. The measurements were performed in RAS and ATR modes (using a slide-on ATR objective, equipped with a conical germanium crystal), in the range 4,000–675 cm^{-1}, at a spectral resolution of 4 cm^{-1}.

2.8.1.3 Experimental procedure

Sample cross-sections were treated for 15 min at room temperature with the blocking solution (5% dried milk in water) then, after washing (3X) with PBS (10 mM phosphate buffer saline, pH = 7.3), they were incubated overnight at 4°C with the anti-chicken egg albumin antibody (primary antibody) diluted 1:500 (v/v) in PBS. Afterwards, the samples were washed (5X) with PBS/milk and incubated for 4h at room temperature with the Fp-labeled anti-rabbit IgG antibody (secondary antibody) diluted 1:10 (v/v) in PBS. Samples were washed again (3X) with PBS and air dried before to be submitted to the ATR-FTIR analysis.

2.8.2 PRELIMINARY RESULTS

First characterization of Fp-labeled anti-rabbit IgG antibody solutions were carried out by RAS measurements. Aliquots (1 µL) of antibody suspensions were applied on a gold mirror and µFTIR spectra were recorded in the reflection-absorption (RAS) mode. In the recorded spectra acquired from both the available antibodies, it was possible to identify two absorption bands

at 1,998 and 2,050 cm^{-1} related to the ν_{CO} of the metal carbonyl in Fp complexes (Figure 2.13).

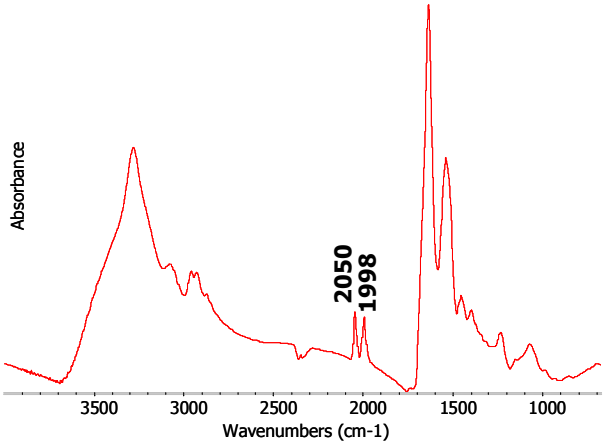

Figure 2.13 – μFTIR RAS spectrum of sample F10-264-1

Due to the complexity of the painting matrix and to its heterogeneity, and in attempt to evaluate the behavior of reagents in FTIR analysis, preliminary investigation were carried out on a number of exemplified standard samples, made by the use of the single layer containing the target protein, without pigments.

After the acquisition of the ATR spectra, chemical maps were elaborated plotting the marker band at 2,050 cm^{-1} in order to verify the Fp-labeled antibody location. The results reveal the presence of the selected peak in correspondence to the whole egg layer (Figure 2.14), which are detectable thanks to the peak at 1,540 (amide II)

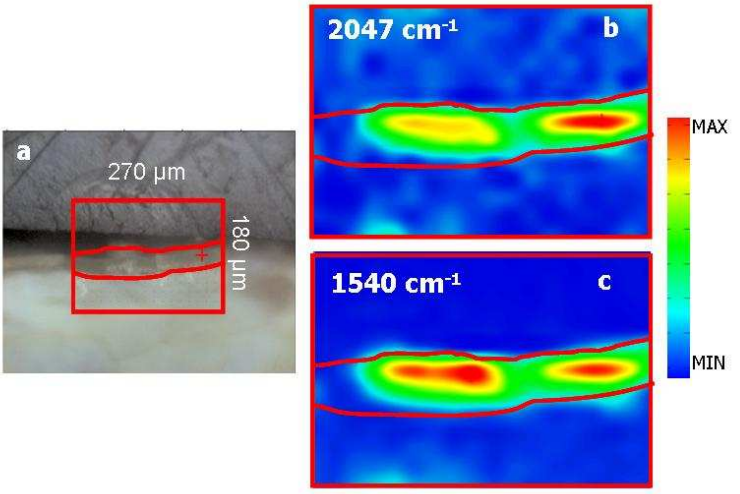

Figure 2.14 – Cross-section of standard sample with a layer of whole egg submitted to the ATR analysis: a) visible microphotographs of the sample under visible light; FTIR false-colour plot representing: b) peak height profile: 2,050 cm^{-1} (Fp-labeled antibody); c) peak height profile: 1,540 cm^{-1} (protein)

2.8.3 FURTHER PERSPECTIVES

The research presented has supplied promising results, particularly with respect to the new detection system proposed for the identification of proteins in paint cross-section, providing a complete characterisation of the sample startigraphy. In fact, the combination of these two analytical approach allows to achieve information regarding both the organic and inorganic materials, on the bases of their absorption bands and, at the same time, to perform a highly selective analysis for the recognition of proteins.

Further researches will be focused on a better evaluation of the approach and of its sensitivity in the identification of proteins in complex samples, presenting complex mixtures of egg (as binding medium) with inorganic pigments, as well as in aged samples.

2.9 CONCLUSIONS

The developed CL immunolocalisation procedure allowed to detect and localise ovalbumin in aged painting cross-sections with a spatial resolution of the order of micrometers (i.e., within the single painting layers) and with little or no interference from several common pigments used in paintings. Moreover, it has been demonstrates the possibility to identify two different proteins in the same painting micro cross-section by exploiting the selectivity of immunological reactions combined with the high sensitivity of CL microscope imaging techniques. Spatial resolution of the order of micrometers was achieved, thus allowing localisation of the target proteins within the single painting layers.

The simultaneous identification of different proteins in micro cross-sections is of particular relevance in the field of Cultural Heritage because painting samples are often very small and available in a limited number, therefore the maximum amount of information must be obtained from each sample. The multiplexed immunolocalisation assay described here was developed using ovalbumin and bovine casein as target proteins because they are often present in binding media, as well as in varnishes and restoration products. Nevertheless, this analytical approach could be extended to the detection of other proteinaceous painting components, such as animal collagen. A higher degree of multiplexing (i.e., the simultaneous detection of three or more proteins) could also be achieved by combining CL imaging with other detection techniques (e.g., fluorescence).

This technique could be complementary to the other techniques used for analysis of the organic components of paintings and provide information useful for studying painting techniques and for authentication of artworks (e.g., by allowing determination of the production period and the origin of the

painting materials). Moreover, the possibility to determine the biological source of a given protein (e.g., fish or rabbit glue) would make the immunolocalisation method relevant also for authentication studies, for example by allowing to determine the production period and the origin of the painting materials.

New detection system are under evaluation, to provide a complete characterisation of the sample startigraphy thanks to the combination with different analytical techniques, widely applied in the field of the cultural heritage.

2.10 BIBLIOGRAPHY

1. Liuveras A, Bonaduce I, Andreotti A, Colombini MP (2010) Anal Chem 82:376–386
2. Messerschmidt RG, Harthcock MA (1988) Infrared microspectroscopy. Theory and applications, Dekker, New York
3. Prati S, Joseph E, Sciutto G, Mazzeo R (2010) Acc Chem Res 43:782–791
4. Wild D (2005) *The immunoassay handbook*, 3rd edn. Elsevier, Amsterdam
5. Chu P, Weiss L (2009) *Modern immunohistochemistry*, Cambridge University Press, New York
6. Kockaert L, Gausset P, Dubi-Rucquoy M (1989) Stud Conserv 34:183–188
7. Johnson M, Packard E (1971) Stud Conserv 16:145–164
8. Jones PL (1962) Stud Conserv 7:10–16
9. Heginbotham A, Millay V, Quick M (2006) J Am Inst Conserv 45:89–105

10. Ramirez Barat B, de la Vina S (2001) Stud Conserv 46:282–288
11. Roda A, Pasini P, Musiani M, Girotti S, Baraldini M, Carrea G, Suozzi A (1996) Anal Chem 68:1073–1080
12. Guardigli M, Marangi M, Casanova S, Grigioni WF, Roda E, Roda A (2005) J Histochem Cytochem 53:1451–1457
13. Bonvicini F, Mirasoli M, Gallinella G, Zerbini M, Musiani M, Roda A (2007) Analyst 132:519–523
14. DeLuca, M. A. (1978) In *Methods in Enzymology*; Academic Press: New York, Vol. 57
15. Kricka, L. J.; Stanley, P. E.; Thorpe, G. H. G.; Whitehead, T. P. (1984) *Analytical Applications of Bioluminescence and Chemiluminescence*; Academic Press: London and New York
16. Marzocchi E, Grilli S, Della Ciana L, Prodi L, Mirasoli M, Roda A. (2008) Anal Biochem 377(2):189-94. Epub 2008 Mar 16
17. C. A. Marquette and L. J. Blum (2006) Anal. Bioanal. Chem., 385, 546
18. F. Barni, S. W. Lewis, A. Berti, G. M. Miskelly and G. Lago (2007) Talanta, 2007, 72, 896
19. Ximenes, V. F. Campa, A. Baader, W. J. Catalani, L.H (1999) Anal Chim Acta, 402:99-104
20. Bronstein, I.; Edwards, B.; Voyta, J. C. (1989) J. Biolumin. Chemilumin., *4*, 99-111
21. Beck, S.; Ko¨ster, H. (1990) Anal. Chem. *62*, 2258-2270
22. R. L. Divi, F. A. Beland, P. P. Fu, L. S. Von Tungeln, B. Schoket, J. E. Camara, M. Ghei, N. Rothman, R. Sinha and M. C. Poirier (2002) *Carcinogenesis*, 23, 2043
23. A. Roda, M. Guardigli, E. Michelini, M. Mirasoli and P. Pasini (2003) Anal. Chem., 75, 462
24. Mirasoli, M. *Venturoli*, S. Guardigli, M. Dolci, L. S. Simoni, P. Musiani, M. and A. Roda (2011) in Chemiluminescence and Bioluminescenze

Past, Present and Future, ed. A. Roda, 401-427 Royal Society of Chemistry,

25. Cennini C, Frezzato F (2004) *Il libro dell'arte*. Neri Pozza Ed., Milano
26. Van Loon A, Keune K, Boon J (2005). In: Parisi C, Buzzanca G, Paradisi A (eds) *Proceedings 8th International Conference on Non-Destructive Investigations and Microanalysis for the Diagnostics and Conservation of the Cultural and Environmental Heritage*, 15–19 May 2005, Lecce, Italy. Italian Society of Non-Destructive Testing Monitoring Diagnostics, Rome
27. Zollner H (1999) Handbook of Enzyme Inhibitors, 3rd Ed. Wiley-VCH, Weinheim
28. 29. Price D, Worsfold PJ, Mantoura RFC (1994) Anal Chim Acta 298:121-128
29. Yuan J, Shiller AM (1999) Anal Chem 71:1975-1980
30. Mirasoli M, Guardigli M, Simoni P, Venturoli S, Ambretti S, Musiani M, Roda A (2009) Anal Bioanal Chem 394:981-987
31. Rej R, Bretaudiere J-P (1980) Clin Chem 26:423-428
32. Cartechini L, Vagnini M, Palmieri M, Pitzurra L, Mello T, Mazurek J, Chiari G (2010) Acc Chem Res 43:867-876
33. Fischer-Durand, N. Salmain, M. Rudolf, B. Dai, L. Jugé, L. Guérineau, V. Laprévote, O. Vessières, A. Jaouen, G. (2010) Anal. Biochem. 407:211-219

Chapter 3

NEW ADVANCES IN THE APPLICATION OF FTIR MICROSCOPY AND SPECTROSCOPY

3.1 INFRARED MICROSCOPY APPLIED TO CULTURAL HERITAGE

After the advent of Fourier transform-based IR (FTIR) spectrometers (late in the 1960s, in parallel with the availability of personal computers), these instruments have slowly begun one of the most widely applied tools for the investigation of cultural heritage materials. In fact, given that many of the inorganic and organic artworks constituents show characteristic absorptions in the mid-IR range (4000–600 cm^{-1}) [1, 2] the use of IR spectroscopy for the examination of paintings and artifacts has been mentioned from its early beginning [3].

In particular, the improvement concerning spectral resolution and detection limits obtained with the transition from dispersive IR to FTIR instruments, allowed their widespread use as suitable tools in conservation issues [4], overcoming drawbacks related to dispersive instruments. In fact they were usually slow, quite limited in spectral resolution and sensitivity and difficultly applicable to the characterisation of artworks samples, due to their small dimensions and complexity.

Subsequently, when micro-sampling accessories for FTIR spectroscopy were introduced in the early 1980s, the following development of FTIR microscopy represented a powerful innovation for the micro-destructive analysis of small samples [5]. Moreover, the recent introduction of mapping and imaging

equipments allows to collect a large number of FTIR spectra on a surface, producing a distribution map of the identified compounds.
The primary advantages of the introduction of accessories and new modalities of analysis is ascribable to the absence of requirements for sample manipulation after its removal from the artworks, such as the dispersion in KBr pellets, which requires a large amount of sample. Conversely, with the FTIR microscopy (and its related accessories), the amount of sample necessary is reduced to less than 1 μg. Furthermore, FTIR microscopy has been widely applied for the characterisation of painting materials as one of the few techniques which allow the stratigraphic detection.

A FTIR microscope consists of a FTIR spectrophotometer combined with an optical microscope, which incorporates all-reflecting optics and aspherical surfaces adapted to the infrared radiation for minimising optical aberrations.
The conventional infrared light source (typically a Globar silicon bar heated to 1500 K), which emits radiation from 1.5 μm up to a few tens of micrometers, is directly directed to the microscope rather than to the spectrophotometer sample chamber, without any modification to the interferometer. The user interface for data acquisition and processing is also the same as for conventional FTIR spectroscopy.
The microscope is designed for observation both in transmission and in reflection mode. A system of dichroic mirrors allows the visible light and the IR radiation to pass through the same optical system, permitting to first visually observe the region of interest and then to record the corresponding IR spectra.
The radiation can be focused on small areas, reducing the amount of material necessary for the analysis and allowing different regions of heterogeneous samples – which cannot be physically separated – to be isolated.

Analysis by FTIR spectroscopy and microscopy may be accomplished in several modes, depending on the amount and type (powder or fragment) of the available samples. In order to achieve the largest amount of information, our laboratory has developed an analytical protocol giving priority to sample conservative techniques within the frame of micro-destructive FTIR spectroscopy techniques [6] (Figure 3.1)

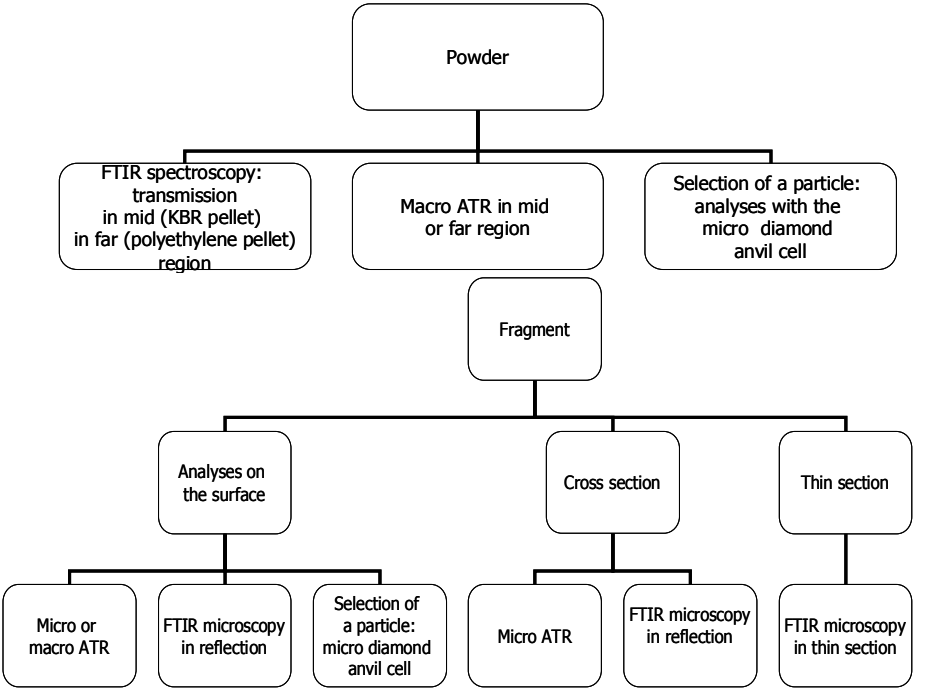

Figure 3.1 - Scheme of the possible analysis in FTIR spectroscopy and microscopy on powder or fragments

In the transmission measurements, the IR beam passing through the sample benefits of a high energy throughput and a resulting high sensitivity. This

explain the large collections of IR transmission spectra produced in the past and their use as reference for comparison with other infrared methods.
The absorption spectra report at each wavelength the absorbance value (A = -log T), which is proportional to both the concentration of the analyte in the sample (c) and the sample thickness (l), (Lambert-Beer's law) in the Equation 3.1 where the extinction coefficient ε·(l·mol^{-1}·cm^{-1}) is a characteristic property of the absorbing material.

$$A=\varepsilon cl = -\log T \qquad (3.1)$$

Transmission analysis is particularly suitable on small particles (sampled from bigger fragments under the stereomicroscope), or on thin film employing IR transparent salt as support (i.e., NaCl window) [7], or using the diamond anvil cell. In the latter case, the particle is placed onto a micro-compression cell made of diamond and pressed in order to squeeze it. The hardness and inertness of diamond allow the analysis of a large variety of samples, including rubbery or reactive ones, without any contamination. The IR spectrum of diamond presents absorption bands between 2500 and 1800 cm^{-1}, a spectral region relatively free from the common characteristic absorption of organic compounds. Moreover, the diamond anvil cell is a simple device that can be placed directly on the stage of a FTIR microscope and, for this reason, it is widely employed to analyse paintings or archaeological materials. It is particularly useful for the analysis of single organic colorants particles, especially when they are mixed with strongly absorbent inorganic salts and organic binders to reduce influence by other components [8].
Recently, the diamond anvil cell has also been proposed for the study of multilayered samples [9]. After careful positioning on a diamond window

followed by compression, the sample stratigraphy can be preserved with only an expansion of each individual layers.

Transmission measurements can be also performed on thin sections obtained after polishing or microtoming an embedded cross section. In order to obtain high-quality spectra, their thickness should be below 15 μm. Thin sections generally prepared by polishing for petrographic studies cannot be used for FTIR spectroscopy since these sections are fixed on a glass slide with glue, which have strong absorbance bands in the mid-IR region. Some soluble adhesives are available but they require for their removal the use of solvents, which are incompatible with the need of avoiding any interaction with the unknown sample. Even though procedures based on microtomy have been proposed as standard methods [1], the possible presence of materials with different hardness may produce an easy deformation of the section, with subsequent particle loss and curling. Alternative methods, i.e., using IR-transparent salts such as silver chloride (AgCl) or potassium bromide (KBr) [10-12], still have some limitations, such as darkening or accelerated corrosion for AgCl.

Reflection methods can be applied for the analysis of either the sample surface or its cross section and they can also be performed directly on the surface of an object without any sample removal and, thus, they have been widely applied on a large variety of materials. If the object is small enough, it can be placed directly on the microscope stage, otherwise a side port reflectance accessory can be used.

At any interface between two materials, an incident radiation is split into a specular reflected light and transmitted beams, in different proportions according to the refractive index ratio of the two materials involved, as described by the Fresnel's equations [13] (Figure 3.2).

$$R = \frac{\left[\left(\frac{n_1 \cos\theta_i - n_2 \sqrt{1 - \left(\frac{n_1}{n_2} \sin\theta_i \right)^2}}{n_1 \cos\theta_i + n_2 \sqrt{1 - \left(\frac{n_1}{n_2} \sin\theta_i \right)^2}} \right)^2 + \left(\frac{n_1 \sqrt{1 - \left(\frac{n_1}{n_2} \sin\theta_i \right)^2} - n_2 \cos\theta_i}{n1 \sqrt{1 - \left(\frac{n_1}{n_2} \sin\theta_i \right)^2} + n_2 \cos\theta_i} \right)^2 \right]}{2}$$

$$T = 1 - R$$

Figure 3.2– Reflection (R) and transmission (T) coefficients for unpolarised incidence light in terms of the incidence angle (θ_i) and the refractive indexes of the first (n_1) and second (n_2) mediums.

If the sample surface is not optically flat, the diffuse reflection component has to be considered. In fact, the diffuse reflected light travels through the sample before being scattered or reflected from internal surfaces. Consequently, *reststrahlen* effects and diffuse reflection may arise and the Kramers-Kronig transformation cannot be applied [14]. Thus the resulted spectra may be of very difficult interpretation.

In order to obtain a highly reflecting surface, a perfect sample planarity has to be achieved by using adequate and strenuous mechanical polishing methods [15], costly advanced techniques such as ion milling system, focused ion beam [16, 17], or ultramicrotomy [18, 19]. As a consequence, very few publications have been so far reported concerning the study of paint cross sections by FTIR microscopy in specular reflection mode [20, 21].

Reflection-absorption measurements can be performed when a thin film (no more than 15 μm) is laid on a metal surface. In such conditions the IR radiation passes through the sample and is reflected back by the metal surface. The thin layer is therefore double-crossed by the IR beams, yielding high-quality spectra comparable to those registered in transmission mode. Nevertheless, reflection-absorption spectrometry (RAS) can be applied in some restricted cases, such as the study of protective coatings on metal

artworks [22] or for the characterization of varnish layers on gilded art objects.

Moreover, it is a simple method, which can be proposed as an alternative to transmission measurements. In fact, samples (films, powders, particles or fibres, etc) can be easily prepared by flattening in the same way as for the analysis with NaCl windows.

Attenuated total reflection (ATR) is based on the principle that total reflection is produced when the incident radiation passes from a higher refractive index material to a lower one with a particular incidence angle, called critical angle. When the incident angle is greater than the critical one, an evanescent wave forms up on the surface of the higher refractive index material (IRE, internal reflection element) and can penetrate the optically less dense medium placed in contact with it, resulting therefore attenuated. The use of ATR has been successfully reported for a large variety of samples, due to the fact that the spectra so obtained are similar to those recorded in the transmission mode. Nevertheless, some distortions of relative intensity and wavenumber shifts, principally at lower wavenumbers, are visible in ATR spectra, since the evanescent wave penetration depth (dp) depends on the refractive index of both the IRE and the material analysed, but is also function of the wavelength, as shown by the equation below (Equation 3.2), where λ is the wavelength of incidence radiation, n_1 the refractive index of IRE, n_2 the refractive index of the sample and θ the incidence angle of radiation on the interface [23].

$$dp = \frac{\lambda}{2\pi n_1 \sqrt{\sin^2 \theta - (n_2/n_1)^2}} \qquad (3.2)$$

Especially, absorption bands at lower wavenumbers are enhanced and those present at higher wavenumbers are less intense or absent. Furthermore, the sample refractive index is function of wavelength, and frequency shifts are also observed, principally at lower wavenumbers.

ATR correction algorithms, proposed by most of the commercially available FTIR software, proved to be not effective in the case of analysis of mixtures, like samples from cultural artefacts. The simplest way to compare ATR and transmission spectra is therefore to create a reference library of known compounds, whose spectra can be subsequently compared with unknown samples. An important advantage of ATR investigation is that it allows the investigation of smaller area maintaining the same aperture, thanks to the magnification factor of the IRE [24]. As an example, the actual investigated area is 25 x 25 μm, in the case for an aperture of 100 μm x 100 μm and an IRE of germanium (refractive index = 4).

In the last decades, FTIR microscopy prospective has been increased by the introduction of mapping and imaging equipments, allowing to collect a large number of FTIR spectra on a surface and to obtain a pattern showing the distribution of different compounds. FTIR mapping systems produce a sequential data collection, using a single-element mercury-cadmium-telluride (MCT) detector, adjustable apertures to select the investigated area and a motorised stage. The spatial resolution is related to the aperture dimensions and to the acquisition method (reflection, transmission or ATR). Furthermore, the overlap between two adjacent surface areas during data collection allows further increasing the spatial resolution. The main disadvantage of the mapping systems is the long time required for acquisition (hours), which may be, however, not so relevant when dealing with important cultural heritage samples.

FTIR imaging consists of a simultaneous and, therefore, faster data collection performed by a multichannel detector where small pixels of about 6 μm are

distributed over a grid pattern (FPA, focal plane array) [25, 26]. This type of detectors allows to record the optical signal entire field of view (FOV) and requires no aperture. Typical IR sensitive focal plane array (FPA) detectors include 64 x 64, 128 x 128 and 256 x 256 elements (pixels) arranged in a regular pattern. Compared to the mapping system, where geometrical apertures are used, the spatial resolution is in this case determined by the pixel dimension. Unfortunately, this yields also a poor spectral quality (low signal-to-noise ratio, S/N) since the photons quantity received by each pixel is inversely related to the number of pixels. For large detectors, this means a low photon quantity. The ATR configuration can provide increased spatial resolution of approximately 5 μm compared to transmission or reflection imaging. The cut-off of the focal plane array detector at 900 cm^{-1} is a significant disadvantage in distinguishing several inorganic compounds with characteristic absorptions below 650 cm^{-1} (i.e., calcite and lead white).

Linear array detectors (raster scanning) have been recently developed combining several mercury cadmium telluride (MCT) detectors with a motorised stage to sequentially scan lines. This system reduces the acquisition time by a factor corresponding to the number of detector elements. The size of individual elements is 25 μm, permitting to obtain high-quality spectra. In transmission or reflection mode, the achieved resolution of 25 μm can be reduced to 6.25 μm using an optical zoom, while in ATR the spatial resolution is reduced by the crystal magnification (~ 6 μm with a germanium crystal).

In recent times, a new integrated FTIR microscope has been designed, offering the powerful combination of a microscope with an incorporated FTIR spectrometer (interferometer, source, laser and detector). The main advantage of this setting is the higher energy compared to conventional systems, where energy losses are due to the radiation optical path from spectrometer to microscope [27].

One of our recent studies shows how this new configuration can increase the system spatial resolution maintaining a high spectral quality.

3.2 THE ANALYSIS OF PAINT CROSS-SECTIONS: A COMBINED MULTIVARIATE APPROACH TO THE INTERPRETATION OF μATR–FTIR HYPERSPECTRAL DATA ARRAYS

As it has been already remarked, the characterisation of organic substances is a difficult task. Two different analytical approaches may be adopted, often in a complementary way: bulk analysis with chromatographic and spectroscopic techniques, or microspectroscopy on cross sections. Chromatographic techniques are widely applied in this field but they require long time sample pre-treatments. Moreover, being bulk analyses, they do not provide the spatial location of the identified compounds. Microspectroscopic techniques can be employed with that specific aim, but the information obtained are sometimes less precise and require the development of different analytical techniques. It is therefore inevitable to adopt the only methodologies proving non-destructive on the sample.

A correct methodological approach can prevent such limitations. For instance, the analysis of the sample surface before the preparation of the cross section is always advisable for the characterisation of preparation layers and the analysis of external varnish layers.

As already reported, attenuated total reflection (ATR) is generally considered as one of the most appropriate approaches in FTIR microscopy of paint cross

sections. It is based on the use of an internal reflection element (IRE), which allows to reduce the investigation areas, in comparison with the reflection mode, thanks to a magnification factor. This results in an optimisation of the spatial resolution, preserving a satisfactory spectral quality.

ATR-μFTIR mapping and imaging systems allow to collect a considerable number of infrared spectra from a bidimensional scansion of the sample surface, collecting information about the spatial distribution of different compounds, with a resolution that is function of the objective aperture dimension, of the stage step selected, and of the reflection index characteristic of the IRE employed.

FTIR chemical maps/images or functional group maps/images can be obtained plotting the intensities of characteristic absorption bands, coded by a chromatic scale, in correspondence with their spatial position on a selected sample area [28, 29]. Collecting a large number of spectra, the sample surface can systematically be studied in both transmission and reflection mode. First, it is possible to achieve a line scan recording spectra at regular intervals across its entire structure either moving the sample stage manually or using a software control [1]. Then, with the help of a motorised stage, molecular mapping or imaging can also be performed on large areas [30]. Each map or image represents spatial position (x, y) and absorption (blue-red colour scale) at a specific wavelength. Overlapping all of the maps/images corresponding to each wavelength, the data set can be represented in four dimensions (three spatial dimensions plus the colour-coded absorption intensity) as a hyperspectral parallelepiped, usally referred to as hypercube (Figure 3.3).

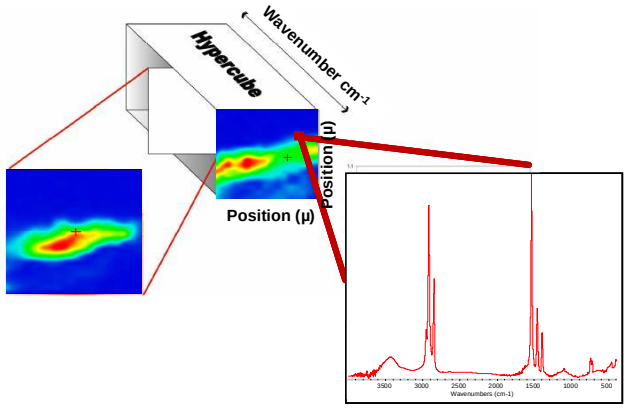

Figure 3.3 – Hyperspectral parallelepiped, or *hypercube*

Nevertheless, by using such a univariate approach, several problems may arise, related to the presence of complex mixtures, which may affect the correct identification and localisation of the compounds. In fact, due to the heterogeneity and complexity of the painting materials, the overlapping of characteristic bands in the region of the middle infrared may occur, as well as variations in their relative intensity. It has been widely demonstrated that, when data sets are constituted by multiple objects and inter-correlated variables, univariate methods – which examine one variable at a time – considerably underutilise the information enclosed therein. Conversely, multivariate approaches are able to consider and represent the whole information in an easily understandable way.

A very small number of applications of multivariate approaches to µFTIR data have been reported so far in the field of painting cross-section investigations. In particular, applications of principal component analysis (PCA) for the elaboration of multivariate chemical maps demonstrated to be a powerful tool in the case for spectra characterised by complex features and/or by unwanted variations arising from the acquisition in the reflection mode [14]. An example of PCA-based chemometric analysis applied to ATR-µFTIR imaging spectra collected using an FPA detector on paint cross-section samples has been also

reported, suggesting the considerable potential of such an approach for this type of studies [31].

The present research is focused on the methodical application and evaluation of a multivariate approach, suitable for processing the ATR-μFTIR hyperspectral data arrays, and for fully interpreting the outcomes, providing useful information for paint cross-section characterisations.

In particular, in order to extract the maximum useful information embodied into the hyperspectral data, an exploratory multivariate approach has been adopted. Moreover, the two approaches for the representation of scores – namely, scatter plots and colour maps – have been integrated in a comprehensive strategy.

Clusters of scores were individuated within the score scatter plots and then, the position of the corresponding objects within a given PC score map were located, thus making possible to understand to which particular part of the sample investigated those points correspond. Furthermore, the spectral profiles of such objects were extracted and interpreted, jointly with an analysis of the loading values, which is functional to individuate the spectral bands that are most involved in defining each sub-area under investigation. Finally, PC false colour images (RGB) were obtained by coding the score values on three selected PCs as the intensity of the red, green, and blue channels, respectively. This generally allowed to illustrate an overall localisation of the painting materials with a single image.

3.2.1 CHEMOMETRICS

Chemometrics is a chemical discipline born for interpreting and solving multivariate problems in the field of analytical chemistry. Svante Wold used for the first time, in 1972, the name chemometrics for identifying the

discipline that performs the extraction of useful chemical information from complex experimental systems [32].

The commonly accepted definition of Chemometrics is below reported: "Chemometrics is the chemical discipline that uses mathematical and statistical methods, (a) to design or select optimal measurement procedures and experiments, and (b) to provide the maximum useful information for chemical problems, by analyzing chemical, physical or theoretical (computed) data"

In the last decade, chemometrics has played a crucial role in the interpretation of spectroscopic data and it has been increasedly employed in the conservation science, to overcome the very limitative vision of the global situation offered by univariate approaches, which consider one variable at a time independently of the others. For instance, they are not able to take into account intercorrelation between variables – a feature that can be very informative, if recognised and properly interpreted.

Conversely, multivariate strategies are able to take into account such an aspect, allowing a more complete interpretation of data structures. However, in spite of their big potential, multivariate methods are generally still less used than univariate tools.

Nowadays, a large number of chemometric techniques is available, giving the possibility of achieving several different results from the analysis of a data set namely:

- recognition of the presence of structures (clusters, correlation) among the objects and/or the variables studied (exploratory analysis, unsupervised).
- deployment of mathematical models for prediction of qualitative responses (classification and class-modelling analysis, supervised).
- deployment of mathematical models for prediction of quantitative responses (regression analysis, supervised).

A bidimensional table is probably the most typical way to arrange, present and store analytical data: conventionally, in chemometrics, each row usually represents one of the samples analysed, while each column corresponds to one of the variables measured.

3.2.2 PRINCIPAL COMPONENTS ANALYSIS

PCA is an unsupervised exploratory method that looks for directions of maximum variance within the multivariate data space, based on the assumption that a high variance (i.e., a high variability) is synonymous with a high amount of information. The directions searched, which are called principal components (PCs), are orthogonal. This implies that they are not inter-correlated and, therefore, that they never account for duplicate information [33].

From a mathematical point of view, the PCs are expressible as linear combinations of the original variables: the coefficients which multiply each variable are called loadings. They represent the cosine values of the angles between the PCs and the original variables. These values may vary between -1 and +1, indicating the importance in defining a given PC: the larger the absolute value of the director cosine, the closer the two directions, thus the larger the contribution of that original variable to the PC. The loading values of the original variables on two selected PCs can be represented on bi-dimensional scatter plots (the loading plots), which give information about the importance of the variables and about their inter-correlation, with respect to the fraction of variance (i.e., information) explained by those PCs.

In terms of matrix algebra, the rotation from the space of the original variables to the PC space is performed by means of the loading orthogonal matrix, **L**:

$$\mathbf{S}_{NV} = \mathbf{X}_{NV}\,\mathbf{L}_{VV} \qquad (3.3)$$

X is the original unfolded matrix, constituted by *N* objects (rows) described by *V* variables (columns), and **S** is the score matrix, containing the coordinate values of the *N* objects on the *V* principal components.

The key feature of PCA is in its high capability for representing large amounts of complex information by way of simple bidimensional or tridimensional plots.

In fact, the space described by two or three PCs can be used to represent the objects (score plot), the original variables (loading plot), or both objects and variables (biplot). For instance, if the first two PCs (low-order) are drawn as axes of a Cartesian plane, we may observe in this plane a fraction of the information enclosed in the original multidimensional space which corresponds to the sum of the variance values explained by the two PCs. Since PCs are not intercorrelated variables, no duplicate information is shown in PC plots.

In the case of almost continuous signals such as IR spectra, it may be useful to represent the loading profiles, eventually superimposed to a selected signal or an average signal profile, in order to directly visualise which parts of the original signals give the highest contribution in defining a particular PC.

3.2.2.1 Preprocessing

In the case of the complex analytical signals arising from FTIR microscopy analysis, a number of preprocessing tools may be employed for three main purposes:

1. elimination or reduction of random noise
2. elimination or reduction of unwanted systematic variations
3. data reduction or compression

Unwanted systematic variations may be due to instrumental hurdles, to the experimental conditions and/or to physical characteristics of the samples. In general, it might be advantageous to avoid unwanted signal variations by improving the experimental settings, but this approach is not always feasible. Furthermore, in many cases, the effort that is needed (complex sample pretreatments, accurate temperature control, and so on) may be so high that it becomes incompatible with the ideal characteristics of a vanguard analytical system, which has to be cost and time saving and as simple as possible [34, 35]. For these reasons, when it is possible, it may be preferred to remove the signal variations afterward, by data preprocessing.

Row preprocessing acts on each single signal, independently of the other ones, and the result is the correction of systematic differences among signals.

3.2.2.2 Row centering

Each signal (y_i), defined by v variables (e.g., the absorption values in a IR spectrum), is corrected individually by subtracting its mean value ($\overline{y}_i$) from each single value ($y_{i,v}$). The values of the row-centered signal ($y_{i,v}^*$) are obtained by:

$$y_{i,v}^* = y_{i,v} - \overline{y}_i \qquad (3.4)$$

After transformation, the mean value of each signal is equal to 0: for this reason, row centering removes systematic location differences, namely baseline shifts, from a set of signals, as it is shown in Figure 3.4

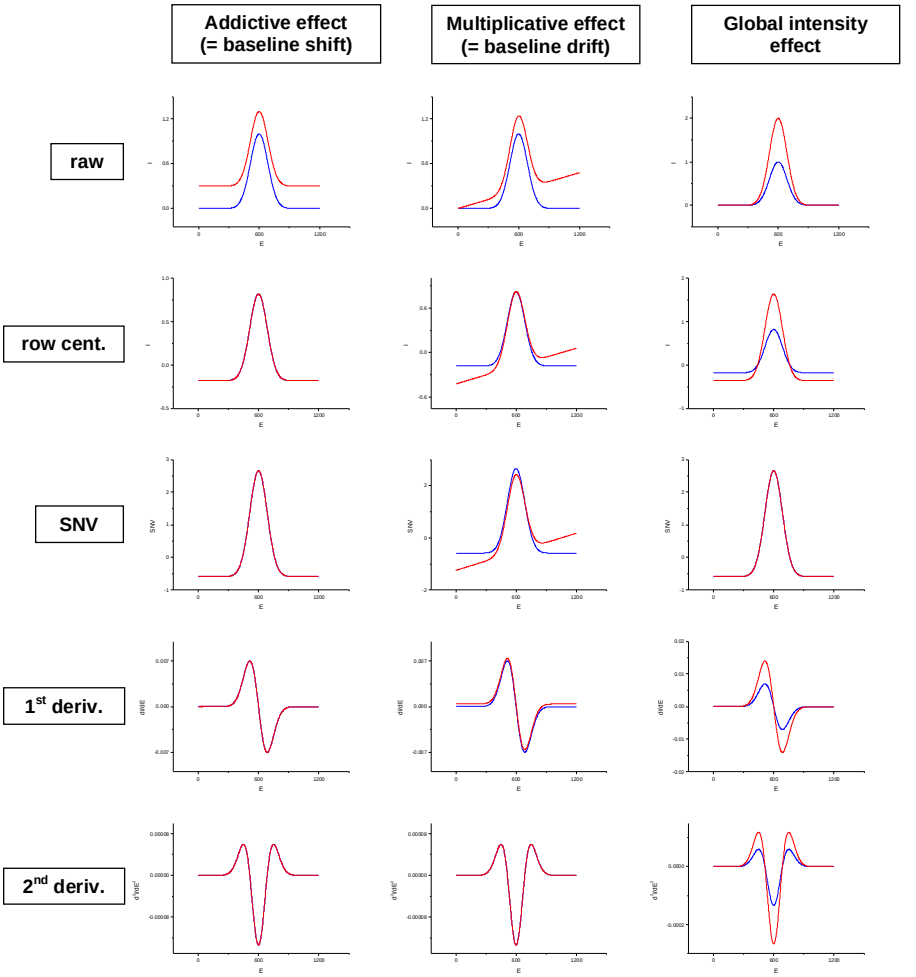

Figure 3.4 - Effectiveness of a number of row pretreatments in eliminating addictive, multiplicative, and global intensity effects.

3.2.2.3 Standard normal variate transform (SNV)

SNV, or row autoscaling, is a mathematical method for signal transformation, particularly applied in spectroscopy, that is useful to remove baseline shifts and to correct for global intensity variations (see Figure 3.4). Each signal (y_i)

is row-centered, as described above, and then scaled by dividing the single values by the signal standard deviation (s_i). The values of the SNV transformed signal are obtained by:

$$y^*_{i,v} = \frac{y_{i,v} - \overline{y}_i}{s_i} \qquad (3.5)$$

After transformation, each signal presents mean value equal to 0 and standard deviation equal to 1: both location and dispersion systematic differences are corrected.

SNV has the peculiarity of potentially shifting informative regions all along the signal range, so that the interpretation of the results referring to the original signals may be deceiving [36]

3.2.2.4 First and second order derivation after smoothing

The numerical differentiation of digitised signals has many uses in analytical signal processing. It allows a signal resolution enhancement, increasing the apparent resolution of overlapping peaks, accentuates small structural differences between nearly identical signals and corrects for baseline shifts and drifts, depending on the derivation order, as shown in Figure 2 [37].

In particular, the first derivative of a signal $y = f(x)$ is the rate of change of y with x (*i.e.*, $y' = dy/dx$), which can be interpreted as the slope of the tangent to the signal at each point. It returns null segments in correspondence to constant bands of the original signal and provides a correction for addictive effects.

The second derivative can be considered as a further derivation of the first derivative ($y'' = d^2y/dx^2$); it represents a measure of the curvature of the original signal, *i.e.* the rate of change of its slope. The second derivative returns null segments in correspondence to bands characterised by a constant

slope in the original signal and provides a correction for both addictive and multiplicative effects.

A disadvantageous consequence of derivation may be an enhancement of the noise, which is usually characterised by high-frequency slope variations. To overcome this hurdle, signals are firstly smoothed, often by using the Savitzky-Golay algorithm, which is a moving window averaging method [38]. A third-degree smoothing polynomial and a window size of 5-15 datapoints are suggested.

Column pre-processing corrects each variable individually and the result is the correction of systematic differences among variables.

3.2.2.5 Column centering

Each variable defining a set of signals (*e.g.* the current values at different potentials in a voltammogram) is corrected individually by subtracting its mean value ($\overline{y}_v$) from each single value ($y_{i,v}$). The column-centered values ($y^*_{i,v}$) are obtained by:

$$y^*_{i,v} = y_{i,v} - \overline{y}_v \qquad (3.6)$$

After transformation, the mean value of each column is equal to 0, so that systematic location differences among variables are eliminated.

3.2.2.6 Column autoscaling

Column autoscaling is often a default data pre-treatment in chemometrics, particularly in the case of variables of different nature. Each variable is corrected individually by subtracting its mean ($\overline{y}_v$) from each of its values

and then dividing by its standard deviation (s_v). The autoscaled values are dimensionless and are computed by:

$$y^*_{i,v} = \frac{y_{i,v} - \overline{y}_v}{s_v} \qquad (3.7)$$

This column pre-processing eliminates systematic location and dispersion differences among heterogeneous variables, giving all of them the same a-priori importance (mean values equal to 0 and standard deviations equal to 1), and enhances differences among the samples. Also in the case of signals like current/potential profiles, in which all the variables have the same nature and measurement unit, column autoscaling may be important, if there are variables characterised by a relatively low mean value and/or standard deviation, which enclose useful information; otherwise, this pre-treatment may decrease the signal-to-noise ratio, since the same weight is given to the noisy parts of the signal and to the informative features.

3.2.3 PCA - MULTIVARIATE CHEMICAL MAPPING

Hyperspectral data are arranged in three-dimensional data matrices with dimensions I x J x V, where I and J are the number of vertical and horizontal points of measurement, respectively, while V is the number of spectral variables recorded for each point (e.g., the absorbance values measured at different wavelengths).

Nonetheless, each point can be considered as an independent object, unfolding the three-dimensional array to a bi-dimensional matrix, structured with $N = I \cdot J$ rows and V variables.

This allows the application of usual chemometric techniques, which generally require bi-dimensional matrices to be processed.

It has been widely demonstrated that, when data sets are constituted by multiple objects and variables, univariate methods – which examine one variable at a time – considerably underutilise the information enclosed therein. Conversely, multivariate approaches are able to consider and represent the whole information in an easily understandable way. Principal component analysis (PCA) – which is one of the most common and efficient tools for multivariate data exploration – was performed, after application of a proper signal pre-processing. The score values can be used to build bi-dimensional scatter plots (the score plots), representing the projections of the data objects into a Cartesian space defined by two given PCs. A score plots gives information about the multidimensional structures existing among the objects, such as similarity, groupings, and trend patterns.

A joint examination of loading and score plots allows to identify the relationships existing between variables and objects, with respect to the fraction of multidimensional space that is accounted for by the two PCs.

Another possibility for representing the object score values is to use a chromatic scale – for example from blue (minimum) to red (maximum score value). This is particularly interesting if the objects are refolded (Figure 3.5) as in their starting configuration. In fact, representing each of them by the colour corresponding to its score value on a given PC, an image arises. Such an image can be considered as a sort of multivariate picture of the sample investigated, because it shows all of the information explained by that PC about the points of the map.

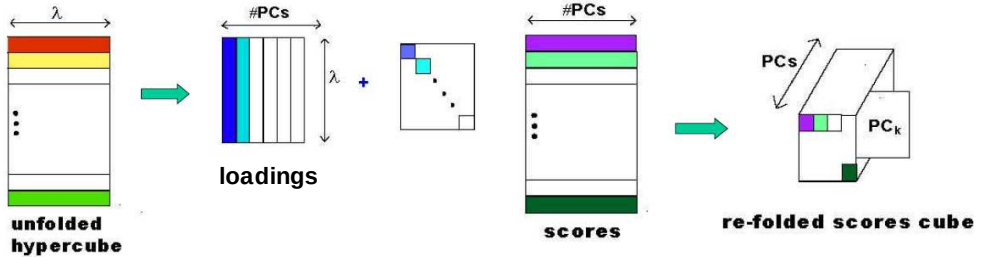

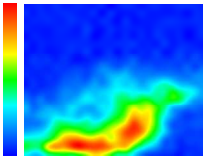

c)

Figure 3.5 - Scheme of application steps of PCA multivariate approach on μFTIR data arrays: a) PCA on the unfolded hypercube; b) Re-folding Scores; c) PC score map obtained

Clusters of scores were individuated within the score scatter plots and then, the position of the corresponding objects within a given PC score map were located, thus making possible to understand to which particular part of the sample investigated those points correspond. Furthermore, the spectral profiles of such objects were extracted and interpreted, jointly with an analysis of the loading values, which is functional to individuate the spectral bands that are most involved in defining each sub-area under investigation. Finally, PC false colour images (RGB) were obtained by coding the score values on three selected PCs as the intensity of the red, green, and blue channels. This generally allowed to illustrate an overall localisation of the painting materials in a single image.

3.2.4 MATERIALS AND METHODS

3.2.4.1 Samples

Three cross-sections, showing different structures and composition have been investigated in order to present suitable multivariate statistical treatments for each case of study, facilitating the extraction of relevant information in complex analytical and conservation issues. In particular, the characterisation of organic substances represent a challenging task. These materials, in fact, are usually present in low concentration and dispersed in inorganic matrix (pigments and ground layers), which have strong absorption bands in the region of middle infrared. Moreover, the characterization of thin organic layer, can be particularly difficult due to chemical variety of original materials and ageing products, as well as the spatial resolution of the instrumentation.
Indeed, the samples invetigated were characterised by the presence of thin and organic layer applied as priming or coating materials. Furthermore, in attempt to evaluate the discrimination power of PCA in the localisation of paint components, the protocols has been also applied on a sample containing organic and inorganic material with similar spectral features, which are not well distinguished with the univariate procedure.

- Sample Erc3

The sample was collected from a mural painting (*Salone Nero*, west wall) of the Roman site of Ercolano (Italy). The study was focused on the characterisation of the state of conservation of the ancient artefact and the recognition and localisation of different conservation treatments applied in the past as surface coatings. In fact, this area shows an overall discoloration effect, probably related to a previous application of water repellent products. The analyses of samples coming from the Herculaneum archaeological sites

were realised within the Herculaneum Conservation Project promoted by the Packard Humanities Institute, in collaboration with the Italian *Soprintendenza Speciale per i Beni Archeologici di Napoli e Pompei* and the British School based in Rome. The fragments were withdrawn *in situ* by Marisa Laurenzi Tabasso (University of Rome *La Sapienza*) and Alessandra De Vita (Herculaneum Conservation Project) within the framework of a joint project entitled: "*Consolidation and fixing techniques of wall painting layers within the Herculaneum archaeological site*".

- *Sample Ef*

The sample was studied within a research project aimed at characterising the painting techniques and at supporting the attribution studies on the 28 portraits of the *Uomini Illustri* collection (oil paintings on wood panels), which is exhibited in the Studiolo of the Ducal Palace of Urbino (Italy). In more detail, the study was carried out on several cross-sectioned samples, in order to identify the painting components and their distribution within the stratigraphic structures. The attribution of the paintings has already been the subject of extensive researches that resulted in the hypothesis for a joint contribution between the Flemish painter Juste de Gand and the Spanish Pedro Berruguete [39]. A particular attention was devoted on the characterisation of the components present in the green areas. In fact, it was noticed that the different green tonalities had been obtained with two different painting techniques, which involved the use of either a mixture of green copper based pigments, calcium carbonate, lead white and/or lead and tin yellow. The *Ef* sample was collected from an area representing the green background within the Euclide's portrait (Figure 3.6).

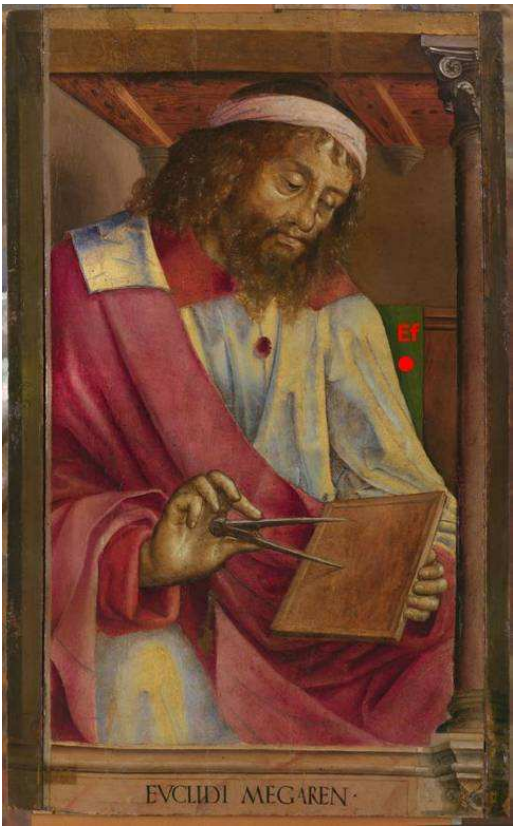

Figure 3.6 – Euclide portrait, painting on wood

3.2.4.2 Sample preparation

Fragments were embedded in potassium bromide (KBr, purchased by Sigma Aldrich) and cross-sectioned. The procedure, previously tested and already published [40], has been applied in order to avoid the interference by absorption bands of the synthetic resins, traditionally employed as embedding material. Briefly, the paint chips was positioned a soft base, which is obtained by pressing 300 mg of KBr into a pellet under low pressure (2 tons for 30 s).

Than, another 300 mg of KBr was added and a pressure of 3 tons for 2 min applied. Afterwards, the pellet (13 mm of diameter and 2 mm thick) is carefully extracted from the holder. Finally, the cross-section was obtained through a dry polishing on silicon carbide papers (Micro-Mesh®) with different grinding (from 2,400 up to 12,000), to achieve a regular and smooth surface and an uniform contact between the ATR crystal and the paint layers.

3.2.4.3 Optical microscopy

The sample cross-sections were primarily observed by means of an optical microscopy, in order to document the stratigraphic morphology of the paint layers. A dark field observation was performed, with an Olympus (Olympus Optical, Tokyo, Japan) BX51 microscopy equipped with a digital scanner camera Olympus DP70. A 100-W halogen projection lamp and a Ushio Electric (USHIO Inc, Tokyo, Japan) USH102D ultraviolet (UV) lamp were employed for the acquisition of visible and fluorescent images, respectively.

3.2.4.4 ATR-μFTIR mapping analysis

A Thermo Nicolet (Thermo Fisher Scientific, Waltham, MA, USA), iN™10MX imaging microscope, fitted with a mercury-cadmium-telluride (MCT) detector cooled by liquid nitrogen, was used for mapping analysis. The measurements were performed using a slide-on ATR objective, equipped with a conical germanium crystal, in the range 4,000–675 cm^{-1}, at a spectral resolution of 4 cm^{-1}. Backgrounds were acquired keeping the slide-on inserted and the ATR objective not in contact with the sample surface.

As for the sample *Erc3*, the analysis was performed spanning an overall area of 184x152 μm^2, using a step of 8 μm in the x-y direction, and an objective aperture of 60x60 μm, corresponding to an investigation area of about 15 μm for each point of analysis. A total of 480 spectra were acquired.

The sample *Ef* was mapped using an aperture of 30x30 μm (with an effective investigated area of about 7.5 μm for each point of analysis) and a step of 4 μm in the x-y direction. The overall area of analysis was of 40x92 μm^2, with 230 spectra recorded.
The dedicate software OMNIC Picta™ (Thermo Fisher Scientific, Waltham, MA, USA), was used for the manipulation of the set of spectra collectively.

3.2.4.5 PCA - Multivariate chemical mapping

All of the multivariate data processing and the chemical mapping were performed, in the present study, by means of self-compiled Matlab routines (The Mathworks Inc., Natick, USA).
In the first case study discussed (sample *Erc3)*, a second-order derivation was applied as the first step, attempting to minimise systematic unwanted variations affecting the signals. Then, the spectral regions were reduced to the ranges 685 – 1,780 cm^{-1} and 2,800 – 3,600 cm^{-1}, eliminating infrared regions affected by environmental and instrumental noise, which prevalently embodies unhelpful information. PCA was performed after a column mean centering.
As for the *Ef* sample, a linear detrending was applied to the signals, in order to correct for baseline unwanted variations. A reduction of the spectral range was realised retaining the same regions and for the same reasons described for the previous case. A mean centering was performed as the column preprocessing on the data matrix, prior to PCA.

3.2.5 RESULTS AND DISCUSSION

3.2.5.1 Sample Erc3

The study on the *Erc3* was aimed mainly at defining the state of conservation of the ancient artefact and at characterising the different conservation treatments superimposed as surface coatings. The investigated area shows, in fact, an overall discoloration effect, probably related to a former application of water repellent products.

The observation of the sample under optical microscopy allowed the recognition of a multilayered structure (Figure 3.7a, b). The ground white substrate (layer 0), is characterised by the presence of big and irregular crystals, and black and brown particles. On the top of it, a brownish layer can be observed. The documentation under UV illumination reveals the presence of two different organic substances, with peculiar visible fluorescence colours, inside that stratigraphy portion. In particular, a first and irregular layer (layer 1, 25 µm thick) can be identified thanks to its strong whitish fluorescence, while a thinner superimposed layer (layer 2, 15 µm thick) shows a bright bluish colour. The ATR-µFTIR measurements were carried out on a representative area (red box in Figure 3.7).

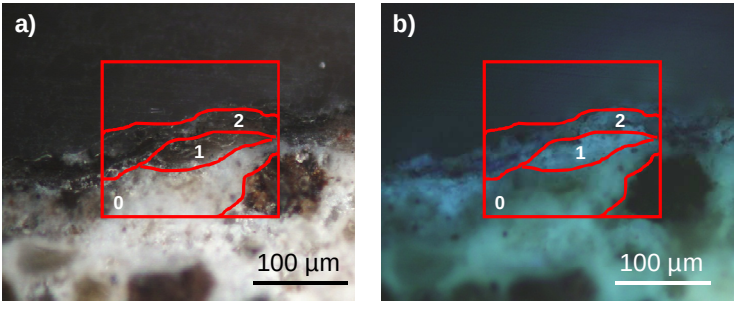

Figure 3.7 - Cross-section microphotographs of sample ECR3 embedded in KBr: a) image under visible light; b) image under UV illumination: the red boxes indicate the selected area for µFTIR-ATR analysis.

A multivariate exploratory study was performed, in order to exploit the maximum relevant information from the spectral features that characterise the points of analysis within the thin selected area. The score map of PC1, reported in Figure 3.8a, identifies the layer 0 (red area, i.e. the highest score values). The average spectral profile extracted from such area (*not shown)* clearly reveals the presence of calcium carbonate as the main component, thanks to the very strong peak at 1,400 cm^{-1} (CO_3^{2-} asymmetric stretching), and to the related absorption band at 875 cm^{-1} (CO_3^{2-} out-of-plane bending). The discrimination between the layers 1 and 2 is observable in both of the PC2 and PC3 score maps (Figure 3.8b, c). In particular, the PC3 map clearly shows the presence of two well-located components related to the uppermost paint layers, according to their different chemical nature.

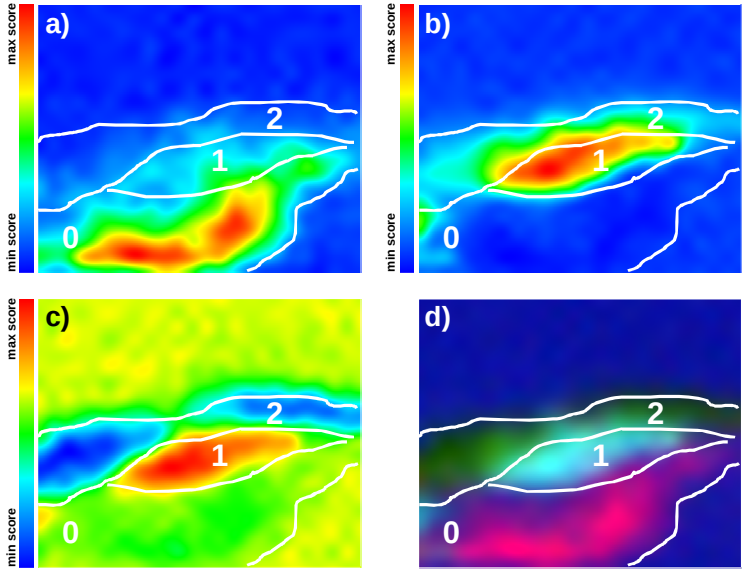

Figure 3.8 - PCA sample *Erc3* - Score maps : a) PC1 b) PC2 c) PC3 d) PC false colour image (RGB). PC1, PC2, and PC3 score values as the intensity of the red, green, and blue channels, respectively

After the preliminary map analysis, PC23 score and loading plots (Figure 3.9a, b) were examined, in order to identify the spectral bands mainly involved in the definition of each layer identified. In particular, in the score plot (Fig. 3a) two different groups of objects are shown, related to high (red squares) and low (green squares) score values along the PC3,. These clusters correspond to the layers 1 and 2, respectively, visualised in the PC3 score map (Figure 3.9c, d). The correspondence with the loadings, located in the matching directions (Figure 3.9b) reveals that a crucial role in describing the layer 2 in the PC3 score map is played by the spectral region around 1,727 cm^{-1}, which is ascribable to the characteristic carbonyl stretching of synthetic resins (e.g., acrylic or polyester resin). On the other hand, peaks around 2,920 and 2,850 cm^{-1} (C-H aliphatic stretching absorption bands) and 1,734 cm^{-1} (ester C=O stretching bands of lipids) represent the spectral variables most important for the definition of the layer 1 in the same map. This information, supported by an examination of the average profile of the spectra corresponding to the selected area (Figure 3.9e), suggests the presence of a natural wax as the principal constituent of the layer 1. This hypothesis is deductible, in particular, by considering the peculiar shape and intensity of C-H stretching absorption bands (typically ascribable to a hydrocarbon with a long alkyl chain), together with the contemporary presence of an ester C=O absorption. As a confirmation, it is possible to notice that the characteristic peaks around 730 and 720 cm^{-1} (ascribable to the C-H rocking absorption bands), which may be considered as markers of such compound, result well detectable in the extracted spectral profile. Furthermore, it is possible to postulate the presence of a superimposed film of a synthetic resin (layer 2).

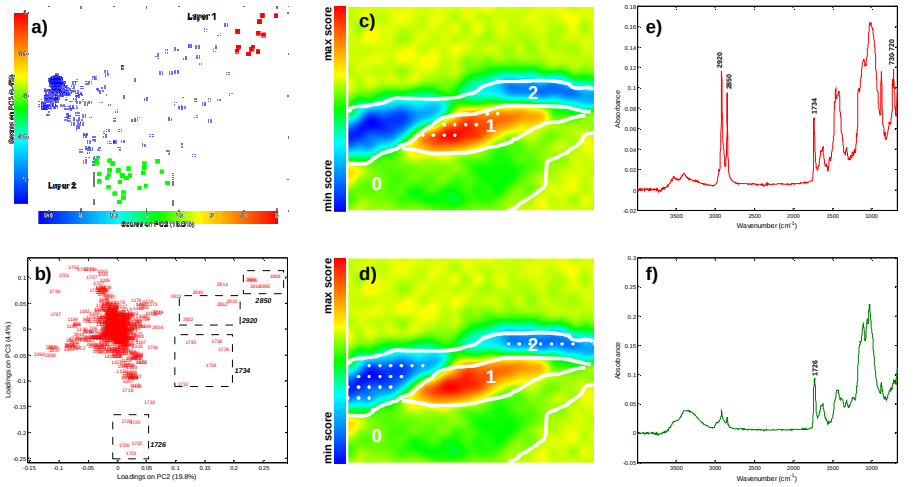

Figure 3.9 - PCA sample *Erc3* - a) PC23 score plot: clusters highlighted in red indicates the objects localised within the PC2 score map, layer 1 (c) and green for objects localised within the PC2 score map, layer 2 (d); the average spectral profiles extracted from the corresponding objects in layer 1 (e) and 2 (f) are shown; b) PC23 loading plot

A multivariate comparison with two pure reference compounds (a bee wax, and an acrylic resin – Paraloid B72) was performed in order to verify such hypotheses. As a first step, the spectra of the two standards were submitted exactly to the same pre-processing as for the map signals; in particular, they were centered with respect to the map data centroid. Then, the two row vectors were post-multiplied by the loading rotation matrix, thus obtaining the corresponding score values, which were employed to project the two reference compounds within the PC23 score-plot (Figure 3.10). By examining this graph, it appears evident that the points characterised by the highest score values on both of the axes (corresponding to the layer 1 – see Figure 3.9) are located exactly in the direction of the wax. Conversely, the points at the lowest score values along PC3 (corresponding to the layer 2 – see Figure

3.9) clearly show a trend towards the Paraloid B72. Such trends can be considered as similarity measurements, thus supporting the identification of the paint materials revealed in the maps and previously exposed. Therefore, although the compounds of layers 1 and 2 present similar spectral features and overlapping of characteristic bands, an excellent differentiation has been made possible, as noticeable in the PC false colour map (Figure 3.8d), which allows the global visualisation of the stratigraphic location of all of the paint materials identified. In this case, the red, green and blue channels were assigned to PC1, PC2 and PC3 scores, respectively.

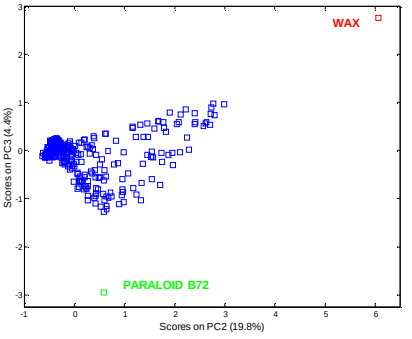

Figure 3.10 - PCA sample *Erc3* - PC23 score plot with inserted the spectra of pure standard compounds used as reference: Paraloid B72 (green square) and wax (red square)

3.2.5.2 Sample Ef

The study on this sample was aimed at identifying and comparing the painting components and their distribution within the stratigraphic structures.
A particular attention was devoted on the characterisation of the components present in the green areas. In fact, it was noticed that the different green tonalities had been probably obtained with two different painting techniques,

which involved the use of either a mixture of green copper based pigments, calcium carbonate, lead white and/or lead and tin yellow.

In the presented case (sample *Ef*) ATR-μFTIR measurements were performed in a portion of the stratigraphy (40x92 μm) containing five different layers (red box in Figure 3.11).

The morphological characterisation of the sample stratigraphy under optical microscopy (Figure 3.11a, b), reveals the presence of a very thin brownish layer (layer 1, 8 μm thick), over a gypsum ground layer, with small white particles dispersed therein. It probably constitutes a priming layer, usually employed in oil paintings in order to limit the absorption of the binding medium from the upper layers to the ground. On the top of it, two green layers (labelled as 2 and 3, respectively) are evident, each of them characterised by a different tonality. In particular, the layer 2 (19 μm thick) presents a darker colour with few and irregular particles dispersed within the homogeneous green matrix. Instead, the upper layer shows a lighter green tonality (layer 3, 22 μm thick). A further external brownish layer (layer 4, 14 μm thick) is well recognisable under UV illumination, thanks to its bright white fluorescence colour.

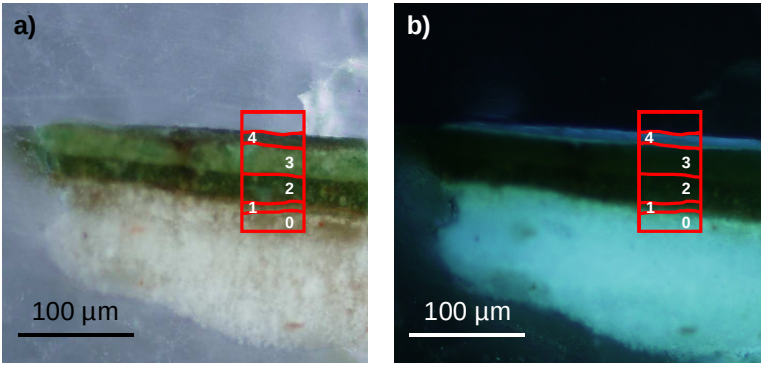

Figure 3.11 - Cross-section microphotographs of sample *Ef* embedded in KBr: a) image under visible light: the red boxes indicate the selected area for μFTIR-ATR analysis; b) image under UV illumination

PCA was performed on the ATR-μFTIR dataset and five PCs were taken into consideration to draw score maps that helped in the explanation of the complex stratigraphic structure (Figure 3.12). In particular, the score map of PC1 (Figure 3.12a) shows a clear localisation of the gypsum ground: layer 0 (red area which corresponds to the highest score values on PC1) well identifiable thanks to the specific absorption bands at 1,105 cm^{-1} associated to the SO_4^{2-} symmetric stretching, which results well visible on the average spectrum extracted (*not shown)*.

In order to achieve a deeper understanding of the painting techniques adopted by the artist, a particular attention was focused on the complete characterisation of the priming layer (layer 1), which was not identifiable by the univariate approach. In details, the PC4 and PC5 score maps show a good discrimination of the mentioned layer from the other painting materials (Figure 3.12d, e).

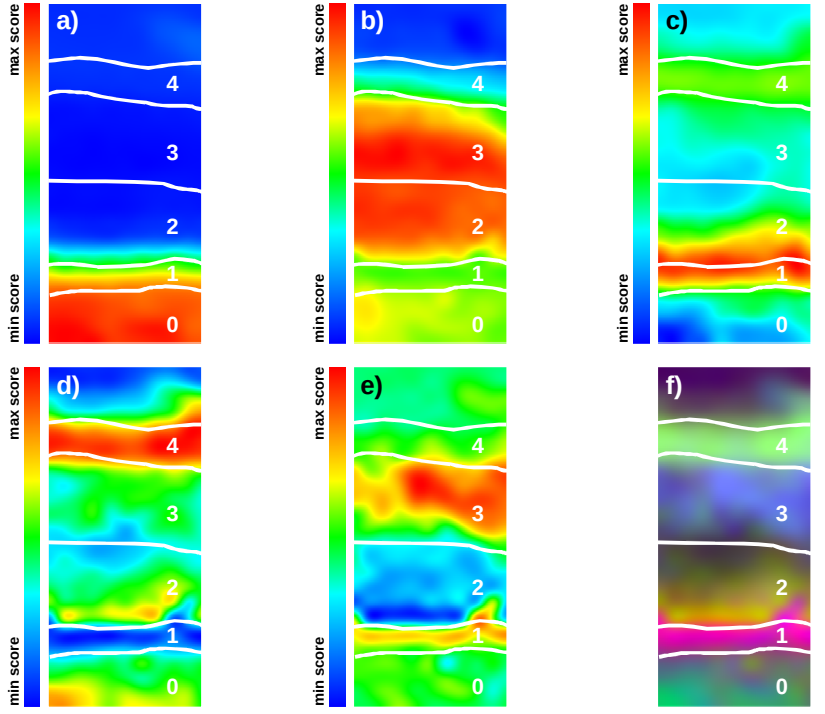

Figure 3.12 - PCA sample *Erc3* - Score maps : a) PC1 b) PC2 c) PC3 d) PC4 e) PC5 f) PC false colour image (RGB). PC3 PC4 and PC5 score values as the intensity of the red, green and blue channels, respectively.

To provide such observations a chemical interpretation, through the examination of the related loadings values both in the matching and opposite (Figure 3.13c), was carried out. This allowed to distinguish the specific contribution of the spectral variables in the description of the layer 1.

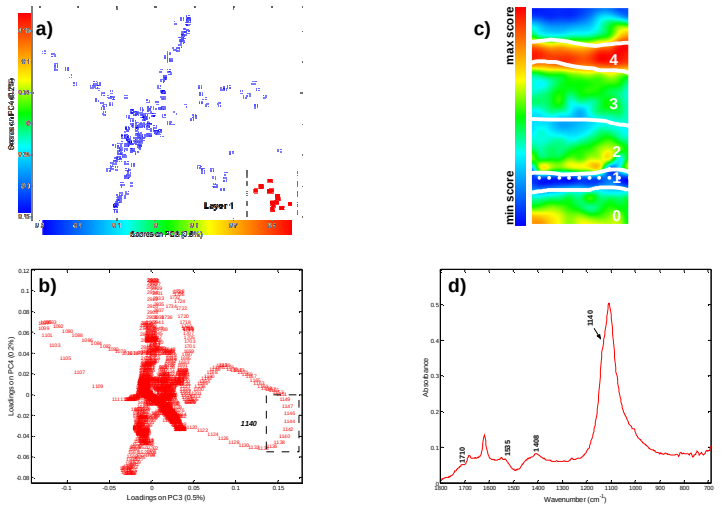

Figure 3.13 - PCA sample *Ef*- a) PC34 score plot: clusters highlighted in red indicates the objects localised within the PC4 score map, layer 1 (c); b) PC34 loadings plot; d) average spectral profile extracted from the corresponding objects in layer 1

In particular, a crucial role seems to be played by a shoulder around 1,140 cm^{-1}, which may be related to the C–O stretching vibration of lipidic substances present in the layer. In fact, it is worth to notice that, in the average spectral profile extracted (Figure 3.13d), several peaks are well recognisable, all ascribable to the presence of an oil-rich layer, probably mixed with some white grains of lead carbonate ($2PbCO_3 \cdot Pb(OH)_2$). Indeed, it is possible to detect the shoulder around 1,710 cm^{-1} (C=O asymmetric stretching band of carboxylic acids) and of the peak around 1,400 cm^{-1} (CO_3^{2-} asymmetric stretching), as well as the weak absorption bands around 1,535 cm^{-1} (COO^- stretching of lead carboxylates).

The score map of PC5 shows a clear discrimination between the two green layers (layer 2, and layer 3, Figure 3.14c, d). The loading analysis (Figure 3.14b) reveals the contribution of the peak at 1,550 cm^{-1} and that the infrared

regions more involved in such differentiation are ascribable to the content of lipid substances (1,735 – 1,710 cm^{-1}, ester and carboxylic acids C=O stretching band), to the amount of carbonate (1,410 cm^{-1}, CO_3^{2-} asymmetric stretching), and calcium carbonate (875 cm^{-1}, CO_3^{2-} out-of-plane bending absorption). Consequently, it is possible to conclude that the characterisation of the layers 2 and 3 is essentially ascribable to variations in the relative amount of these components, as well as to the rather addition of lead carbonate. This last pigment may be revealed in single point analysis, given the presence of a peak at 680 cm^{-1} (CO_3^{2-} in-plane banding band), which – however – was removed from the data matrix to be submitted to multivariate analysis, due to the too low signal-to-noise ratio, as described in the PCA paragraph.

On the other hand, concerning the identification of the green pigment employed, it was not possible to detect unambiguously the absorption bands typically representative of the hypothesised presence of the verdigris – copper acetate – (band at 1,610 cm^{-1} assigned to the COO asymmetric stretching of the carboxylate groups coordinate to the Cu^{2+} ion). In addiction, one of the most intense absorption bands, in the mentioned layers, corresponds to the peak at 1,550 cm^{-1}, which can be related to the presence of lead carboxylates (lead acetate). Such compounds may derive from the interaction between the lead-based pigment and the siccative oils, probably used as binding media. The exact composition of the complex mixture constituting this layer is still under investigation.

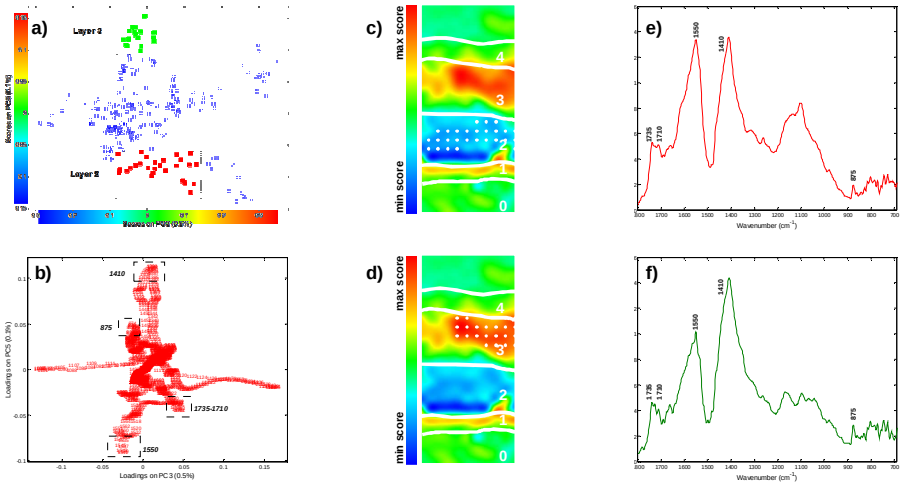

Figure 3.14 - PCA sample *Ef* - a) PC23 score plot: clusters highlighted in red indicates the objects localised within the PC5 score map, layer 2 (c) and green for objects localized within the PC5 score map, layer 3 (d); the average spectral profiles extracted from the corresponding objects in layer 2 (e) and 3 (f) are shown; b) PC35 loading plot

It is worth to point out that, such a clear localisation and identification of both the green layers is not achievable by the univariate method. In fact, peculiar absorption bands were selected and employed to perform a comparative univariate mapping. As Figure 3.15 clearly reveals, neither the peak at 1,410, 1,550, nor the band at 1,735 – although characteristic – were helpful to discriminate the two green layers, if considered independently one at a time.

The layer 4, probably related to an uppermost varnish layer, appears well located in the PC4 score map (red area, Figure 3.16c), and it is characterised by a strong absorption band at 1,730 cm^{-1} (C=O stretching), as revealed by a joint analysis of scores and loadings (figure 20a, b, PC34 score and loading scatter plots), as well as the peak around 2,930 cm^{-1} (C-H aliphatic stretching absorption bands).

Finally, a PC false colour image (RGB) was obtained by coding the PC3, PC4, and PC5 score values as the intensity of the red, green and blue channels, respectively (figure 3.12f). Such a comprehensive map shows a global discrimination between all the layers, on the basis of their different chemical nature.

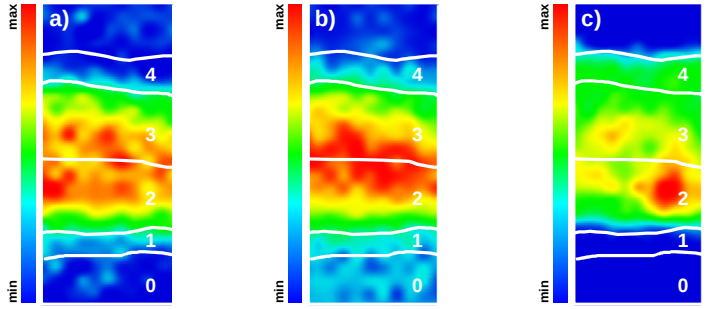

Figure 3.15 - ATR mapping sample *Ef* – univariate FTIR false-colour plot representing: a) peak area profile at 1410 cm^{-1} (carbonate) b) peak area profile at 1550 cm^{-1} c) peak area profile at 1735 cm^{-1} (siccative oil)

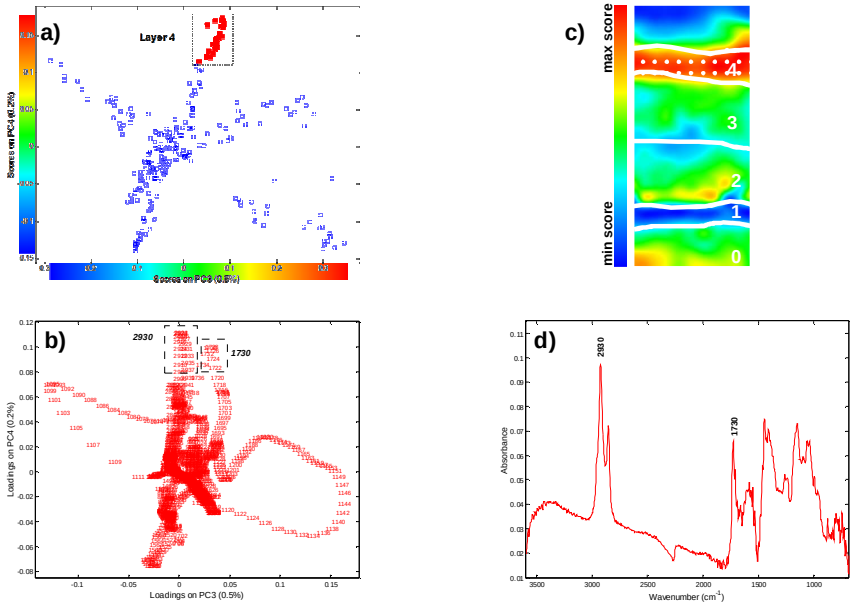

Figure 3.16 - PCA sample *Ef* - a) PC34 score plot: clusters highlighted in red indicates the objects localised within the PC4 score map, layer 4 (c); b) PC34 loading profile; d) average spectral profile extracted from the corresponding objects in layer 4

3.2.6 CONCLUSIONS

The combined multivariate methodology applied in this study proved to be a powerful approach for the analysis of data obtained from hyperspectral mapping techniques. The results demonstrate the potential of chemometric method applied for the characterisation of paint cross-sections and their crucial role in the extraction of meaningful information starting from complex multivariate data.

Moreover, the research highlights the importance of a joint examination of PCs score maps together with several chemometric tools (e.g., identification of cluster of scores the related PC score map, extracting the average spectral

profiles and creation of PC false colour image) may be systematically performed and employed to extract information otherwise inaccessible.

3.3 APPLICATION OF ATR-FAR INFRARED SPECTROSCOPY TO THE ANALYSIS OF NATURAL RESINS

The present research has been focused on the application of FTIR spectroscopy in the far infrared region (FarIR) as an alternative method for the characterisation of natural resins. To this purpose, standards of natural resins belonging to four different categories (sesquiterpenic i.e elemi, shellac; diterpenic, i.e. colophony, Venice turpentine; diterpenic with a polimerised components, i.e. copal, sandarac; triterpenic, i.e. mastic and dammar) used as paint varnishes have been analyzed by FarIR spectroscopy in ATR mode.

In the past, tree and insect secretions have been extensively employed in art, as well as in conservation and preservation of art works, thanks to their useful chemical and physical behaviour, including water insolubility, adhesive and coating properties. Different natural resins were mainly used for decorative and varnish purposes since very ancient times for their excellent glasslike capability. A great number of recipes and preparation procedures are documented in literature [41-42]. Resins mixed with a drying oil were the earliest type of varnish blend, whereas spirit varnishes were introduced only in the 16th century. In addition, such biopolymers were mixed with different

organic compounds and additives in order to obtain a suitable binding medium [43].

Resins are composed of complex mixtures of terpenoids derived by isoprene. They can be distinguished by their carbon atom numbers into sesqiterpenic (terpenic compounds with 15 carbon atoms), diterpenic (terpenic compounds with 20 carbon atoms) and triterpenic (terpenic compounds with 30 carbon atoms).

Shellac is a sesquiterpenic resin secreted by an insect (*Kerria lacca*, *Keriidae* family, *Hemiptera* order) that infects host trees. The raw lac is scratched from branches and purified through crushing, sieving and water washing procedures. It is mainly composed by polyesters of oxy acids, which can be dissolved in alcohol, low percentages of waxy substances and low molecular polymers derived by poly hydroxyl acids. Elemi is a malleable material containing a considerable amount of liquid sesquiterpenes and a fraction of triterpenic components. The most common type of elemi is obtained from species of the Bursaceae family, growing in the Philililippines. Diterpenic resins belong mainly to the Coniferae class (Pinaceae, Cupressaceae, Auracariaceae). Pinaceae resins (i.e. colophony, Venice turpentine, Strasbourg turpentine) are characterized mainly by the presence of abietane and pimarane acids. Cupressaceae (i.e. sandarac) and Auracariaceae (i.e. Manila copal) are composed by labdane acids, in particular by a polymerised fraction derived by communic acids. Triterpenic resins (i.e. dammar and mastic) contain C30 isoprene derivatives showing different basic skeletons, mostly tri- or pentacyclic. Monoric, oleononic, masticadienonic and dammararolic acids are some of the most important triterpenoid components. Mastic can be found on many Mediterranean coasts since it is secreted by the *Pistacea lentiscus* shrub, while dammar is derived from trees of the Dipterocarpaceae family, growing in the Far East [43].

Several analytical techniques have been so far employed for the identification of resins and the characterisation of their degradation pathway. In particular, GC-MS [44-46] can provide specific information on molecular composition, biological source and degradation effects. However, it is a destructive technique, not allowing the possibility to repeat the analysis and confirm the result.

Py-GC/MS has been widely employed for the characterisation of natural resins [47-49]. This technique is actually less time consuming than GC-MS because no sample pre-treatment is required. It also allows to overcome the problem related to the solubility decrease in long time aged resins.

In the last decades vibrational spectroscopic methods (infrared and Raman) have been optimized to overcome the drawbacks related to bulk analyses, developing portable instruments (for in situ analyses) and microscope based techniques (for stratigraphical investigations). In particular infrared spectroscopy has been widely used thanks to its versatility and ability to provide information on both organic and inorganic materials [50]. Since its first introduction, IR spectroscopy has been applied to the examination of paintings and artefacts mainly in the MidIR range 4000–600 cm^{-1} [2]. When micro-sampling accessories for FTIR spectroscopy were introduced in the early 1980s, the following development of FTIR microscopy became an essential tool in the micro-destructive analysis of small samples [51]. Moreover, the recent introduction of mapping and imaging equipments allows to collect a large number of FTIR spectra on a surface, producing a distribution map of the identified compounds. FTIR spectroscopy can also be used for non-destructive analyses in form of portable instrument. In the recent times fiber optics have been employed for the development of portable instruments both in the VIS-NearIR and in the MidIR range [52-53]. Even though FTIR spectroscopy appears to be particularly flexible, only IR-active compounds can be detected. Moreover, the characterisation of the organic

substances is a difficult task and only the main class can often be distinguished.

In the field of resinous materials, for instance, FTIR techniques are mainly helpful in recognising their presence, thanks to the presence of both the acid stretching band at around 1690 cm^{-1} and the ester triplet due to C-O stretching vibrations at around 1230, 1160 and 1090 cm^{-1} (characteristic also of drying oils) [54-55]. Even though the different resins show some particular features [4], FTIR is mainly applied as a preliminary and non-destructive technique to detect the presence of resinous materials. The subsequent identification of the resins may be accomplished by other techniques, such as GC-MS [56]. FTIR spectroscopy has also been employed to study the ageing effects on natural resins [57-58], which leads to oxidation cross linking reactions or hydrolysis, depending on the resin typology.

Raman spectroscopy and microscopy have been successively employed for resins characterisation [59-68]. In particular high wavelengths laser excitation (i.e. 1064, 780, 785 nm) has been applied to reduce the fluorescence effects. Despite inherently weaker Raman effect in the near infrared region (signal is almost 350 times lower than spectra obtained by using a 250 nm laser, because of the inverse dependence between molecular scattering intensity and excitation wavelength), the strong reduction of fluorescence effects allows the determination of different resin specimens [59, 63]. A specific protocol based on the interpretation of the FT- Raman spectra has been developed for the discrimination of diterpenoid and triterpenoid resins [59], considering ageing processes such as oxidation and hydrolysis. The discrimination protocol takes into account the entire spectrum with particular attention to bands from about 3000 to 500 cm^{-1}. The region from 1200 to 200 cm^{-1} is typical of the vibrations of v(CC), ρ(CH), δ(CCH) and δ (CCO) groups. However, the comparison of resin samples in this region may be difficult because of the inherent weakness of the spectra [61]. Moreover, in some

cases the resins specimen shows fluorescence emissions even in these conditions, which may invalidate their correct classification [59].

In order to avoid a sensible reduction of the Raman signal due to the use of FT lasers, Lau et al. have proposed to employ SERS Raman spectroscopy [68] with the application, on a metal surface *ad hoc* prepared, of a drop of a solution containing the extracted resin .

This research is aimed at evaluating the use of FTIR spectroscopy in the far infrared region (FarIR) to propose an alternative and complementary technique for the characterisation of natural resins. FarIR spectroscopy is widely employed in different fields, such as astrophysics, cation exchange and interactions in ceramics, as well as lattice vibrations in the field of polymer crystallization. Since 1969, several studies have highlighted the analytical potential of FarIR spectroscopy for the investigation of minerals in the 200-50 cm^{-1} region [69]. Furthermore, recent studies document the application of FarIR spectroscopy in both transmission [70] and ATR modes [71-74] as a valid alternative method for the characterization of the compounds inactive in the MidIR (different inorganic pigments and corrosion products). As far as the authors know, the application of FTIR spectroscopy in the FarIR region for the investigation of organic substances has not yet been carried out. To this purpose, standards of natural resins used as paint varnishes have been analyzed by FarIR spectroscopy in ATR mode, obtaining promising results. Moreover, the discrimination between spectral data was magnified and verified using principal component analysis (PCA).

The ability of the method for identification purposes in real matrices was tested by the analysis of historical samples. The results were compared to those obtained from a complementary methodology based on analytical pyrolysis.

3.3.1 ATR-FAR INFRARED SPECTROSCOPY

The infrared range of the electromagnetic spectrum covers the wavelength region from 25 μm to 1 mm, which conforms to the wavenumber range 40,000-100 cm^{-1}. It is split in the Near-IR (NIR), the Mid-IR (MIR) and the Far-IR (FIR) regions.

The vibrations occurring in molecules are fundamental vibrations, which are quantised in specific energy levels. They can be divided in two main categories: internal and external vibrations. The internal vibrations take place within a single molecule, while the external vibrations involve two or more molecular units (they are also called lattice or crystal vibrations). Lattice vibrations have lower frequencies than the internal vibrations, in particular, those for organic compounds are usually at frequencies lower than 400 cm^{-1}. Inorganic compounds absorb at even lower frequencies due to the presence of heavier atoms. In general, as the atomic mass is increased the bond length between the atoms will be longer, and the vibrational excitation energy becomes lower (this corresponds to higher wavelength and lower wavenumbers).

The Far-IR (FIR) region is defined as below 400 cm^{-1}. Indeed, FIR spectroscopy is a well known technique used as an alternative way for collecting spectra of many inorganic pigments and corrosion products found on art objects.

Among the available techniques, the far infrared region is accessible by employing either transmission spectroscopy or attenuated total reflection (ATR). The latter allows obtaining spectra which are comparable to those in transmission mode (PE pellets) [70-71] with the great advantage of needing a much lower amount of sample and being considerably less time-consuming, not requiring any sample preparation at all.

For these reasons, in the field of Cultural Heritage, ATR measurements are desirable.

However, particular attention is required in the examination of ATR spectra: it is well known, in fact, that ATR spectra look more distorted than the transmission ones in terms of both bands intensity and shifts towards lower frequencies [72-75].

Concerning the ATR depth penetration [72-75], on the bases of the equation reported by Harrick [76-77] it can be argued that the depth of penetration of the IR beam in ATR spectroscopy is considerably higher in the FIR region than in the MIR region However n_2 is not a constant in particular for strong absorption bands and Equation 3.1 must take into consideration the effect of *anomalous dispersion* of the sample refractive index [73].

According to [74] a more fully way to express the absorbance, considering the *anomalous dispersion* explained above, is given by the following expression (Equation 3.8):

$$A = \left(\log_{10} e\right)\frac{n_2}{n_1}\frac{E_0}{\cos\theta}\frac{d_p}{2}\alpha \qquad (3.8)$$

For this reason ,strong absorption bands may shift towards lower frequencies as n_2 can change considerably and as d_p is much different on one side of the absorption band than on the other side this causes band distortion toward lower frequencies.

3.3.2 MATERIALS AND METHODS

3.3.2.1 Standard resin

All the standard materials, purchased from Kremer, are listed below:

1. Elemi
2. Shellac
3. Colophony
4. Venice turpentine
5. Sandarac
6. Copal
7. Dammar
8. Mastic

The solid samples were analyzed as samples in a powder form, collected from the bulk specimen. Venice turpentine (which is in the liquid form) was analysed only after preparing a resin film obtained by its solubilisation in ethyl alcohol and application on a glass slide support.

Two historical samples have been examined. One (BP) was collected from a yellow area of the "La Battaglia di Cialdiran", an oil painting on canvas dated back to the 16th century, the work of an unknown artist conserved in the Regional Museum of Mirto Palace, Palermo, Italy. The second (PMB7) was a gilded leather sampled from a painted wall hanging dated to the 17th century.

3.3.2.2 FarIR spectroscopy

A Thermo Nicolet Nexus 5700 spectrometer, using a solid-substrate beamsplitter operating in the FarIR region of 700-90 cm^{-1}, was employed. A Parker/Balston self-contained purge gas generator was used to minimize interference bands generated from ambient moisture. During the collection of

spectra, the outlet pressure was set at 30 psi/bar, while the outlet flow control at 9 (dimensionless).

The ATR spectra were registered by a diamond ATR Smart Orbit™ accessory (from Thermo Optec) both in the MidIR (DTGS detector with a KBr window) and in the FarIR (DTGS detector with a polyethylene window) region (Figure 3.17). The diamond crystal has a refractive index of 2.4, with a single bouncing refractive infrared beam at 45° angle of incidence. Analyses were performed on samples in a powder form by grinding the bulk resins, or in small fragments after sampling thin films from resin. Measurements were carried out at a spectral resolution of 4 cm^{-1}, with a physical mirror rate of 0.6329 cm s^{-1}. Approximately, less than 0.5 mg of material was required for each measurement. Several replicate spectra were collected for each resin specimen.

The historical samples were analysed placing the external surface of the fragments on the macro ATR crystal, simply applying a pressure to optimise the contact.

Figure 3.17 - ATR Smart Orbit™ mounted on a Thermo Nicolet Nexus 5700 spectrometer

3.3.2.3 Chemometric analysis

Spectral data were processed by principal component analysis (PCA) employing the chemometric package V-PARVUS [ref]. Matrix dataset was composed with intensity values of peaks as variables (columns) and spectra in the range 670-150 cm^{-1} as objects (rows). Standard normal variate (SNV) transformation and column centering were applied as pre-treatments on the matrix dataset. SNV was specially applied in order to remove baseline shifts and to correct for global intensity variations [80].

3.3.2.4 Analytical pyrolysis

The historical samples BP and PBM7 were analysed by off-line pyrolysis with a CDS 1000 Pyroprobe (Platinum filament coil) following the procedure proposed by Torri *et al.* [81]. Breefly, samples were pyrolysed at 700 °C for 60 seconds, evolved pyrolysis products were sampled by solid phase microextraction (SPME) with a carboxen-PDMS fiber. The fiber was inserted into the injector port kept at 280 °C of a 6850 Agilent HP gas chromatograph connected to a 5975 Agilent HP quadrupole mass spectrometer. Analytes were separated by a HP-5MS fused-silica capillary column (stationary phase poly[5% diphenyl/95% dimethyl]siloxane, 30 m, 0.25mm i.d., 0.25 µm film thickness) using helium as the carrier gas. Mass spectra were recorded under electron ionization (70 eV) at a frequency of 1 scan s^{-1} within the 12–450 *m/z* range. The following thermal program was used: 35 °C for 5 min, then 10 °C min^{-1} until 310 °C, followed by a column cleaning at 310 °C for 3 min. GC-MS traces of real samples were compared to those derived from analytical pyrolysis of standard resins.

3.3.3 RESULTS AND DISCUSSION

The use of a macro diamond accessory had three main advantages: no sample manipulation was required; the amount of sample was reduced, according with conservation purposes; the varnish applied as external layer on historical samples could be directly analysed just positioning the external sample surface onto the ATR crystal.

3.3.3.1 Standard resins

The different resin specimens have been analysed both in the MidIR and in the FarIR region. The ATR- MidIR spectra (Figure 3.18) showed extremely similar profiles.

In fact, it is difficult to identify not only the different resins but also more generic categories such as: a) sesquiterpenic resins, b) diterpenic resins containing abietane compounds, c) diterpenic resins containing polymerised communic acid, d) triterpenic resins cannot be discriminated.

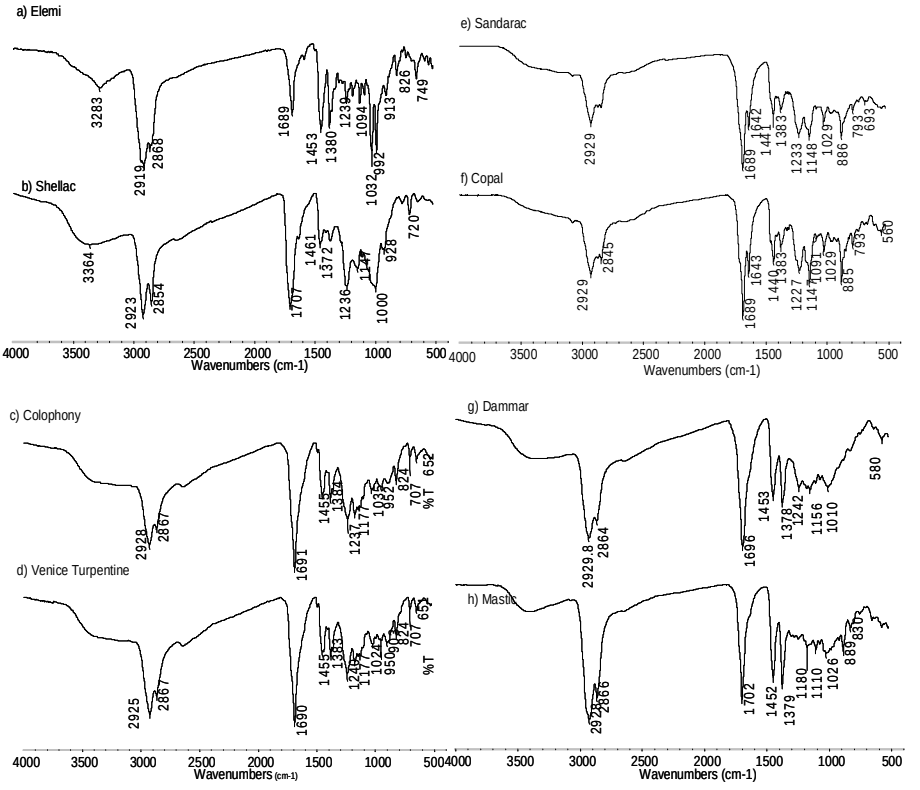

Figure 3.18 - MidIR spectra obtained in ATR of a) elemi, b) shellac, c) colophony, d) Venice turpentine, e) sandarac, f) copal, g) dammar, h) mastic

On the other hand, FarIR analyses allowed the identification of specific bands for each investigated category as shown in Table 3.1.

Elemi and shellac show characteristic FarIR spectra (Figure 3.19a, b) which allow a clear distinction between them. Some similarities, in terms of absorption values, can be observed comparing the elemi spectrum with the mastic and dammar ones, even though the resins specimens can be easily distinguished (Table 3.1).

Elemi	Shellac	Colophony	Venice turpentine	Sandarac	Copal	Dammar	Mastic	Approx assignment
				696 (m)	695 (m)		692 (w)	
				685 (m)				
					675 (m)			
		658 (s)	652 (s)			658 (m)		
663 (s)								υ CC [25]
	646 (m)						646 (m)	δ CCC [25]
638 (w, sh)						638 (m)		δ CCC [25]
		611 (w)	610 (w, sh)		617 (m)			
						601 (w)		
590 (m)								
				581 (m)	583 (m)	580 (s)	583 (s)	
	572 (m)							
562 (m)		561 (m, sh)	560 (m, sh)	556 (m)	563 (m)			δ CCO [31]
		540 (s)	538 (m)					δ CCO [25]
528 (m)						530 (s)	526 (m)	δ CCO, δ CCC [24]
				520 (m)	520 (m)			
	518 (s)							
498 (m, sh)					491 (w)			
		478 (w)	475 (w)				471 (m)	δ CCC [27]
460 (m)	460 (m)					458 (m)		δ CO [31]
		449 (w)		449 (m)	447 (m)		451 (w)	δ CCO [26,27]
433 (m)							431 (w)	

		417 (m)	422(w)					
	411 (m)							
				397 (s)	395 (s)			
		393 (m)	387 (m)					
367 (m)				363 (m, sh)	362 (m, sh)			δ CCC [31]
	356 (w)					351 (m)		
		345 (m)	347 (w)					
340 (m)	341 (w)						338 (s)	
	313 (w)			310 (w)		318 (w)		τ (CCC), τ (CCO) [24]
294 (m)	195 (w)	290 (m)	286 (m)					
							269 (w)	
265 (w)	265 (m)			260 (m)	265(m)			τ (CH_3) [26, 27]
		253 (w)	252 (m)					
						243 (m)		
229 (m)								
	212(m)				212 (m)			
				199 (m)			199 (w)	
189 (m)								
					169 (w)	169 (m)	170 (m)	

Table 3.1 - Resins absorptions in the FarIR region. s: strong; m: medium; w: weak; sh: shoulder

Diterpenic resins have a common peak at around 395 cm^{-1} but they also show particular features allowing to distinguish *Pinacea* resins, such as colophony and Venice turpentine (Figure 3.19c, d), from diterpenc resins containing polymerised communic acid, such as sandarac and copal (Figure 3.19e, f). Colophony and Venice turpentine are characterised by the presence of peaks at around 540 and 475 cm^{-1}, while sandarac and copal have peaks at 520 and 260 cm^{-1} (Figure 3.19c, f).

Triterpenic resins show significant similarities in all the collected spectra having common features, such as the peak at about 580 cm^{-1}. Some differences can be noticed between the two triterpenic resins which can be used to discriminate them, such as the band at 658, 638 and 351 cm^{-1} typical of dammar and bands at 646 and 338 cm^{-1} mainly present in mastic resin (Figure 3.19g, h).

Previous studies on the characterisation of natural resins performed by Raman spectroscopy allowed the approximate assignment of frequency values in the vibrational mode [59-68]. A comparison with the data reported in the literature was made, in order to identify possible transitions, which are detectable both by the infrared and the Raman spectroscopy. FarIR spectra are indeed different from Raman ones, but there are common absorptions. In particular the following vibrations υ CC , δ CCC , δ CCO, δ CCC, δ CO , τ (CCC), τ(CCO) and $\tau(CH_3)$ have been tentatively assigned in Table 1. The presence of vibrational modes active only in the FarIR region further confirms that the two techniques may complement each other in the characterisation of natural resins.

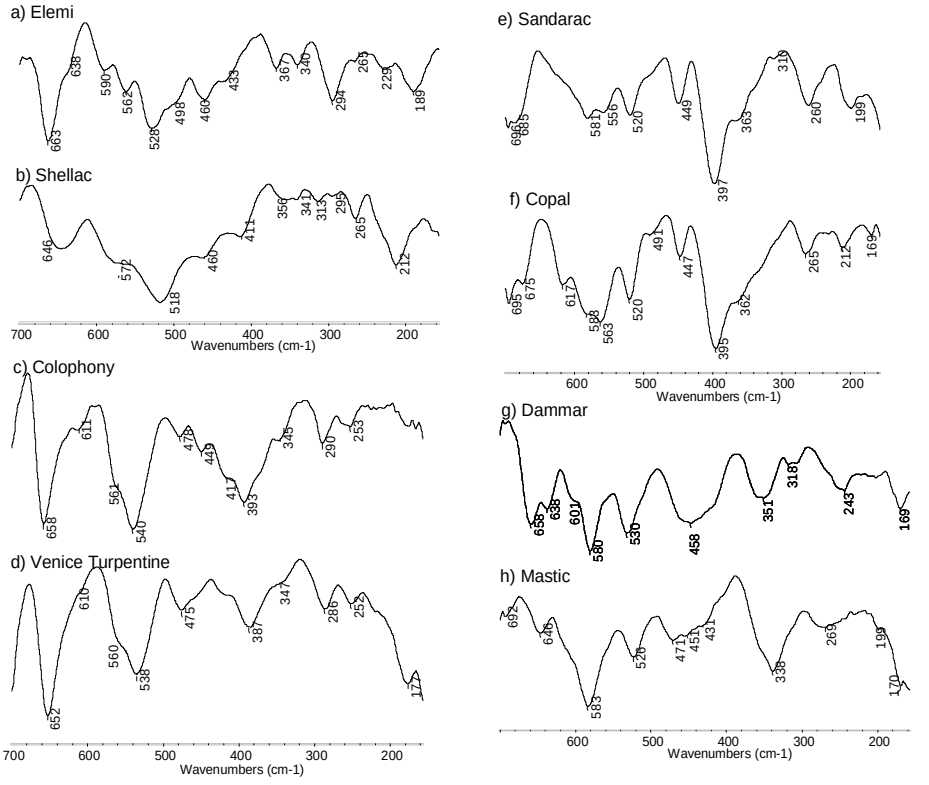

Figure 3.19 - FarIR spectra obtained in ATR of a) elemi, b) shellac, c) colophony, d) Venice turpentine, e) sandarac, f) copal, g) dammar, h) mastic

3.3.3.2 Historical samples

The cross section photomicrographs of the BP sample shown in Figure 3.20 allows to clearly identify the presence of an organic protective applied as external layer. This may be revealed by the strong whitish fluorescence visible under UV light, which is not influenced by the pollution of the embedding material because the sample was embedded in KBr [40].

Figure 3.21 shows the BP spectrum in the FarIR region obtained in macro ATR on the external surface (corresponding to layer 2 in figure 4). From the MidIR spectrum (not reported) the carboxylic acids band (1716 cm^{-1})

suggests the presence of a natural resin, but its identification resulted rather difficult.

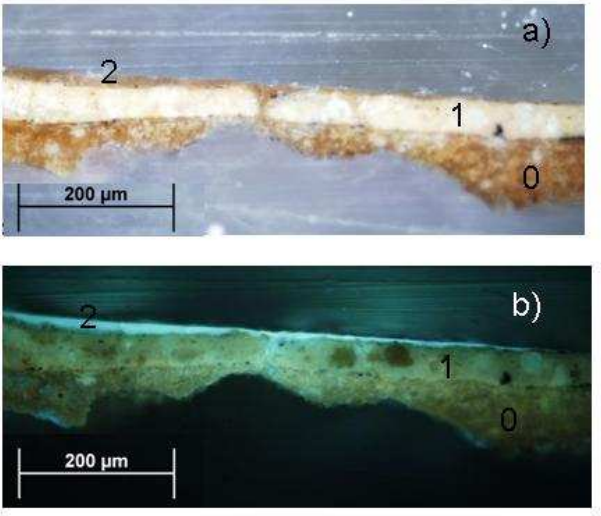

Figure 3.20 - Cross section photomicropraphs under a) visible and b) UV light of the KBr embedded BP cross section (Layer 2: varnish; layer 1: pigmented layer composed by yellow ochre, lead white, calcite, siccative oil; layer 0: preparation composed by gypsum)

The FarIR spectrum was more informative and, when comparing it with the dammar profile (Figure 3.21b), different analogies can be noticed in the position and shape of the bands (i.e., bands at 638, 580, 530, 458, 351 cm^{-1}).

The occurrence of dammar in this sample, suggested by FarIR data, was supported by analytical pyrolysis. Chromatograms in full scan obtained from off-line pyrolysis of sample BP and dammar are shown in figures 6a and 6b, respectively. A cluster of peaks with retention times and mass spectra corresponding to those of dehydrogenated sesquiterpenes $C_{15}H_{22}$ specific of dammar [47] were revealed in both of the samples. In particular, the mass

chromatograms at *m/z* 159 in Figures 3.22c and 3.22d show a peak at 19.3 min tentatively identified from its mass spectrum (Figure 3.22e) as calamenene (4-isopropyl-1,6-dimethyl.1,2,3,4-tetrahydro-naphthalene), a distinctive marker of dammar resin [82].

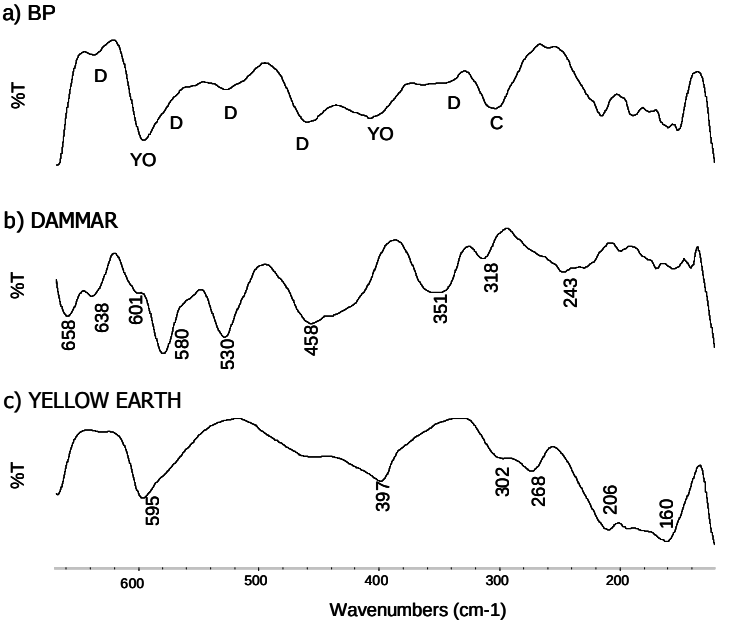

Figure 3.21 - FarIR spectra obtained in ATR of a) BP sample, b) dammar (D) c) yellow ochre (YO): C: calcium carbonate

The interpretation of FarIR spectrum was complicated by signal contributions arising from the matrix, in particular from silicate-based pigments (Figure 3.21c), such as a yellow earth (595 and 397 cm^{-1}), and calcium carbonate (307 cm^{-1}) [78]. These compounds derived from the underlying yellow layer (layer 1 in figure 4) after the sample squeesing due to the contact with the ATR crystal, as it was confirmed by micro FTIR in ATR in the MidIR range directly on the stratigraphy.

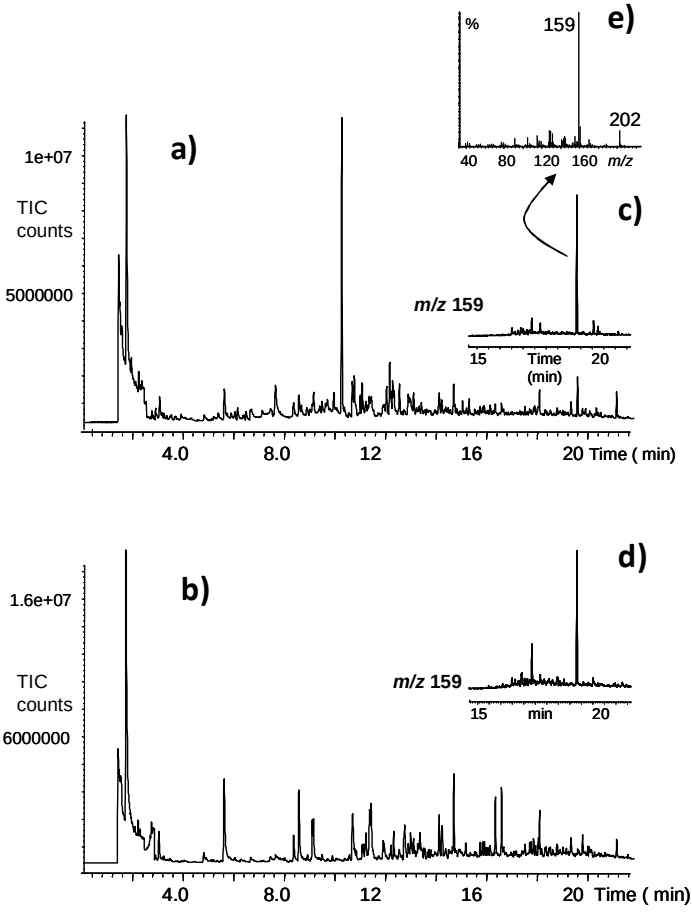

Figure 3.22 - GC-MS of pyrolysate from a) sample BP and b) dammar resin; mass chromatograms at *m/z* 159 expanded in elution region of dammar markers ($C_{15}H_{22}$ bicyclic sesquiterpenoids) of c) sample BP and d) dammar resin, e) mass spectrum of the GC peak at 19.3 min, tentatively identified as calamenene

This represents a limitation of the method because, in order to obtain meaningful spectra, it is necessary to apply a pressure which might partially disaggregate the sample. Moreover, strong absorbent inorganic salts may present bands overlapping with the signal arising from the resins. In this case

the resin layer, as shown in the stratigraphy (Figure 3.20b) is homogeneously present and, although very thin, its spectrum can be still detected. To overcome this problem, a new system is being developed, aimed at analysing small particles, sampled under the stereomicroscope from the external layer, in the transmission mode using an IR condenser.

The cross section of sample PMB7 is reported in Figure 3.23. Gilded leathers in the past were usually made by gluing a very thin leaf of tin or silver over the support, which was afterwards varnished with an oleo-resin binder (mainly shellac, sandarac or colophony) mixed with yellow dyes [2].

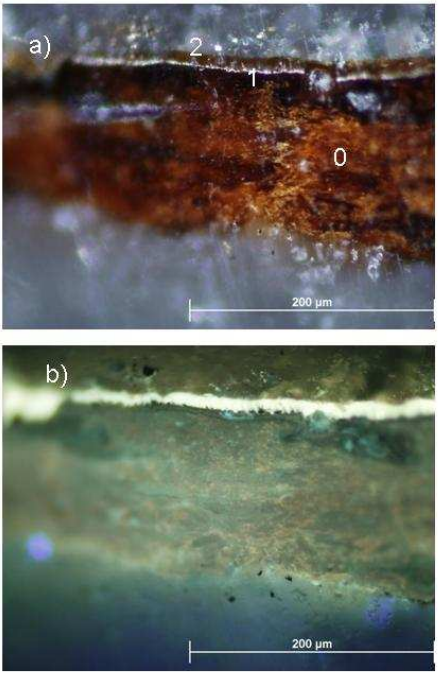

Figure 3.23 - Cross section photomicrographs under a) visible and b) UV light of the KBr embedded PMB7 cross section (Layer 2: gold varnish, Layer 1: silver leaf, Layer 0: leather)

Micro FTIR analyses in the MidIR range have been performed by reflection-absorption spectroscopy (RAS). The varnish layer is, in fact, 20 μm thick and the metallic leaf allows to reflect back the infrared light so that the final spectrum is similar to that obtained in transmission.

As for the sample BP, the presence of resinous materials is suggested by the carboxylic acids band (1704 cm^{-1}) but it is not possible to assign the spectrum to any particular resin. On the other hand, the FarIR spectrum (Figure 3.24) shows the absorption at 540 and 393 cm^{-1}, suggesting the presence of a diterpenic resin without the polimerised component (i.e., colophony or Venice turpentine). In particular, colophony appears among the ingredients mentioned by old recipes [42]. Peaks 592 and 340 cm^{-1} may derive from the underlying leather support (Figure 3.24c), while the other unknown peaks might be connected to the dye used to provide the gilded coloration.

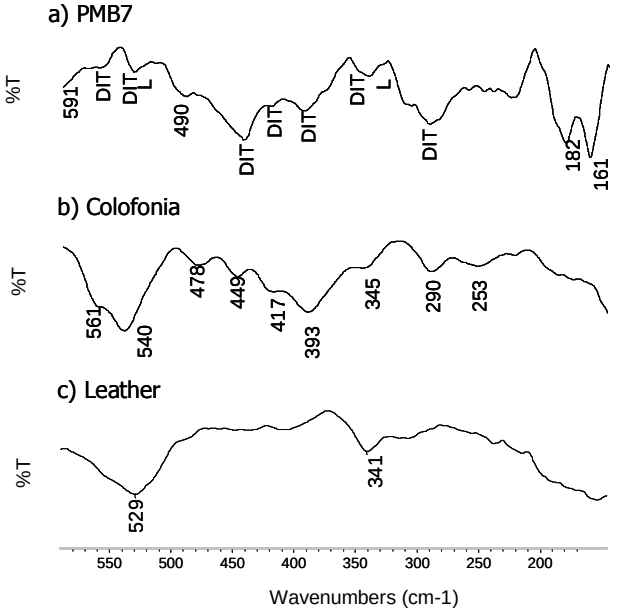

Figure 3.24 - FarIR spectra obtained in ATR of a) PMB7 sample, b) Colophony c) Leather (DIT: diterpenic resin without a polimerised component; L: leather)

Further investigations aimed at characterising the possible presence of organic dyes (i.e., saffron, aloe, antraquinonic dyes) are still being carried out by FarIR/MidIR spectroscopy as well as other techniques such as Raman spectroscopy and HPLC-DAD.

About 0.5 mg of the organic layer was scraped off from the same fragment. The sampling was performed under the UV illumination of an optical microscope, in order to better localise the higher fluorescence generated by the varnish layer. However, analytical pyrolysis of sample PBM7 failed to confirm the occurrence of resins since the MS-pyrograms were dominated by intense peaks associated to the thermal degradation products of proteins derived by the leather support.

3.3.3.3 Data analysis

A statistical multivariate analysis was performed in order to evaluate the dispersion of the data and to better characterise the different resins, since principal component analysis (PCA) is usually employed for data exploration purposes, outliers detection, visualisation of graphical clustering and evaluation of the information present in the spectral signals [83].

PCA was performed both on MidIR and on FirIR data and the results were compared. The PC12 score plot obtained with MidIR spectra is reported in Figure 3.25. These two PCs are able to clearly discriminate only some resins, such as dammar, mastic, shellac and elemi, while they are not effective for the diterpenic resins with or without the polymerised fraction. Moreover, the resins dispersion between the replica spectra is in some cases comparable with the dispersion between different standards (i.e., mastic and Venice turpentine dispersions). Furthermore, PCA is not able to correctly identify which resin is present in the historical sample BP. Indeed, the two available replicates are positioned in a region far from all of the analysed resins.

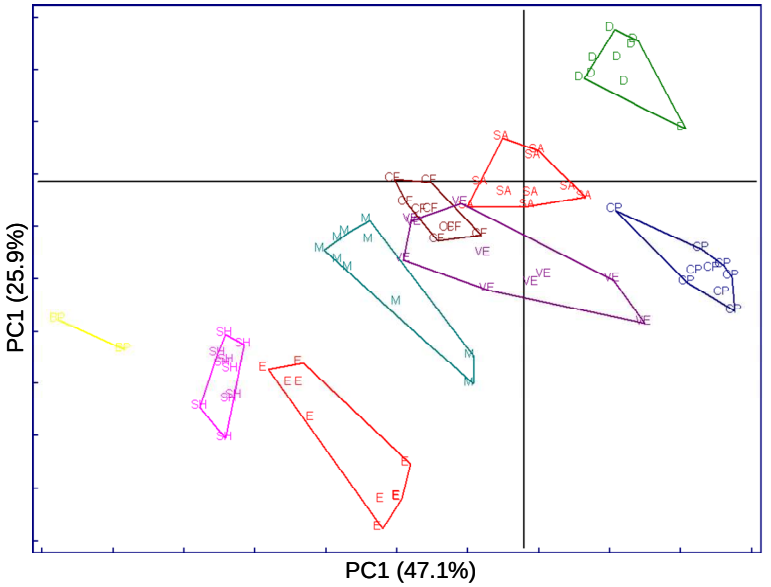

Figure 3.25 - PC12 score plot resulting from PCA of the resins MidIR spectra (minimum 9 replicates for standards, 2 replicates for the BP sample); BP: historical sample; CF: colophony; CP: copal, D: dammar; E: elemi; M: mastic; SA: sandarac; SH: shellac; VE: Venice turpentine

This may suggest that the MidIR region is more influenced by the presence of other specimens present in the historical sample, which affect the PCA results.

The PC12 score plot obtained with FarIR spectra is reported in Figure 3.26. These two PCs are able to well identify four clustered groups, thanks to the lower variability of replica spectra compared with the dispersion between the different standards. It can be noticed that the four categories described are clearly separated. The statistical multivariate approach allowed to distinguish resins belonging to the same categories (i.e., mastic from dammar, shellac from elemi). This was not true when considering diterpenic resins and diterpenic with the polymerised fraction: although copal and sandarac appeared separated, the spectral profiles resulted extremely similar and the

differences might become even less evident when analysing historical/aged samples.

PCA confirmed the interpretation also in the case for the historical sample BP. Even though the FarIR spectra contain other compounds, the four replicates are positioned within the dammar region. One replicate is slightly shifted, probably because of a greater influence by the other compounds arising for the underlying layer. It was not possible to apply PCA on the sample PMB7 because the small fragment available allowed to perform just one FarIR and Py/GC-MS analysis.

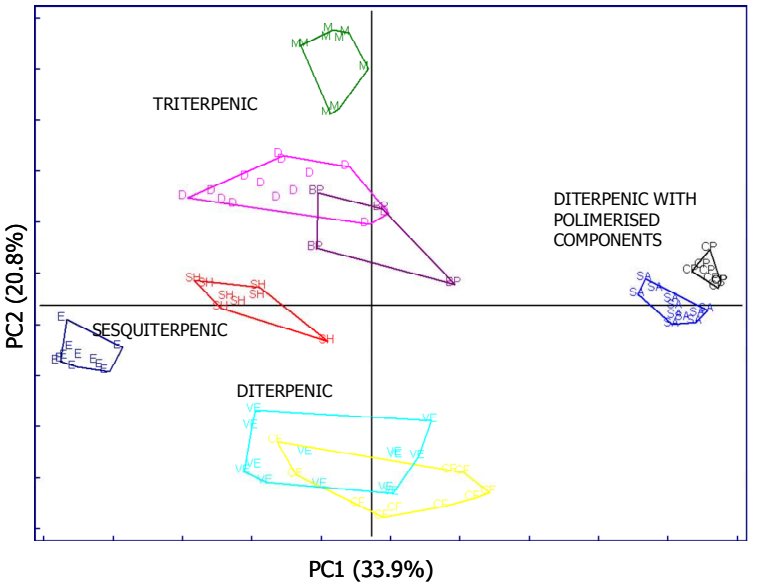

Figure 3.26 - PC12 score plot resulting from PCA of the resins FarIR spectra (minimum 8 replicates for standards, 4 replicates for the BP sample); BP: historical sample; CF: colophony; CP: copal, D: dammar; E: elemi; M: mastic; SA: sandarac; SH: shellac; VE: Venice turpentine

The Fisher weights (FW) [84-85] were calculated as discrimination indices, in order to provide an estimation of the discriminative ability of each PC in terms of separation between two categories (Tables 2, 3).

For MidIR data, the FW (Table 3.2a) were generally lower than those obtained for the FarIR spectra (Table 3.2b). This suggests that the resins were less discriminated in the former case. It is interesting to notice the high FW values calculated between the BP classes and all of the resin classes, that indicate that, in this case, PCA is unable to identify the historical sample composition.

Fisher weights referred to the FirIR spectra highlighted the discriminative ability of PC1 and PC2 in the distinction of the resin specimens under investigation, according to their chemical nature and to the information achieved from the observation of the spectra. In particular, the highest values of FW were related to the separation between clusters of different terpenic categories, while the FW of both PC1 and PC2 showed still significant but lower values within classes of resins belonging to the same category, except for colophony and Venice turpentine. Moreover, it was extremely interesting to find out that the low FW values (PC1: 1.1, PC2: 1.2) between the BP sample and the dammar spectra confirm the characterisation of the unknown varnish as dammar.

	PC1 FW	PC2 FW
CP - E	33.0	6.8
CP - M	27.4	0.0
CP - CF	40.2	2.8
CP - D	3.2	28.0
CP - SH	172.9	6.9
CP - VE	5.5	0.0
CP - SA	13.2	6.3
CP-BP	164.3	4.5
E - M	0.2	4.3
E - CF	2.3	12.8
E - D	22.0	32.0
E - SH	5.3	0.9
E - VE	2.6	6.7
E - SA	8.2	16.3
E - BP	17.4	2.9
M - CF	0.9	1.2
M - D	17.2	12.4
M - SH	8.7	2.8
M – VE	1.6	0.0
M - SA	5.5	2.7
M - BP	22.6	1.2
CF - D	25.0	17.8

a)

	PC1 FW	PC2 FW
CP - E	812.8	21.5
CP - M	316.7	45.2
CP - CF	18.7	75.0
CP - D	55.9	14.4
CP - SH	138.4	1.5
CP - VE	28.9	44.3
CP - SA	2.5	3.3
CP-BP	35.5	1.2
E - M	81.2	81.55
E - CF	18.9	26.4
E - D	10.9	50.24
E - SH	12.9	6.22
E - VE	11.6	12.9
E - SA	420	6.3
E - BP	22.18	10.3
M - CF	0.9	133
M - D	0.7	13.6
M - SH	4.5	47.7
M – VE	0.0	103.7
M - SA	146.4	56.3
M - BP	0.3	14.3
CF - D	1.7	104.8

b)

Table 3.2 - Fisher weights calculated as a measure of the between classes variance to within class variance ratio for a) MidIR spectra and b) FarIR spectra; BP: historical

sample; CF: colophony; CP: copal, D: dammar; E: elemi; M: mastic; SA: sandarac; SH: shellac; VE: Venice turpentine

3.3.4 CONCLUSION

This study allowed to propose FarIR-ATR spectroscopy as a complementary tool for the identification of natural resin. Compared with MidIR spectroscopy, FarIR analyses allow to better distinguish sesquiterpenic, diterpenic, diterpenic with polymerised communic acid and triterpenic resins. Moreover, PCA of spectral data permits in some case (i.e., dammar and mastic, shellac and elemi) to distinguish between resins belonging to the same category, although an evaluation of the spectral changes in resin derived by the oxidation and hydrolysis process occurring with ageing is being carried out to better understand the technique diagnostic performances.

Even though the ageing effect has not been evaluated yet, the method has been tested on historical case studies. In the first case (sample BP), this method allowed to confirm the results obtained with the analytical pyrolysis. On sample PMB7, the bulk analyses approach was not effective in the identification of the resin due to the strong signals arising from the leather support. In this case, FarIR spectroscopy allowed the identification of the resin. Actually, thanks to its flexibility, PMB7 sample did not disaggregate after the contact with the crystal and the analyses could be specifically focused on the external surface, even though a small influence of the leather support is present.

FIR spectroscopy has the disadvantage of producing less intense spectra and of being difficult to perform on a microscopic scale. It can be therefore used as a complementary technique to Raman spectroscopy and to the traditional FTIR spectroscopy in the MidIR region.

A particularly interesting field of application may be that of the control of the cleaning procedures during restoration.

3.4 BIBLIOGRAPHY

1. Derrick, M. R.; Stulik, D.C. (1999) Infrared spectroscopy in conservation science, The Getty Conservation Institute: Los Angeles
2. Casadio, F.; Toniolo, L. (2001) J. Cult. Heritag, 2001, 2(1), 71-78
3. Gettens, R. J. Science in the art museum, Scientific American, 1952, 187(1), 22-27
4. Low, M. J. D.; Baer, N. S., Studies in Conservation, 1977, 22, 116-128
5. Messerschmidt, R. G.; Harthcock, M.A. (1988) Infrared microspectroscopy. Theory and applications. Marcel Dekker: New York,
6. S. Prati, E. Jospeh, G. Sciutto, R. Mazzeo (2010), Accounts of chemical research, ISSN 0001-4842, vol. 43, n. 6, 792-801
7. Gillard, R. D.; Hardman, S. M. (1994) Studies in conservation, 39(3), 187-192.
8. Bruni, S.; Cariati, F. (1999) Vibrational Spectroscopy, 20, 15-25
9. Cotte, M.; Susini, J. (2008) Journal of Analytical Atomic Spectrometry, 23, 820 - 828.
10. Pilc, J.; White, R. (1955) National Gallery Technical Bulletin, 16, 73-84.
11. Langley, A.; Burnstock, A. (1999) in 12th Triennial Meeting of ICOM Committee for Conservation, James & James: Lyon, 234-241.
12. Van der Weerd, J., R.; Heeren M. A. (2004 Studies in conservation, 49(3), 193-210.

13. Griffiths P, De Haseth JA (2007) Fourier Transform Infrared Spectrometry 2rd edn. John Wiley & Sons Inc, New Jersey
14. Rosi, F. Miliani, C. Federici, A. Brunetti, B.G. Sgamellotti, A. Clementi, S. (2010) Anal. Bioanal. Chem. 399(9), 3133-3145
15. van Loon A, Keune K, Boon JJ (2005) In: Art'05 – 8th International Conference On The Non Destructive Investigations And Microanalysis For The Diagnostic And Conservation Of The Cultural And Environmental Heritage, Lecce
16. Lins A, Giannuzzi LA, Stevie FA, Price B, Tucker M, Gutman, N (2001) MRS Proc 712: 113-118.
17. Boon JJ, Asahina S (2006) Microsc and Microanal 12: 1322-1323.
18. Mazel V, Richardin P, Debois D, Touboul D, Cotte M, Brunelle A, Walter P, Laprévote O (2007) Anal Chem 79: 9253-9260.
19. Cotte M, Checroun E, Mazel V, Solé VA, Richardin P, Taniguchi Y, Walter P, Susini J (2009) e-PS 6: 1-9.
20. Bruni S, Cariati F, Casadio F, Toniolo L (1999) Vib Spectrosc 20: 15-25.
21. van der Weerd J, Brammer H, Boon JJ, Heeren RMA (2002) Appl Spectrosc 56: 276-283.
22. Dannenberg, H.; Forbes, J. W., Infrared Spectroscopy of Surface Coatings in Reflected Light, Anal. Chem., 1960, 32(3): 365-370
23. Reffner, J. A.; Martoglio, P.A., Uniting Microscopy and Spectroscopy, in Practical Guide to Infrared Microspectroscopy, Marcel Dekker: New York, 1995, 41-84
24. Lewis, L.; Sommer, A. J., Attenuated Total Internal Reflection Microspectroscopy of Isolated Particles: An Alternative Approach to Current Methods, Applied Spectr., 1999, 53, 375-380.
25. Lewis, E. N.; Treado, P. J.; Reeder, R. C.; Story, G. M.; Dowrey, A. E.; Marco, C.; Levin, I. W., Fourier Transform Spectroscopic Imaging

Using an Infrared Focal-Plane Array Detector., Anal. Chem., 1995, 67, 3377-3381.

26. Chan, K. L. A.; Kazarian, S. G., Appl. Spectrosc. 2003, 57, 381-389
27. Joseph E, Prati S, Sciutto G, Ioele M, Santopadre P, Mazzeo R (2010) Anal Bioanal Chem 396:899-910
28. Treado, P. J. and M. D. Morris (1993) Infrared and Raman spectroscopic imaging Microscopic and spectroscopic imaging of the chemical state. M. D. Morris. New York, Marcel Dekker**:** 71-108
29. Krishnan, K., J. R. Powell, et al. (1995) Infrared microimaging. Practical Guide to Infrared Microspectroscopy. H. J. Humecki. New York, Marcel Dekker**:** 85-110.
30. Harthcock, M. A. and S. C. Atkin (1988) Imaging with Functional Group Maps Using Infrared Microspectroscopy Appl. Spectrosc. 42(3): 449-455.
31. Spring M, Ricci C, Peggie DA, Kazarian S (2008) Anal Bioanal Chem 392:37-45
32. Wold, S. (1972) Spline Functions, a New Tool in Data-Analysis. Kemisk Tidskrift 84, 34-37.
33. Oliveri, P. Casolino, M.C. and Forina, M. (2010) Chemometric Brains for Artificial Tongues in: S. Taylor (Ed) Advances in Food and Nutrition Research , 61 - 2, 57-117
34. Valcárcel, M., and Cárdenas, S. (2005) Vanguard-rearguard analytical strategies. Trends Anal. Chem. 24, 67-74
35. Vlasov, Y., Legin, A., Rudnitskaya, A., Di Natale, C., and D'Amico, A. (2005) Nonspecific sensor arrays ("electronic tongue") for chemical analysis of liquids: (IUPAC technical report). Pure Appl. Chem. 77, 1965-1983
36. Fearn, T. (2009) The effect of spectral pre-treatments on interpretation. NIR News 20, 16-17

37. Taavitsainen, V. M. (2009) Denoising and Signal-to-Noise Ratio Enhancement: Derivatives. In "Comprehensive Chemometrics, Vol. 2" (S. D. Brown, R. Tauler, and B. Walczak, eds.), pp. 57-66. Elsevier, Amsterdam.
38. Savitzky, A., and Golay, M. J. E. (1964) Smoothing and Differentiation of Data by Simplified Least Squares Procedure. Anal. Chem. 36, 1627-1639.
39. Mazzeo, R. Menu, Amadori, M.L. Bonacini, I. Itié, E. Eveno, E. Joseph, E. Lambert, E. Laval, E. Prati, S. Ravaud, E and Sciutto, G. (2011) Studying Old Master Paintings: Technology and Practice. Marika Spring (ed.). Archetype Publications. London, 44-51
40. Mazzeo, R.; Joseph, E.; Prati, S.; Millemaggi, A. (2007) Attenuated Total Reflection-Fourier transform infrared microspectroscopic mapping for the characterization of paint cross-sections Anal. Chim. Acta 599, 107-117
41. Thompson DV Jr (1954) Il libro dell'arte, the craftsman's handbook of Cennino d'Andrea Cennini. Dover, New York;
42. Thomson R. (2005) In Conservation of leather and related materials, Butterworth Heinemann, 88-91;
43. Mills J.; White R. (1999) in Organic material in museum objects, 2d ed.Oxford, Butterworth Heinemann, 95-129
44. Andreotti A.; Bonaduce I.; Colombini M.P.; Gautier G.; Modugno F.; Ribechini E. (2006) Anal. Chem., 78: 4490-4500;
45. Domènech-Carbò M.T.; Kuckova S.;. de la Cruz-Canizares J.; Osete-Cortina L. (2006) J. Chrom.A 1121: 248–258
46. Doménech-Carbò M.T. (2008) Anal. Chim. Acta 621: 109–139;
47. Chiavari G.;. Fabbri D.; Prati S. (2002) Chromatographia 55: 611–616;

48. Shedrinsky S.M.; Wampler T.P.; Baer N.S. (1987), Wiene Berichte veber Naturwissenschaft in der Kunst 4: 12-25;
49. Osete-Cortina L.; Domènech-Carbò M.T. (2005) J. Chromatogr. A 1065: 265-278;
50. Manso, M., Carvalho, M.L. (2009) Spectr. Acta B 64:482;
51. Messerschmidt, R.G.; Harthcock, M.A., Infrared Microspectroscopy. Theory and Applications (1988) Marcel Dekker. New York;
52. Ricci, C.; Miliani, C.; Brunetti, B.G.; Sgamellotti, A. Talanta (2006) 69.1221-1226;
53. Bacci, M. , Sens. Actuat. B (1995) 29 (1-3) 190-196;
54. Katsibiri O.; Howe R.F. (2010) Microchem. J. 14-23
55. Feller R.L. (1954) Science 120: 1069-1070;
56. Cartoni G.; Russo M.V.; Spinelli F.; Talarico F. (2003) Annali di Chimica 93: 849–861;
57. Scalarone D.; Lazzari M.; Chiantore O. (2003) J. Anal. Appl. Pyrol. 68–69:. 115–136.
58. Nevin A.; Comelli D.; Osticioli I.; Toniolo T.; Valentini G.; Cubeddu R. (2009) Anal Bioanal Chem 395:2139–2149
59. Edwards H.G.M.; David A.R.; Brody R.H. (2008) J. Raman Spectr. 39: 966–971.
60. Edwards H.G.M.; Falk M.J.; Quye A.(1997) J. Raman Spectrosc. 28: 243-249.
61. Edwards H.G.M.; Sibley M.G.; Heron C. (1997) Spectrochim. Acta Part A 53: 2373-2382
62. Edwards H.G.M; Farwel D.W.; Daffner P.L. (1996) Spectrochim. Acta A 52: 1639-1648
63. Brody R.H.; Edwards H.G.M; Pollard A.M. (2002) Biospectr. 67: 129–141.

64. Brody R.H.; Edwards H.G.M; Pollard A.M. (2001) Spectrochim. Acta A 57: 1325-1338.
65. Vandenabeele P.; Ortega-Aviles M.; Castilleros D.T.; Moens L. (2007) Spectrochim. Acta A 68: 1085-1088.
66. Vandenabeele P.; Grimaldi D.M; Edwards H.G.M; Moens L. (2003) Spectrochim. Acta A 59: 2221-2229.
67. Vandenabeele P.; Wehling B.; Monees L.; Edwards E.; de Rev M.;. van Hooydonk G. (2000) Anal. Chim. Acta 407: 261-274.
68. Lau D.; Livett M.; Prawer S. (2008) J. Raman Spectr. 39: 545-552
69. Karr C.; Kovach J.J. (1969) Appl Spectrosc 23:219-223
70. Kendix, E.; Moscardi, G.; Mazzeo, R.; Baraldi, P.; Prati, S.; Joseph, E.; Capelli, (2008) J Raman Spectrosc. 39: 1104–1112;
71. Kendix, E.L.; Prati, S.; Joseph, E.; Sciutto, G.; Mazzeo, R. (2009) Anal. Bioanal. Chem. 394: 1023-1032;
72. Reffner JA, Martoglio PA (1995) In: Humecki HJ (ed) Practical Guide to Infrared Microspectroscopy. Marcel Dekker, New York, pp 41–84;
73. Averett LA, Griffiths PR, Nishikida K (2008) Anal Chem 80:3045–3049
74. Nunn S, Nishikida K (2003) Thermo Scientific Application Note 01153
75. Harrick NJ, du Prè FK (1966) App Opt 5:1739–1743
76. Harrick NJ (1965) J Opt Soc Am 55:851–857
77. Vahur, S.; Knuutinen, U.; Leito, I. (2009) Spectrochim. Acta A 73: 764–771;
78. Vahur, S.; Knuutinen, U.; Leito, I. (2010) Spectrochim. Acta A 75: 1061-1072;
79. Prati, S.; .Joseph, E.; Sciutto, G.; Mazzeo, R. (2010) Acc. Chem. Res. 43: 792–801;
80. Barnes J.; Dhanoa M.S.; Lister S.J. (1989) App. Spectrosc. 43:772-777;
81. Torri C.; Fabbri, D.; (2009) Microchem. J. 93: 133–139;

82. Dutta S., Mallick M., Bertram N., Greenwood P.F., Mathews R.P. (2009) Intern. J. Coal Geol. 80: 44–50;
83. Esteban M, Arino C, Diaz-Cruz JM (2006) Trends Anal Chem 25:86–92;
84. Harper AM, Duewer DL, Kowalski BR, Fashing JL (1977) In Kowalski BR (ed) Chemometrics: Theory and Application, ACS Symposium;
85. Oliveri, P.; Baldo, M. A.; Daniele, S.; Forina, M. Anal. Bioanal. Chem. (2009) 395:1135–1143.

Chapter 4

SAMPLE PRE-TREATMENTS:

DEVELOPMENT OF NEW SAMPLE CROSS-SECTION PREPARATION PROCEDURES

As already highlighted, the characterisation and localisation of different layers in a complex paint matrix are fundamental for achieving a profound knowledge of the nature and conditions of constituent materials, aiming at taking adequate decisions on the conservation and preservation procedures to be adopted.

On these bases, the preparation of sample cross-sections represents a crucial step in the examination of stratigraphies. In fact, the small and fragile paint chip collected from the artwork surface needs to be embedded in a support, which should be able to hold the sample in the correct orientation. The embedding procedure is accomplished by grinding, polishing or microtoming the block to produce either cross-sections or thin sections, discovering the complete layer structure to be submitted to analysis. In particular, the observation of mounted paint cross-section under optical microscopy allows the recognition of painting structure and morphology, providing information on the painting technique, overpainting and other restoration measures, prior to the application of specific elemental and molecular investigations.

To this aim, different types of synthetic resin have been widely employed. In particular, in the mid-twentieth century, [1] polyester resin was introduced and it is nowadays commonly used in the investigation of cultural objects.

On the other hand, the stratigraphical characterisation of the organic substances may be considerably limited by the sample preparation. In fact, organic substances, used as binders or varnishes, are usually a minor

constituents in samples. Furthermore, embedding polymeric media can interact with them, due to the pollution phenomena which can arise during the preparation processes.

Even if in some cases the infiltration effect can be considerated optimal, thanks to the consolidation effect that is particularly useful in the polishing and microtoming approaches (allowing the preservation of their physical integrity during polishing), it is well known that absorption bands from the polymer embedding resin may influence FTIR spectra. This is due to the high sensitivity of infrared spectroscopy to the presence of infiltrated resin.

In fact, this can negatively affect the characterisation of the organic components with special reference to the outermost varnish layer and preparation ground. For example, when the cross-section is analysed with spectroscopic techniques, the resin absorption bands may overlap with those characteristic of the organic paint components, affecting the results and requiring particular attention in the interpretation. In many cases, the strong absorption bands of synthetic resins in the middle infrared region makes the identification of a binder very difficult or impossible, since it is usually present in very low concentration in the paint stratigraphy, showing small marker peaks.

The contribution of the resin may be removed by mathematical subtraction of its spectral profile from the sample spectrum [2]. However, this process is critical and requires particular attention in order to avoid gross errors, such as over-subtraction and lose of information.

Moreover, it is worth noting that sample materials may show a partial solubility in liquid prepolymer [1]. In particular, problems were reported to occur in the identification of wax-based finishing layers [3], due to the high capability of the embedding medium to dissolve such natural organic substances.

The penetration of liquid embedding plastic in the porosities and cavities of samples may also affect the visual examination of stratigraphies under optical microscope [1], causing discoloration and darkening of the sample especially in white and ground preparation layers.

In an attempt to overcome such drawbacks, alternative materials were evaluated and tested.

The use of infrared-transparent salts as embedding materials for cross-sections was deployed in order to avoid the contamination of the embedding resin and to improve the detection of organic substances, thanks to their transparency within the diagnostic region (4000 – 400 cm^{-1}). First attempts focused on the potentialities of potassium bromide (KBr), which is the traditional salt employed in transmission analysis – performed on pellets obtained by grounding the sample together with KBr powders and applying a pressure with a hydraulic press.

Pilc and White proposed the KBr thin section preparation method [2]. Difficulties in the preparation of layered samples have been reported concerning the lack of flexibility for microtome sectioning of such inorganic materials. In fact, the attempts to expose the paint surface by cutting thin sections have proven generally unsuccessful due to the brittle nature of KBr. In a more recent publication, a new method was proposed for the preparation of a thin cross-section embedded in KBr, by polishing the pellet on both sides until a thin slide remains [4]. The procedure, based on the well-known approach in petrography, proposed a cold-flowing KBr to act as a glue.

The performances of a different salt have been investigated – silver chloride (AgCl), which showed particular advantages thanks to its softness and malleability, avoiding the high pressure necessary in the KBr embedding method. However, darkening and accelerated corrosion processes determine the requirement for a rapid examination of the samples. In fact, silver

chloride is sensitive to light and this makes the preparation difficult, limiting the possibilities of inspecting the fragment being sectioned.

Recently, a variation of the already reported KBr thin section preparation method was proposed, together with other infrared transparent salts, for the analysis of cross-sections in ATR mode [5]. The study reveals that the procedure, the detection of organic substances, is significantly improved thanks to the absence of a contaminating embedding material. In addition, the KBr embedding system also leads to better observations of paint cross-sections under ultraviolet illumination, thanks to the absence of the embedding resin fluorescence contribution.

The KBr cross-section is prepared by means of a macro-micro pellet die (Figure 4.1). First, some KBr powder is pressed into the pellet under a low pressure (2 tons for 30 sec) in order to achieve a soft base where to transfer the multi-layer fragment. The paint fragment is then positioned with the surface parallel to the base and more KBr powder is added. After a second low pressure application (3 tons for 2 minutes), the pellet (13 x 3 mm) is extracted and dry-polished transversally using a specifically developed brass holder equipped with silicon carbide cards with successive grid from 1,000 up to 12,000.

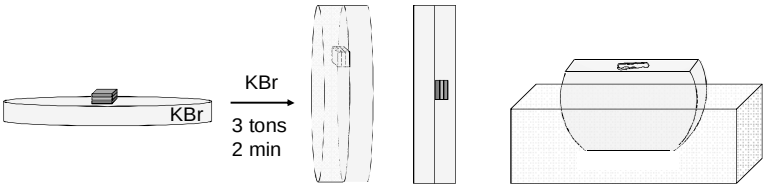

Figure 4.1 - Preparation of paint cross-sections embedded in KBr into a macro-micro pellet die: the sample is positioned parallel to a KBr pellet previously gently pressed. Some KBr powder is added to cover the sample and all the system is pressed into a new pellet which is further inserted in a polyester resin support and polished.

However it is important to note that KBr is a hygroscopic material and, consequently, the spectral quality is reduced during the acquisition and the effect is particularly detectable during the first 20 minutes of FTIR measurements. Therefore, other infrared salts presenting a minor hygroscopicity were investigated, such as calcium fluoride (CaF_2) and barium fluoride (BaF_2) [6].

Both for CaF_2 and for BaF_2, the embedding procedures were adapted to compact the salts in pellets. Nevertheless, the results achieved with CaF_2 were not successful, as the paint fragment embedded was not visible. The signal-to-noise ratio (S/N) value between 4000 and 3800 cm^{-1} were measured for a period of 2 hours, mapping an area on the preparation layer of similar paint fragments embedded in either KBr or BaF_2.

The BaF_2 embedded sample shows, after about 60 minutes, a rather low improvement of the spectral quality with respect to KBr and, furthermore, the pellet appears to be more fragile.

On the other hand, the polishing procedure is still a delicate step, due to the high fragility of the inorganic salts, if compared with an organic resin.

As an alternative to the KBr embedding system, various barrier coatings have been tested to prevent the infiltration of the embedding resins [7]. Recently, cyclododecane ($C_{12}H_{24}$) was proposed as a temporary consolidant to prevent the embedding resin pollution [8]. Cyclododecane has been used in the conservation field mainly as a temporary consolidant or hydrophobic barrier coating for aqueous treatments of water-sensitive works of art, thanks to its capability to sublimate at room temperature [9-10]. The proposed method foresaw the consolidation of the porous sample with a saturated solution of cyclododecane in toluene (80% w/v) or with melted cyclododecane. The sample was subsequently embedded in resin and cut by microtomy. The cross-section was not analysed before 24 hours had passed, allowing time for

the complete sublimation of cyclododecane. Even if the proposed method limits interferences from embedding materials, the authors also report different drawbacks such as the significant sample manipulation required, and the possible reduction of the sample stability after sublimation of cyclododecane.

Another key issue to be considered is the cross-section roughness when FTIR microscopy, both in ATR and reflectance mode, has to be performed. Indeed, its optimisation could allow a better ATR crystal/sample surface contact or optimise diffuse reflection effects.

Planar surfaces enable the maximisation of the specular components, which is responsible for the presence of distorted peaks, which appear with a first-derivate-like shape [11]. Corrections such as the Kramer-Kroming's (K-K) transform algorithm [12] is applicable, to convert reflectance spectra into transmission ones. However, if a diffuse reflection component is present at some point due to a different local roughness, the correction does not allow one to obtain readable spectra [13]. Another strategy may be to obtain a rough enough surface in order to maximise the diffuse reflection.

Some research studies have already been carried out by employing the fast ion milling (FIM) [14-17] or controlled sample polishing systems [4], even though a complete standardised and repeatable method has not been so far developed.

The present research work focuses on the comparison of traditional preparation procedures in terms of superficial morphology and pollution of the sample and on the development of alternative approaches.

In particular, starting from the previous results obtained in our research group, a particular attention has been devoted to the performances of the infrared-transparent salt sodium chloride (NaCl) as the embedding material, thanks to the encouraging preliminary results obtained. In fact, the

investigated system showed high performances in terms of physical stability. Moreover, it is less hygroscopic than the KBr.

Concerning the evaluation of different polishing approaches, standard samples – obtained with a layer of lead white mixed with oil on a gypsum ground and embedded in various materials (by the application of traditional and alternative systems) – were polished under different conditions. In particular, both wet and dry procedures were deployed, in order to evaluate the effects of water interaction with the paint components and of the spreading of materials over the paint layers during the dry polishing.

At the same time, an attempt was made to overcome drawbacks related to the use of water as a lubricant and cooling medium.

Finally, the well-known KBr embedded method was optimised using the inorganic salt as a barrier against the resin infiltration. In fact, the double embedding system (with KBr and polyester resin) increases the physical stability of inorganic salts and it is also suitable to be employed as a polishing sample holder.

A particular attention has been focused on the use of an advanced polishing system in order to compare its performance in terms of roughness surface and pollution with the traditional approaches. To this aims, different sample typologies have been submitted to the argon ion milling polisher, evaluating the effectiveness in combination with different embedding methods.

Argon ion milling is a conventional approach in the preparation of mineral sections thinned to electron transparency for transmission electron microscope (TEM) analysis [15]

More recently, the cross section polisher (CP) system has been also employed in the preparation of paint cross-section trough a broad argon ion beam [16-17].

The system consists of a specimen chamber with a TMP vacuum system, an optical microscope for sample positioning. After evacuating the specimen chamber, the investigated region is irradiated with a broad argon ion beam with an accelerating voltage range of the beam between 2 and 6 kV. In order to prevent beam striations and to achieve uniform etching in heterogenous samples characterised by the presence of materials with different hardness, the specimen stage can be rotated by 30 degrees during the ion beam milling, and the specimen stage can be rocked by 30 degrees [16].

The main advantages of this system are related to the high quality of the sample surface, which can be obtained without the pollution of embedding media.

Moreover, it has been demonstrated that the improvement of surface quality allows the recognition of complex structures and particle dispersed into a layer.

4.1 APPLICATION OF IMAGING TECHNIQUES FOR THE COMPARISION OF DIFFERENT PAINT CROSS-SECTION PREPARATION PROCEDURES

In order to compare the performance of different preparation procedures and their effects on the sample superficial morphology and with regard to the embedding media pollution, a round-robin was organised in the frame of the European project CHARISMA. In detail, a sample collected from a wooden panel painting was divided into 6 small fragments, which were sent to each of the involved partners.

The cross-sections were investigated by the application of an integrated analytical approach aimed at evaluating the effects on the sample surface and on the outcomes for each methodology. Optical microscopy, environmental scanning electron microscopy (ESEM), and laser confocal microscopy were used together with FTIR microscopy, both in ATR and in total reflectance modes.

4.1.1 MATERIALS AND METHODS

4.1.1.1 Sample ROND13

The sample was collected from a painted wooden panel attributed to Baldassarre Carrari (1460-1516) and exposed at the MAR (Art Museum of Ravenna city, Italy). The sampling area is located in the gilded halo of the Virgin (Figure 4.2).

The sample ROND13 shows a complex stratigraphy characterised by the superimposition of several layers. Figure 4.3 shows the micro-photomicrograph acquired under optical microscope of one of the cross-sections, while the descriptions of the different layers are reported in Table 4.1.

Figure 4.2 - a) Virgin with Christ and Saints by Baldassarre Carrari, 1570 (MAR Museum, Ravenna, Italy), b) Magnification of the sampling area

In detail, under optical microscope it is possible to observe a white ground (layer 0) with a grey layer on the top (layer 1). Three green layers are evident, each of them characterised by a different tonality (layer 2, 3 and 4). A further brownish layer (layer 5) is present and it is probably related to the gold foil as a mordant. The uppermost discontinuous layer (layer 6) is easily recognisable under UV illumination thanks to its bluish fluorescent colour.

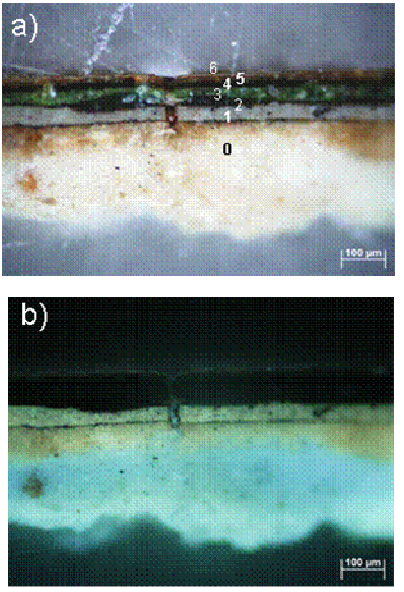

LAYER	THICKNESS (µm)	COLOUR
6		Brown
	2-3	Gold leaf
5	10-15	Beige-brown
4	15	Dark green
3	15-30	Light green
2	8-40	Dark green
1	30	White grey
0	-	Brownish White

Figure 4.3 - Sample ROND13: microphotographs of the cross-section (original magnification 200x): a) image under visible light; b) fluorescent image under UV illumination (330 – 385 nm). Table 4.1: description of ROND13 paint stratigraphy

4.1.1.2 Sample preparation procedures

The different embedding and polishing procedures, which were applied on small fragments of the same real sample by the various laboratories involved, are reported in Table 4.2.

SAMPLE NAME	EMBEDDING MATERIALS	POLISHING PROCEDURES
ROND13_1	1. Epoxy resin	Silicon carbide grinding for wet grinding using different *grit sizes (up to 4000)*
ROND13_2	1. PVA to fix the sample 2. Polymethyl methacrylate 3. Plexiglas (PMMA) cubes	Silicon carbide grinding for wet grinding using different *grit sizes (up to 4000)*
ROND13_3	1. KBr pellets	Silicon carbide grinding for dry grinding using different *grit sizes (up to 12000)*
ROND13_4	1. KBr pellets	Silicon carbide grinding for dry grinding using different *grit sizes (up to 4000)*
ROND13_5	1. Cyclododecane ($C_{12}H_{24}$) coating 2. Epoxy resin	Removal of resin excess by cutting (no polishing procedures were performed)
ROND13_6	Polyester resin	Argon ion milling

Table 4.2 – Embedding and polishing procedures investigated

The sample ROND13_2 was prepared following a procedure optimised at the KIK IRPA institute (Belgium), shown in Figure 4.4. A plexy glass bar was sawn

into cubes of 1 cm^3 (A), then the sample was fixed on its cube with a drop of PVA glue (B). At this stage a small quantity of resin was applied (C). After a few minutes, a second cube was positioned on top of the resin without applying too much pressure in order to preserve the sample integrity (D). The cross-section obtained was then polished (E).

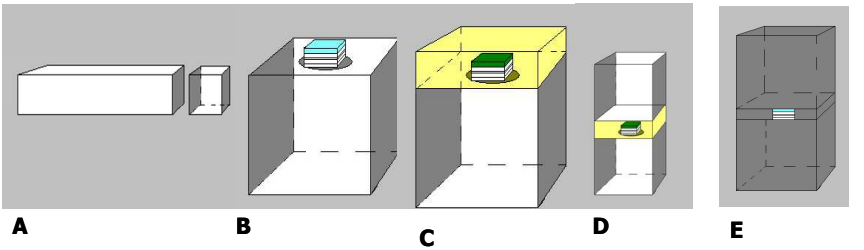

Figure 4.4 - Scheme of ROND13_2 embedding procedure

Both of the KBr embedded samples (ROND13_3 and ROND13_4) were prepared following the already reported procedures. The polishing approach was performed by two different operators up to different grit sizes.

The procedure for the preparation of the sample ROND13_5 is based on the use of cyclododecane ($C_{12}H_{24}$), a commercially available cyclic alkane, which melts at 58°C, dissolves in a wide number of low-polarity solvents, and sublimates at room temperature [8]. After the consolidation of the sample using a saturated solution of cyclododecane in toluene (80% w/v) applied under vacuum, a barrier coating was produced with melted cyclododecane, to ensure complete encapsulation and prevent resin infiltration. The resin-embedded sample was dried by exposure to blue light (440 nm), and the block was microtomed to reveal the sample stratigraphy.

The last sample (ROND13_6) was prepared by embedding the paint chip in polyester resin and polished using a JEOL cross section polisher (CP) (Figure 4.5). The sample area was submitted to the argon ion beam for 12 hours.

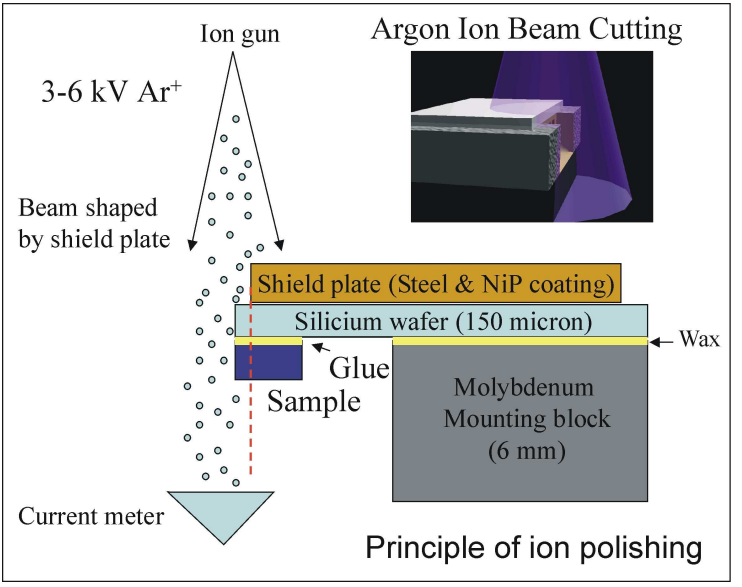

Figure 4.5 - Polyester resin embedded sample submitted to the argon ion milling, scheme of the technique principles (courtesy of JEOL Europe, Paris)

4.1.1.3 Optical microscopy

Dark field observations were performed using an optical microscope Olympus BX51M equipped with fixed oculars of 10x and objectives with different magnifications (5, 10, 20, 50, and 100x). Visible and ultraviolet light were respectively provided by a 100 W halogen projection lamp and an Ushio Electric USH102D lamp. Cross-section photomicrographs were recorded with a digital scanner camera Olympus DP70 directly connected to the microscope.

4.1.1.4 Confocal Laser Scanning Microscope

The documentation of sample surface morphologies were carried out with the use of a LEXT microscope purchased from Olympus, equipped with a motorised revolving to prevent contact with a specimen during an objective lens change. The 408 nm laser diode was combined with optics specifically designed for operation at this wavelength. 2D and 3D colour images were acquired at different magnifications (5, 10, 20, and 50x) by a combination of the laser image with the full colour bright field image in the computer system.

4.1.1.5 Scanning electron microscope

The elemental analysis have been carried out using a Zeiss EVO 50 EP extended pressure scanning electron microscope (EP-SEM) equipped with an INCA EDX detector. Due to the environmental pressure operation (70 Pa), no conductive coating was needed and the cross section has been directly analysed without any further preparation.

The parameters have been set at a 25 kV accelerating voltage, with a working distance between 9 and12.5 mm. Both backscattered (BSE) and secondary (SE) electrons images have been acquired for surface documentation and characterisation.

The INCA energy software has been used for acquisition and elaboration of data.

4.1.1.6 ATR-μFTIR mapping analysis

A Nicolet iN™10MX raster scanning microscope, fitted with an MCT detector cooled by liquid nitrogen, was used in order to perform ATR mapping. The mapping measurements were performed both in reflection and in ATR mode, using a slide-on ATR objective with a conical germanium crystal, in the range 4000–675 cm^{-1}, at a spectral resolution of 4 cm^{-1} and with 32 scans. For all

of the investigated samples, an aperture of 60x60 µm (corresponding to an investigation area of about 15 µm for each point of analysis) was employed, with a step of 7 µm in the x-y direction. The dedicated software OMNIC Picta™ (Thermo Fisher Scientific, Waltham, MA, USA) was used for the manipulation of the set of spectra collectively.

4.1.1.7 Chemometric analysis

Spectral data were processed by principal component analysis (PCA) and by employing the chemometric package V-PARVUS [19].

For reflectance spectra, a matrix dataset was composed with intensity values of peaks as variables (columns) and spectral vectors in the range 1800 - 700 cm^{-1} as objects (rows). A mean centering was performed as the column preprocessing on the data matrix, prior to PCA. In order to investigate the spectral physical differences, no row pre-treatments were applied. Their effects, in fact, are usually related to the magnification of chemical compositional variability, minimising the physical distortions [20].

In the chemometric analysis of ATR spectra extracted from the light green layer (layer 3), a total of 235 spectra extracted from chemical maps were utilised in the spectral range of 3800 – 2750 cm^{-1}, and 1800 – 700 cm^{-1}. A second order derivative and column centering were applied as a row and column pre-treatment on the matrix dataset in order to correct for baseline shifts and drifts [21].

4.1.2 RESULTS AND DISCUSSION

4.1.2.1 Evaluation of sample morphology

Confocal microscope analyses highlighted the negative role played by water when used as a lubricant during the polishing procedure. The effect is dramatic in the presence of water soluble materials, such as the gypsum grounds or proteinaceous binding media. Thus, the use of water can be considered as a relevant discriminating factor in the different approaches.

In Figures 4.6a and 4.6b, 3D confocal laser microscopy images of the two samples polished in wet conditions are reported (ROND13_1, ROND13_2). It can be noticed that the irregularity of the surface is localised, as expected, at the level of the preparation composed of gypsum.

On the other hand, the sample ROND13_5, which was obtained by microtoming, shows a similar effect and discontinuities probably due to different materials hardness.

Samples obtained by cutting argon ion milling (ROND13_4) and dry polishing (ROND13_5, ROND13_6) present a more regular and flat surface.

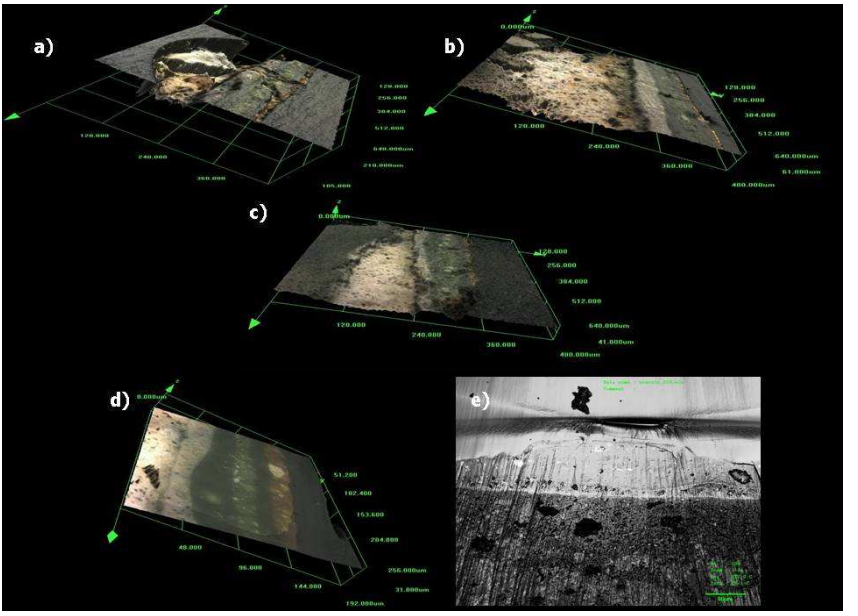

Figure 4.6 - 3D confocal microscopy images of a) ROND13_1, b) ROND13_2, c) 3D confocal microscopy images of ROND13_5, d) 3D and e) 2D confocal microscopy images of ROND13_6

The sample ROND13_4 shows a planar sample surface in the 3D confocal image (Figure 4.6d), while a sort of curling effect is appreciable in the 2D confocal image (Figure 4.6e), due to a difference in the etching rate, probably derived by the presence of voids in the sample.

To evaluate the effect of polishing, the two samples were prepared by different laboratories using different card grit (up to 12,000 for the sample ROND13_3, up to 4,000 for the sample ROND13_4).

As expected, the polishing procedure clearly affects the sample morphology, as shown by the bidimensional image obtained in confocal microscopy (Figures 4.7c,d). In the sample ROND13_4, in fact, the marks produced by the polishing procedure on KBr splattered on paint layers are clearly visible.

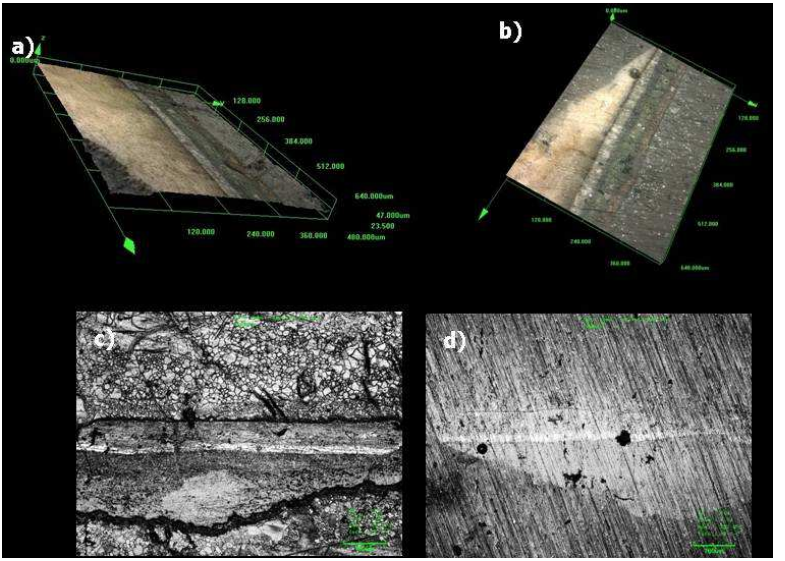

Figure 4.7 - Confocal microscopy images of a) 3D, ROND13_3, b) 3D, ROND13_4, c) 2D ROND13_3, d) 2D, ROND13_4

ROND_13 cross sections were analysed by μFTIR in the reflection mode with the aim of evaluating how the sample preparation affects the repeatability and the reproducibility of the spectra measured in each single layer. In particular, spectra were acquired on the layer 4, and processed by principal component analysis (PCA). The chemometric analysis was applied just to compare the data dispersion in the frame of each sample, rather than to compare the position of each group, which might be affected by several factors. It is known, in fact [9], that reflection spectra are highly influenced by the sample morphology.

PC12 plots show that the sample preparation has a considerable effect on the data repeatability. In particular, the spectra registered on ROND13_3 and ROND13_6 are the less dispersed (Figure 4.8).

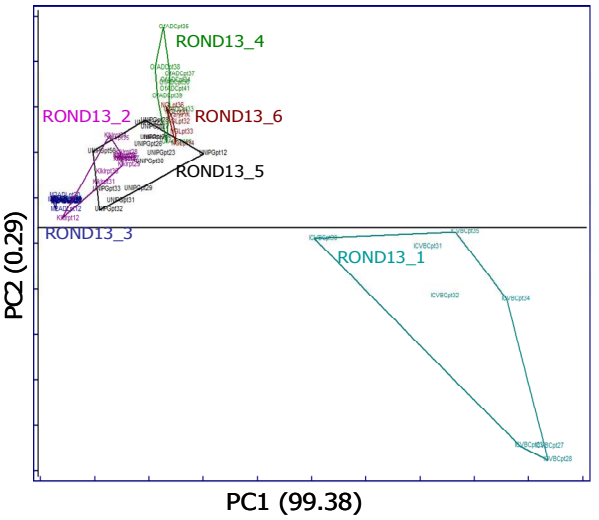

Figure 4.8 - PC12 score plot performed on spectra acquired in total reflection mode on layer 4

4.1.2.2 Evaluation of the sample pollution and location of organic and inorganic substances

Micro ATR mapping analyses were performed on all the samples, in order to understand how preparation methods interferes more in the localisation of the different organic and inorganic components.

In Table 4.3 the composition of the different layers is reported, with the indication of the bands employed to obtain the false colour chemical maps. The sample is composed of a gypsum preparation (layer 0). A layer composed of lead white mixed with a lipidic binder is applied on it (layer 1). Three green layers (2-4) are subsequently present and are related to the seat painted under the Virgin. They are composed by copper acetate or resinate with lead white and a small amount of calcite in an oily binder. Both copper and lead carboxylates can be detected in the FTIR spectrum. Copper acetate-resinate bands (around 1605 and 1445 cm^{-1}) can be detected only as shoulders in some cross-sections, however its presence was confirmed by micro Raman

analysis (data not shown). In all of the samples, spectra related to layers 2-4 are dominated by the bands at 1550 cm^{-1} and 1404 cm^{-1}, suggesting the presence of lead acetate, which may be formed by the interaction of the original verdigris and lead white. The correct assignment of the bands and the interaction between copper acetate and lead based pigments is still under investigation.

Layer n.	***Thickness (μm)***	**Colour**	**Composition**	**FTIR marker band**
6		Brown	Calcium oxalate Silicate	1321 911
	2-3	Gold leaf		
5	10-15	Beige-brown	Bole Lead white Calcite Lipidic binder	3695 837 870 1740
4	15	Dark green	Copper acetate-resinate Lead acetate Lead white Lipidic binder	1602 1550 837 1740
3	15-30	Light green	Copper acetate-resinate Lead acetate Lead white Lipidic binder Copper oxalate	1602 1550 837 1740 1321
2	8-10	Dark green	Copper acetate-resinate Calcium oxalate Lead acetate Lead white Lipidic binder	1602 1321 1550 837 1740
1	30	White grey	Lead white Lead carboxylates Lipidic binder	837 1740
0	400	Brownish White	Gypsum	1160

Table 4.3 – Compositional layer description of ROND13 stratigraphy. For each component, the FTIR marker bands used for the creation of chemical false colour images are reported

A layer of bole and oil was applied onto the green background (layer 5) to fix the gold leaf of the Virgin's halo. It can be noticed that only in the two samples embedded in KBr – ROND13_3 and ROND 13_4 – the uppermost layer of varnish can be seen. In the other samples, the varnish might have been covered by the embedding medium or completely dissolved due to the interaction. Only from the ROND13_3 sample, it was possible to obtain spectra from the external layer, which suggest the presence of oxalates arising by deposition or by deterioration of the organic protective and silicates.

Two problems occurred during the ATR mapping on the different samples:

- displacement of the investigated area due to the movement of the crystal (registration of spectra from an area different from the selected one);
- achievement of good contact between crystal and sample surface (which affects the quality of spectral signal).

The crystal can move due to several factors:

- if the surface is irregular with areas at different levels;
- if it comes into contact with materials of different hardness.

Moreover, the spectral profile depends on the sample morphology and, in particular, on the contact between the internal reflection element and the sample.

In all of the samples, an area comprising the gypsum preparation layer was selected for mapping. A slight movement of the crystal was registered in each cross-section. In the organic resin embedded samples ROND13_1, ROND13_2, and ROND13_5, the displacement of the crystal might be due to the irregularities present in the preparation layer. In the first two samples, the lack of planarity is due to the wet polishing treatment, while in the cut, sample areas at different levels are present, mainly in the layer 0, which is the most porous and the least hard. Moreover, in these three samples, there

is no contact between the crystal and the preparation layer. In the ROND13_1 sample, which from the confocal microscope appears to be the least irregular one, no signal can be registered in layer 1.

The false colour correlation maps of the embedding media (data not shown) clearly show that both ROND13_1 and ROND13_2 are affected by the resin pollution, even if, in the last case, the contamination seems to be less evident. Consequently, the map ester and the acid bands related to the organic binder in both of the samples cannot be discriminated from the contribution of the embedding resin.

In the sample ROND13_5 it was found that cyclododecane, after having exerted its barrier action, indeed sublimates at room temperature within a few hours, leaving no trace. Moreover, the use of the cut method prevents the spreading of the resin due to the polishing procedure. μ-FTIR ATR analyses show that the treatment seems to be effective in reducing the sample pollution, enabling the mapping of the organic components. Indeed, only the external layer is partially contaminated.

In the two KBr embedded samples (ROND13_4 and ROND13_5), the ATR displacement occurred, probably due to the fact that KBr is particularly soft, so as the crystal may partially sink. However, thanks to the uniform planarity all over the sample, the preparation layer could be easily mapped. In ROND13_4, the employed KBr resulted to be contaminated by an unidentified compound characterised by absorptions at 1725, 1270, 1120, and 830 cm^{-1}. It can be noticed that, due to the dry polishing, the sample is polluted by KBr, and the band at 1725 cm^{-1} prevents the identification of the organic substances. On the other hand, in the ROND13_5 sample, pure KBr was employed and this allowed an easy mapping and identification of the organic substances. However, even in this sample, KBr particles were detected on the sample surface by SEM-EDX analysis, and it cannot be excluded that intra-layers contaminations may arise from softer materials.

In ROND13_6, the crystal moved both horizontally and vertically in an area in which the stratigraphy was not complete (layer 5 is missing). The displacement probably depended on the presence of craters created by ion milling. Indeed, the sample is particularly small and 12 hours of treatment produced drops between the unpolished region and the polished one. This led to the presence of different level areas, which probably negatively affected ATR analyses. The situation should be improved by just extending the ion mill treatment in order to extend the planar surface.

In order to achieve a deeper understanding of the sample preparation performance in ATR-μFTIR mapping, spectral data were processed by principal component analysis (PCA). A matrix dataset was created with intensity values of peaks as variables (columns) and spectra – recorded during the ATR-uFTIR analysis performed on the light green layer (layer 3) for each sample under investigation (classes) – as objects (rows).
The PC12 score plot allows to identify different clustered groups, thanks to the lower variability of replica spectra compared with the dispersion between the different classes, except for the ROND13_3/ROND13_1 classes, which present a partial overlap. Moreover, the loading analysis (data not shown) allowed the identification of the variables that are most involved in the definition of each PC and, consequently, in the discrimination between classes.
As expected, the PC12 score and loadings bi-plot (Figure 4.9) magnified the crucial role played by the absorption bands around 1726 cm^{-1} for the separation of the ROND13_4 spectra from all the others.

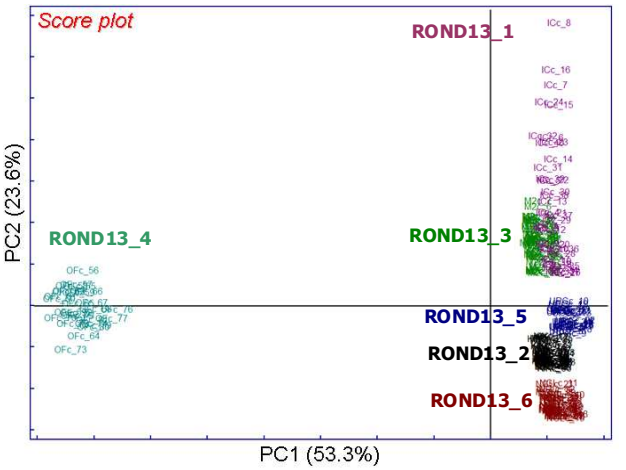

Figure 4.9 – PC12 score plot

In addition, the dispersion along the PC2 of the ROND13_1 spectra is extremely visible, due to the influence in the scatter effect of the peak around 1508 cm^{-1}, probably related to the effect of the embedding resin pollution. In fact, the mentioned peak together with the one at 1244 cm^{-1} can be considered as embedding resin markers, as they are detectable in all of the spectra extracted from the light green layers (Figure 4.10).

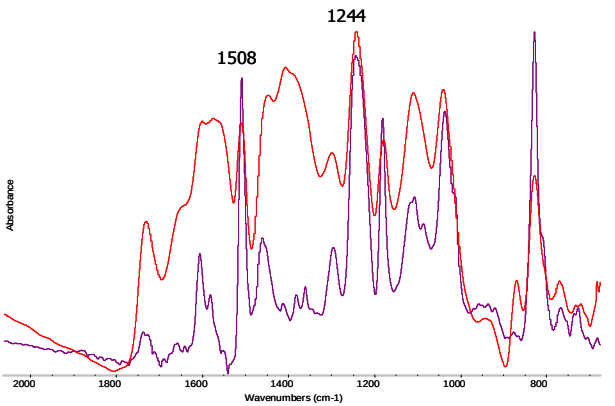

Figure 4.10 – ATR-FTIR spectra. Red profile: spectrum extracted from the green layer of sample ROND13_1; blue profile: spectrum of the embedding resin

4.1.2.2 Comparison between ROND13_3, ROND13_5, and ROND13_6

ROND13_3, ROND13_5, and ROND13_6 (Figure 4.11) shown to provide the best performances in terms of preventing the sample pollution.

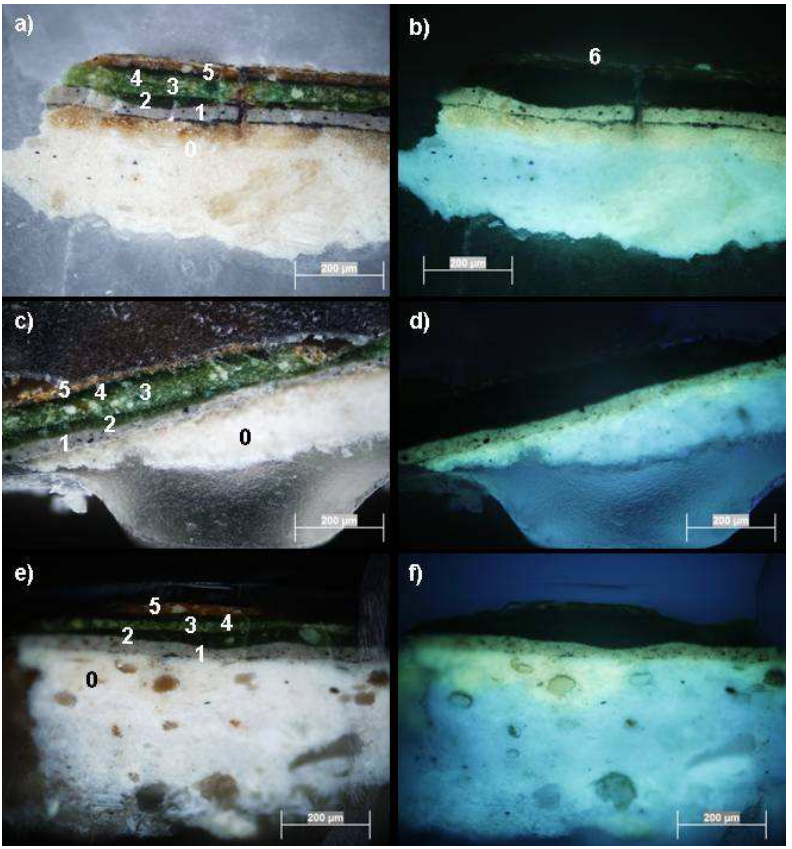

Figure 4.11 – Cross-section photomicrographs a) ROND13_3 visible microscopic image b) ROND13_3 fluorescent image under UV illumination b) ROND13_5 visible microscopic image b) ROND13_5 fluorescent image under UV illumination a) ROND13_6 visible microscopic image b) ROND13_6 fluorescent image under UV illumination

μFTIR-ATR chemical maps for the three sample are reported in Figures 4.12, 4.13, 4.14, respectively. As already described, in the ROND13_5 sample it was not possible to map the preparation layer made of gypsum.

In all of the three cross-sections, the lead white layer has been correctly mapped, using the marker peak at 837 cm^{-1}. In both ROND13_3 and ROND13_4, the bole layer has also been identified, which seems to be absent in the ROND13_6, as previously described. It is worth mentioning that in none of the samples it has been possible to identify organic substances in the gypsum layer normally mixed with an inorganic substance (such as gypsum, calcium carbonate or kaolin). One of the typical Italian preparations was composed of gypsum and animal glue [19]. In this case, the amount of the organic binder was probably below the instrument detection limit.

It can be noticed that in the ROND13_6 sample, the resolution between the acid and the ester bands is well defined, in particular in the green layers 2 and 4. In ROND13_3, the resolution is maintained in the green layers, while in the layer 1, the two bands cannot be distinguished and in some points the spectra are noisy due to a bad contact with the crystal. In the ROND13_5 sample, the resolution is worse, especially in the layers 2 and 4, even if the two bands can be still detected. Furthermore, the KBr embedded sample is noisy in the region around 1600, probably due to the presence of hygroscopic KBr particles. This does not allow to distinguish the contribution of the band at 1620 cm^{-1}. This band is clearly evident in the ROND13_6 sample and, together with the band at 1318 cm^{-1}, it may be ascribed to calcium oxalate.

In the green layers, spectra present interesting peaks in the region around 1350 –1250 cm^{-1}. In ROND13_6, two defined bands at 1377 and 1350 cm^{-1} are present, together with a well defined peak at about 3570 cm^{-1}. Both of the peak and the related substances were investigated. Unfortunately, due to the movement of the crystal, it was not possible to determine the presence of this compound in the layer 2 or 3. In ROND13_3, the band at 1377 and 1350

cm^{-1} is present only as a shoulder, while the OH absorption is completely absent. On the contrary, in the sample ROND13_5, these absorptions were not detected, while a band at 1360 cm-1 may suggest the presence of copper oxalate in the layer 2, even if the region around 1600 is not defined enough. The presence of different compounds in the three samples can be explained considering the fact that the different layers are not homogeneous and only a small fraction of the samples have been mapped.

In ROND13_5, it was possible to register spectra corresponding to the external brown layer (layer 6), with results showing that it is composed of calcium oxalate and silicate, as previously described. However, the signals are weak and noisy, and it is not possible to identify the protective employed, which is responsible for the fluorescence registered (Figure 4.11b).

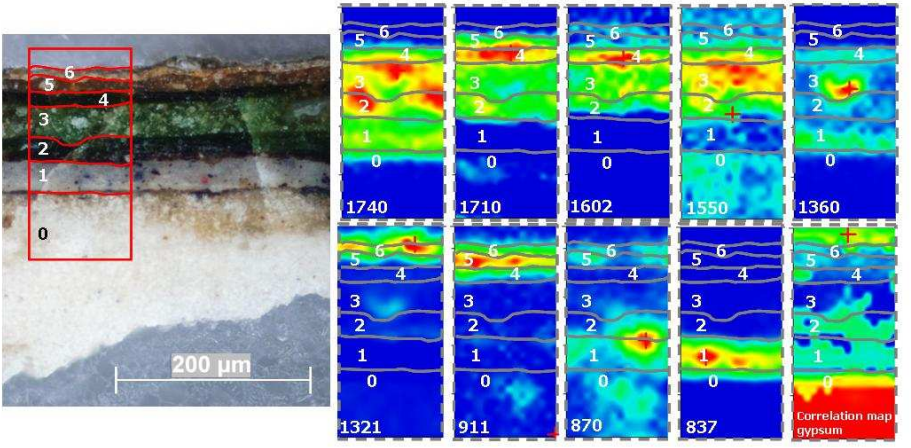

Figure 4.12 – False colour plots of the different paint components Sample ROND13_3. The marker bands employed are reported. The red square indicates the investigated area on photomicrographs under visible light.

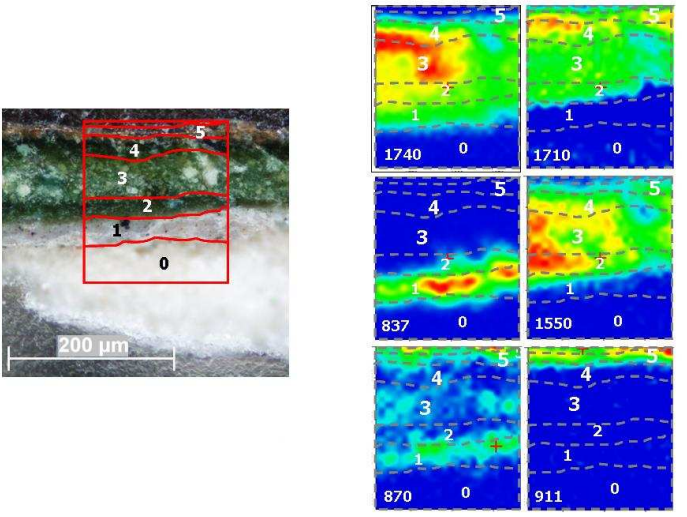

Figure 4.13 – False colour plots of the different paint components Sample ROND13_5. The marker bands employed are reported. The red square indicates the investigated area on photomicrographs under visible light.

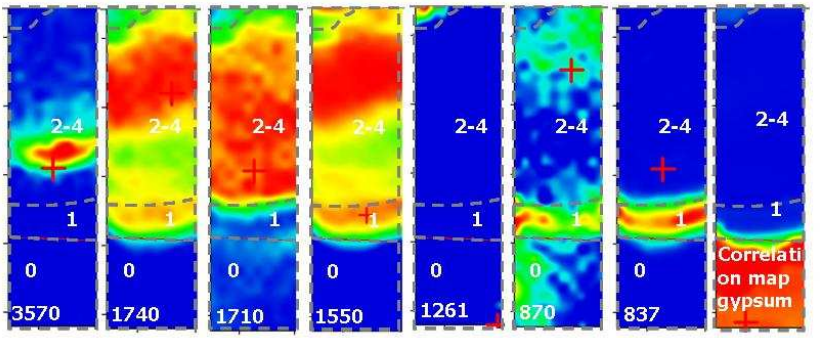

Figure 4.14 – False colour plots of the different paint components Sample ROND13_6. The marker bands employed are reported. Due to the crystal displacement (in both vertically and horizontally direction) it was not possible to report the exact investigated area in the visible image.

4.2 DEVELOPMENT OF ALTERNATIVE CROSS SECTION PREPARATION METHODS

The use of infrared-transparent salts as embedding material for cross sections has been introduced in order to avoid the contamination of the synthetic embedding resins and to provide the detection of organic substances.

In particular, stratigraphical analyses by means of FTIR microscopy can be negatively affected by the cross-section preparation.

In the present research work, alternative approaches to the embedding KBr system have been investigated and compared.

Sodium chloride (NaCl) has been selected thanks to its high performances in terms of physical stability, cost and its reduced harmful effect in comparison with KBr.

In order to improve the standardised approach for both of the salts, a new embedding method has been optimised, using a double embedding system (with an inorganic salt and a polyester resin). In this case, the inorganic salt has the function of a barrier against the resin infiltration and it is suitable for a polishing sample holder. Furthermore, the embedded samples obtained have been submitted to alternative polishing approaches (such as argon ion milling), in order to overcome some drawbacks related to the pollution effects occurred with the dry polishing procedures.

4.2.1 MATERIALS AND METHODS

4.2.1.1 Standard samples

Standard samples have been collected from mock-ups prepared in laboratory according to traditional painting techniques [14] and simulating the stratigraphy of ancient easel paintings. In details, the pigment layer have been obtained using a mixture of lead white ($PbCO_3 \cdot Pb(OH)_2$) with different binding media: linseed oil (6BO), animal glues (4CB), or whole egg tempera (5BT). Then, a preparation layer made of gypsum and rabbit glue was applied. Pigment and gypsum have been obtained from Zecchi (Florence, Italy), while rabbit glue and linseed oil have been purchased from Phase (Bologna, Italy).

4.2.1.2 Reagents

Inorganic salts (KBr and NaCl) have been used at analytical grade, purchased by Sigma-Aldrich Co. (St. Louis, MO).

Polyester resin for sample embedding (SeriFix Resin and SeriFix Hardener) has been purchased from Struers A/S (Ballerup, Denmark).

4.2.1.3 Sample preparation procedures

The samples prepared from mock-ups (with size of a few mm^2) have been carefully observed under a binocular stereo microscope and then cross-sectioned and submitted to different analytical investigations. Different embedding and polishing procedures have been performed and compared.

Historical samples have been treated with the new double embedded system, both with KBr and NaCl.

4.2.2.1 KBr double embedding system

Samples were previously embedded in KBr following the standard procedure [5]. Briefly, the micro fragment was placed in a macro-micro pellet die where a previous KBr pellet-bed (2t for 1 min) had been prepared and covered with additional KBr and then pressed (3t for 2 min). Afterwards, the pellet obtained was reduced in the external part and submitted to the polyester resin embedding procedure. The dry polishing approach was carried out by the use of silica abrasive papers (purchased from Micro-Surface Finishing Products Inc., Wilton, IA) with grit from 1,000 to 12,000, to obtain a high-quality surface in terms of planarity and roughness. A polishing sample holder has been employed in order to ensure a high level of surface planarity and the reduction of surface roughness.

4.2.2.2 NaCl embedding system

The paint chips is placed on a soft base, which is obtained by pressing 300 mg of NaCl into a pellet under low pressure (1 tons for 15 s). Then, another 300 mg of NaCl was added and a pressure of 3 tons for 2 min was applied. Afterwards, the pellet (13 mm of diameter and 2 mm thick) was carefully extracted from the holder. Finally, the cross-section was obtained through a dry polishing on silicon carbide papers (Micro-Mesh®) with different grinding (from 2,400 up to 12,000).

For the creation of the double embedding system, the procedure reported above has been followed.

4.2.1.4 Instrumentation

Dark field observations have been performed using an optical microscope Olympus BX51M equipped with fixed oculars of 10x and objectives with different magnifications (5, 10, 20, 50, and 100x). Visible and ultraviolet radiations were respectively provided by a 100 W halogen projection lamp

and an Ushio Electric USH102D lamp. Cross section photomicrographs were recorded with a digital scanner camera Olympus DP70 directly connected to the microscope.

The documentation of the sample surface morphologies have been carried out with the use of a LEXT microscope purchased by Olympus equipped a 408 nm laser diode, combined with optics specifically designed for operation at this wavelength. 2D and 3D images have been acquired at different magnifications (5, 10, 20, and 50x). Roughness profile and area measurements have been performed.

The elemental composition was determined using a Zeiss EVO 50 EP extended pressure scanning electron microscope (EP-SEM) equipped with an INCA EDX detector. Data analysis was carried out by the use of INCA Energy software.

The analytical SEM instrument (JSM-6610) developed by JEOL (JEOL Ltd, Japan), coupled with a low-vacuum chamber has been also used for elemental and morphological analysis of samples.

The ATR-FTIR mapping measurements have been performed both in reflection and in ATR modes using a Thermo Nicolet iN™10MX raster scanning microscope, fitted with an MCT detector cooled by liquid nitrogen and a conical germanium crystal. Spectra were recorded in the range 4000–675 cm^{-1}. Data collection and post-run processing were carried out using the OMNIC Picta™ software (Thermo).

A IB-09010 JEOL cross section polisher (CP) using ultra pure argon (99.9999%, purity grade 6.0), have been employed in the argon ion milling polishing procedures. The instrument creates a cross-section by irradiating the sample with an ion beam along the edges of the shield placed on it in the dry-evacuated chamber.

4.2.3 RESULTS AND DISCUSSION

4.2.3.1 KBr double embedding system

The KBr embedding method present some specific drawbacks mainly related to the inorganic salt brittleness and hygroscopicity. Indeed, the use of the double embedded system has been proposed in attempt to improve the original performances of the approach.

The use of an external coating made by a polymeric resin is aimed at the physical stabilization of the fragile KBr pellet as well as at its protection from atmospheric humidity. On the other hand, the presence of the salt can be considered as a barrier to the infiltration of the resin into the porous layer of the paint sample.

A significant advantage achieved is related to the possibility to employ the polishing sample holder coupled with suitable supports designed to fit with paint cross-section embedded in resin (Figure 4.15).

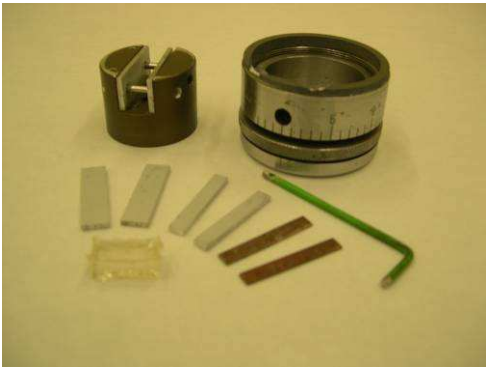

Figure 4.15 – Polishing sample holder

The holder has been designed in order to reduce the influence of operators during the preparation procedures, obtaining more constant and reproducible

results. In fact, the approach usually requires a certain practice and may be affected by a not appropriate manipulation.
In particular, the small and fragile cross-sectioned surface of KBr may present evident irregularities.
Moreover, it is worth to say that the planarity of the sample surface is particular important in μFTIR analysis in both ATR and total reflection modes. In the first case, in fact, the condition of stratigraphic sample surface play a crucial role in the contact between sample and crystal, to which the quality of the spectral signal is related.

In order to evaluate the performances of the semi-automatic polishing approach, two samples collected from the same mock-ups obtained with a layer of lead white mixed with oil (6BO) over a gypsum ground and treated following the same embedding procedure (double embedding system) have been submitted to two different polishing methods: with or without the use of the sample holder. Finishing polishing steps are reported in Table 4.4.

SiC paper grade	Time (min)
1000	1
6000	2
8000	4
12000	8

Table 4.4 – polishing steps followed in preparation procedure with and without the sample holder

Laser confocal microscope has been employed in the surface morphology analysis (Figure 4.16a and 4.16b).

As expected, the use of an appropriate sample holder is particularly helpful in obtaining planar surfaces. In fact, thanks to the constant and homogeneous pressure on the whole cross-sectioned surface a high quality in terms of roughness can be achieved.

In addition, the preliminary results have been also confirmed by the comparison of data obtained from roughness measurements performed on white paint layers of the investigated samples (Table 4.5).

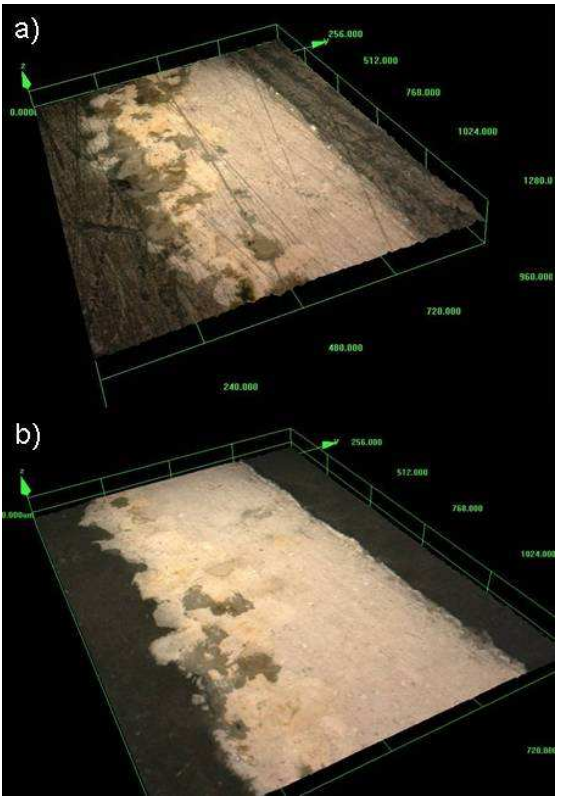

Figure 4.16 – 3D colour confocal images (magnification: 200x) - Standard samples 6BO embedded in KBr and polyester resin polished by: a) manual procedure, b) semi-automatic procedure

The data related to the surface texture can be quantified by the vertical deviations of a real surface from its ideal form. The roughness parameter

usually employed is the *Ra* parameter [22], which is a statistical descriptors that gives an estimation of the average behaviour of the surface height. It is one of the most effective surface roughness measurements commonly adopted in the general engineering practice.
High *Ra* values indicate rough surfaces. On the contrary, smooth surfaces are characterised by lower values.

Polishing procedure	**Layer**	***Ra* value**
Manual	White paint layer	0.54
Semi-automatic	White paint layer	0.35

Table 4.5 – *Ra* values of white paint layers acquired on standard samples

Another key point on the evaluation of the new embedding system potentialities was related to the pollution due to the spreading of the embedding materials on the paint layer. Moreover, this effect is usually amplified during dry polishing procedures.
Specific investigations have been carried out in order to identify the presence of polyester embedding resin on the KBr barrier and on the sample stratigraphy.
Results achieved by the application of μFTIR-ATR analysis on standard sample cross-sectioned with the alternative method, allowed the characterisation of both organic and inorganic substances and their localisation.
The investigated sample has been made by the application of a pigment layer (lead white with linseed oil) on the top of a gypsum preparation layer.
As shown in Figure 4.17, a white paint layer it is well recognisable in the chemical map by using the absorption band at 1735 cm^{-1} for the identification of oil and the marker band of lead white at 838 cm^{-1}. The C=O ester peak of

oil, which could present an overlap with the embedding resin, has been selected in order to verify the absence of resin within the investigated area. In fact, it results well located in correspondence with the painting layer, and no contamination effect can be detected on the KBr surface around the stratigraphy.

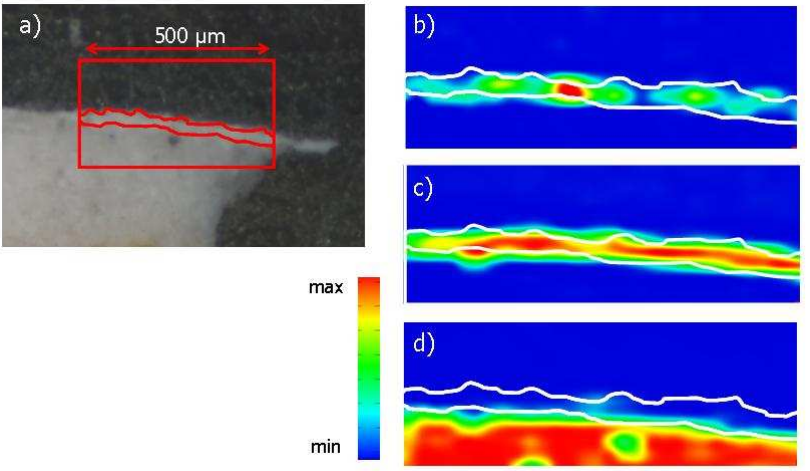

Figure 4.17 – a) Cross-section microphotographs of sample 6BO under visible light; FTIR false-colour plot representing: b) peak area profile: 852-820cm^{-1} (lead white); c) peak area profile: 1754-1712cm^{-1} (siccative oil); d) peak area profile: 1170-1016 cm^{-1} (gypsum)

Alternative polishing method were also investigated.

In particular, argon ion milling was performed combining different preparation procedures, in order to identify and define the most appropriate approach in artwork sample pre-treatments.

Standard sample 6BO has been prepared according with the method proposed. A first characterisation has been carried out by elemental analysis, aimed at identifying the KBr pollution on the sample stratigraphy.

Moreover, both backscattered (BSE) and secondary (SE) electrons images in the tomography mode have been acquired for surface morphology documentation.

Elemental maps of potassium (K) and brome (Br) show the presence of KBr on the gypsum ground and on the support (Figure 4.20). It can be related to the heterogeneous surface and cavities presented in such layers.

The ion beam allowed to obtain a flat and regular surface, which is appreciable in the 3D confocal colour image acquired after the treatment (Figure 4.18b) as well as in the backscattering images (Figure 4.19). Details visible in the ion milled surface magnified sharp differences between elements, revealing particulars in the micron and submicron particle size range.

Furthermore, the elemental analysis performed on the ion polished sample surface reveals the absence of inorganic salt contamination thanks to the milling effect.

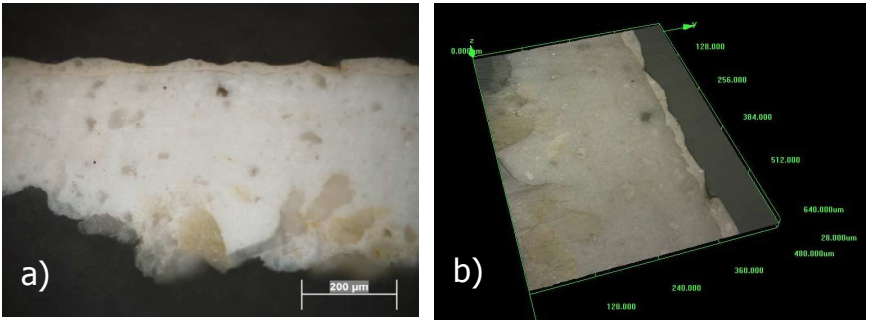

Figure 4.18 - a) Cross-section microphotographs of sample 6BO under visible light; b) 3D colour confocal image (200x)

Before Ion Milling

After Ion Milling

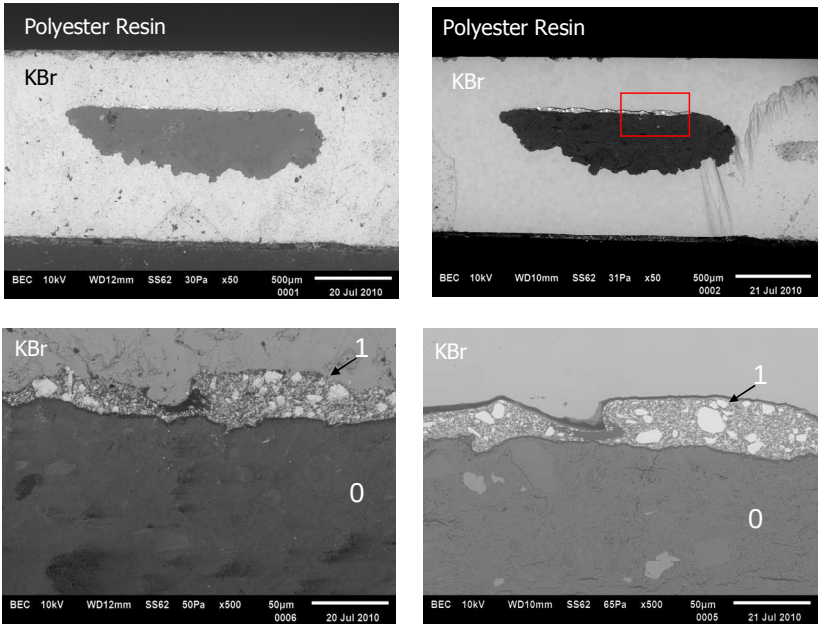

Figure 4.19 - Scanning laser microscopy: BEC image. Standard sample 6BO before and after the argon ion milling polishing procedure.

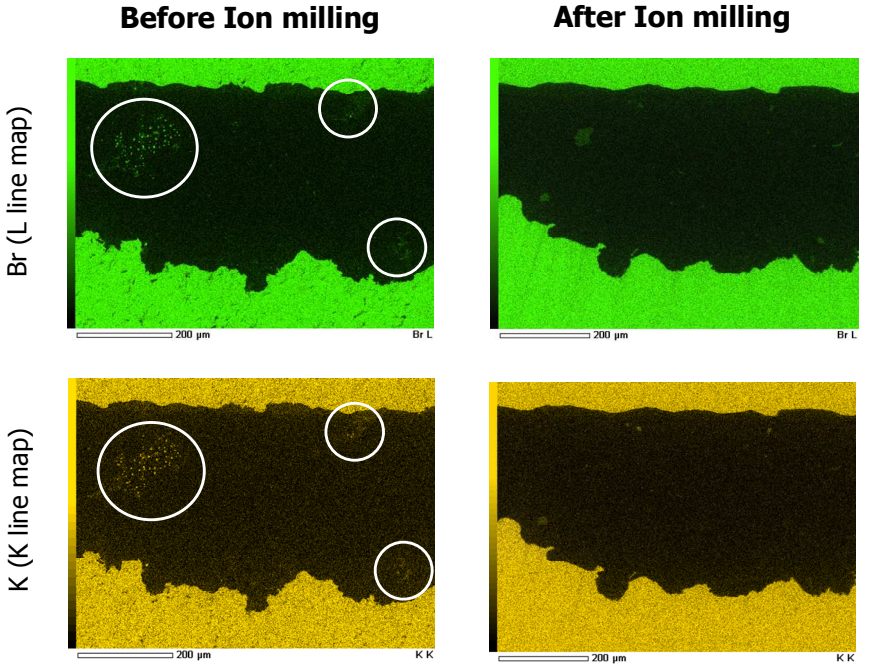

Figure 4.20 – Elemental mapping analysis performed on the sample 6BO before and after the argon ion milling polishing procedure. The white circles in the images before the treatment localize the presence of KBr on the sample stratigraphy

4.2.3.2 NaCl embedding system

Studies on the NaCl embedding system have been carried out in attempt to propose a valid alternative to the KBr one. In particular, NaCl has been selected thanks to its lower hygroscopicity and cost than KBr (solubility of NaCl: 35.8 g/100g of H_2O).

Moreover, another important aspect is related to the harmful of KBr and its effect on the masculine fertility.

Another difference between the two investigated salts is related to the infrared-accessible spectral range. In particular, it is comprised between 4000 and 650 cm^{-1} for the NaCl, while the transparent region for the KBr is bigger

(4000 – 400 cm^{-1}). Indeed, this aspect is particularly important in transmission analysis with the traditional spectrophotometers. On the other hand, in infrared microscopy investigation, it cannot be considered as a limitation, according with the detector spectral range.

Moreover, a particular attention has been paid on the performance in terms of physical stability. Initially, investigation has been performed by the use of optical and infrared microscopy.

Micro FTIR-ATR analysis performed directly on the cross sections revealed higher physical resistance of NaCl to the ATR crystal pressure, as shown in the 3D confocal images acquired after the mapping analysis on both the KBr and NaCl embedded samples, using the same pressure and dimension of the investigated area (Figure 4.21).

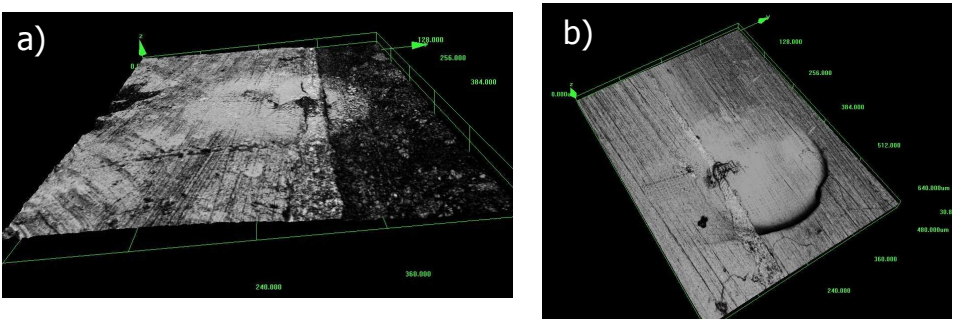

Figure 4.21 – 3D confocal image (magnification: 200x) acquired after the μFTIR-ATR analysis on standard samples 6BO embedded in a) NaCl and b) KBr

Consequently, a low pressure is needed to obtain a good contact and improve the quality of the spectrum, avoiding problems related to the displacement of the ATR crystal during the mapping analysis.

Also for the NaCl embedding system, the contamination of the salts on the paint layers has been investigated through elemental maps. The analysis

reveals the presence of few grains of the salts into the cavities of the support (data not shown).

4.3 CONCLUSIONS

The research work presented allowed the comparison between different embedding and polishing methods. In particular, it was demonstrated that wet polishing may cause dissolution of water-soluble materials, so that it should be avoided. Moreover, the non-homogeneous area created in the sample impede its analyses with micro FTIR in the ATR mode. The use of organic embedding media causes a significant pollution of the sample. This effect may be reduced if a pre-treatment with cyclododecane is performed, and the cross-section is obtained by cutting, or if the resin cross-section is polished by ion milling. KBr embedding was the procedure most effective to avoid the resin pollution. In particular, only in the two samples embedded with this inorganic salt was the external protective layer conserved. However, evidence of pollution of KBr was found. This could lead one to obtain noisy spectra in the region around 1600. The cyclododecane treated and cut sample represents a good compromise in identifying the organic substances, even if the presence of irregularities on the surface leads locally to less sensitive and less defined spectra. The ion milled sample provides intense and well-resolved spectra. Even if the method creates a crater on the surface, an extending the time of the treatment, it provide a larger planar surface.

Regarding the alternative preparation procedures, the research allowed to develop an new embedding system and polishing approaches in order to improve the traditional methods.

The well known KBr embedded method was optimised using the inorganic salt as a barrier against the resin infiltration, obtaining promising results. In fact, the double embedding system (with KBr and the polyester resin) showed high performance in terms of physical stability and it is also suitable for a polishing sample holder, which is needed in order to obtain a high-quality surface.

The evaluation of the effect of resin pollution during the polishing procedures by μFTIR analysis did not show any significant results.

Moreover, it was demonstrated that the use of NaCl as embedding material is particular useful and present several advantages in comparison with KBr. Indeed, the high performances in terms of physical stability allowed to achieve a good contact between ATR crystal and sample surface with a lower pressure, avoiding deformation of the investigated area and improving the quality of the spectral signal.

Different preparation procedures have been optimised and combined, showing the high performance obtained and related to the surface planarity and roughness as well as to embedding sample pollution. In particular, the use of the argon ion polisher system has been confirmed as one of the most appropriate approaches in the polishing of paint cross-sections. On the other hand, due to the limited accessibility and to the cost, it cannot be proposed as a routine methodology.

On these bases, further research analyses will be focused on the use of alternative solvents for wet polishing, in attempt to overcome drawbacks related to the dry polishing methods and to the use of water as cooling medium.

4.4 BIBLIOGRAPHY

1. Plaster, J. (1956) Stud. Conserv. 2:110-57
2. J. Pilc, R. White, Natl. Gallery Tech. Bull. 16 (1995) 73
3. Godla, J. 1990 M.A. thesis, Antioch University, West Townsend, Mass.
4. J. Van der Weerd, R.M.A. Heeren, J.J. Boon (2004) Stud. Conserv. 49 193
5. Mazzeo, R. Joseph, E. Prati, S. Millemaggi, A. (2007) Anal. Chim. Acta *599*, 107-117.
6. S. Prati, E. Jospeh, G. Sciutto, R. Mazzeo (2010), Accounts of chemical research, ISSN 0001-4842, vol. 43, n. 6, 792-801
7. Derrick, M. Souza, L. Kieslick, T. Florsheim, H. Stulik, D.J. (1994) Amer. Instit. Conserv. 33 227
8. C.M. de Fonjaudran, A. Nevin, F. Piqué, S. Cather (2008) Anal Bioanal Chem 392 77–86
9. Jäegers E, Jäegers E (1999) Brit Mus Occas Pap 135:37–42
10. 5. Muros V, Hirx J (2004) JAIC 43:75–89
11. Hopfe V, Korte EH, Klobes P, Griihlert W (1993) J Mol Struct 293:245-248
12. Chalmers JM, Everall NJ, Ellison S (1996) Micron 27:315-328
13. Rosi, F. Miliani, C. Federici, A. Brunetti, B.G. Sgamellotti, A. Clementi, S. (2010) *Anal. Bioanal. Chem. 399(9),* 3133-3145
14. J.J. Boon, S. Asahina (2006) Microsc. Microanal. 12 13227
15. Heaney, P.J. Vincenzi, E.P. Giannuzzi, L.A. Livi, K.J.T. (2001) American mineralogist, 86:1094–1099
16. Ogura, K. Kamidaira, M. Asahina, S. and Erdman, N. (2007) Microsc Microanal 13 (Suppl 2)

17. Boon, J. J. van der Horst, J. (2008) Proceedings of the ICOMCC Paintings Working Group meeting on Grounds, by Archetype Publishers London. Ed J. Townsend

18. Thompson DV Jr (1954) Il libro dell'arte, the craftsman's handbook of Cennino d'Andrea Cennini. Dover, New York

19. Forina, M., Lanteri, S., Armanino, C., Casolino, C., Casale, M., & Oliveri, P. (2009). V-PARVUS 2009, Dip. Chimica e Tecnologie Farmaceutiche e Alimentari, University of Genova, available (free, with manual and examples) from authors or at http://www.parvus.unige.it

20. Harper AM, Duewer DL, Kowalski BR, Fashing JL (1977) In Kowalski BR (ed) Chemometrics: Theory and Application, ACS Symposium

21. Oliveri, P.; Baldo, M. A.; Daniele, S.; Forina, M. Anal. Bioanal. Chem. (2009) 395:1135–1143

22. Wooding, R. A. Bradley E. F. and Marshall J. K. (1972) Boundary-Layer Meteorology, 5:285-308

Acknowledgements

My sincerest thanks to all who have helped and supported me in this research work

Prof. Rocco Mazzeo
Dr.ssa Silvia Prati
Dr.ssa Marta Quaranta
Dr. Emilio Catelli
Dr.ssa Edith Jospeh

Prof. Aldo Roda
Dr.ssa Luisa Stella Dolci
Dr.ssa Angela Buragina
Prof. Massimo Guardigli

Dr. Paolo Oliveri